Aus dem Institut für Experimentelle Schmerzforschung
der Medizinischen Fakultät Mannheim
(Direktor: Prof. Dr. med. Martin Schmelz)

Specific activation of nociceptor subgroups
by slowly depolarizing electrical stimuli

Inauguraldissertation
zur Erlangung des Doctor scientiarum humanarum
(Dr. sc. hum.)
der Ruprecht-Karls-Universität
zu
Heidelberg

vorgelegt von
Sabrina da Silva Soares

aus
Rosário do Sul-RS-Brasilien
2023

Dekan: Prof. Dr. med. Sergij Goerdt
Referent: Prof. Dr. rer. nat. Roman Rukwied

TABLE OF CONTENTS

LIST OF ABBREVIATIONS

A-CAP: A-fibres compound potential

ADS: Activity dependent slowing

ANOVA: Analysis of variance

AP: Action potential

$CaCl_2$: Calcium chloride

C-CAP: C-fibres compound potential

CGRP: calcitonin gene related peptide

CMi: Mechano-insensitive nociceptors

CN: Silent cold-sensing nociceptors

CNS: Central Nervous System

$corL_S$: Corrected latency for sine wave

CTX: μ-conotoxin PIIIa

DFG: German research foundation

DAPSYS: Data acquisition processor system

DMSO: dimethyl sulfoxide

DRG: Dorsal root ganglion

e-thr: electrical threshold

GDNF: Glial cell line-derived neurotrophic factor

HEK293: Human embryonic kidney cells grown in tissue culture

HEPES: Zwitterionic sulfonic acid buffering agent

H_2O: Water molecule

HT: Mechano-thermo-chemo sensitive or polymodal nociceptors

HCN2: Potassium/Sodium hyperpolarization-activated cyclic nucleotide-gated ion channel 2

IB4: *Griffonia simplicifolia* isolectin B4

KCl: Potassium chloride

KH_2PO_4: Potassium dihydrogen phosphate

L_R: latency for rectangular stimulus/conduction delay

LT: Low-threshold mechano-sensitive fibres

Na^+: Sodium ion

NaCl: Sodium chloride

Na_2HPO_4: Di-natriumhydrogenphosphate

NaOH: Sodium hydroxide

Na_V: Sodium channel

nC: nanocoulomb

$MgCl_2$: Magnesium chloride

ms: milliseconds

m/s: meters per second

m-thr: mechanical threshold

PBS: Phosphate-buffered saline

PCR: Polymerase chain reaction

pH: Potential of hydrogen

ProTx: Pro-toxin II and III

q_R: charge for rectangular stimulus

q_S: charge for sine wave stimulus

QST: Quantitative sensory testing

QTRAC: Threshold tracking software

RNA: Ribonucleic acid

SD: Standard variation

SDS: Slow depolarising stimulus

TAAK: Twik-related arachidonic-acid stimulated K+ channel

TG: Trigeminal ganglion

TREK1: Twik-related K+ channel

TRPA1: Transient receptor potential cation channel, subfamily A, member 1

TRPM8: Transient Receptor Potential Cation Channel, subfamily M, member 8

TTX-R: Tetrodotoxin resistant

TTX-S: Tetrodotoxin sensitive

VGSC: Voltage gated sodium channel

VHT: Very-high threshold nociceptors

WPI: World Precision Instruments-Stimulators

XEN907: Xenon 907

1 <u>INTRODUCTION</u>

1.1 Nociception

Nociceptors are primary sensory neurons specialized in the detection of noxious stimuli, such as high mechanical pressure, extremes of temperature or chemical irritants, including endogenous mediators like low pH.[1] This specialized apparatus includes the expression of ligand-gated ion channels and G-protein coupled receptors to transduce the noxious stimuli as well as a unique range of voltage-gated sodium channels (VGSC), key determinants of neuronal excitability. The terminals of VGSC transduce generator potentials into electrical signals, initiate and propagate the action potentials to the central nervous system (CNS), finally releasing neurotransmitters in the dorsal horn of the spinal cord.[2] At the level of the spinal cord the nociceptive input is processed in a complex fashion, culminating in the information being transmitted to the brainstem and thalamus and ultimately to cortical networks.[3,4] The activation of the central nociceptive system will determine the perception of pain (Fig. 1).

Modified from https://www.nature.com/articles/nri3621.
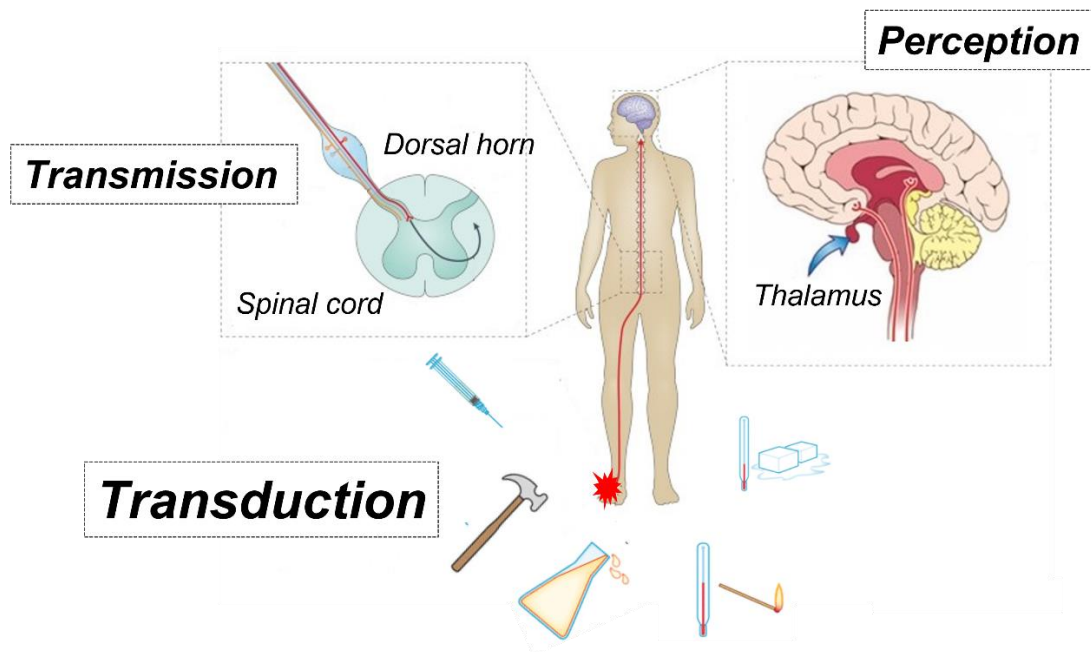
Figure 1: Nociception: The noxious stimulus is detected by peripheral sensory neurons and transduced into electrical signals. The electrical signals or action potentials are carried to the spinal cord where a modulation of this electrical signal occurs, and the information is then transferred to the brain where pain perception takes place.

Pain is protective and adaptive and has the function to warn the individual to escape and protect the injured area during the healing process. This concept includes both nociceptive and inflammatory pain. Yet, when pain extends well beyond healing of the initial injury, remaining for a period of weeks to years, it is considered as chronic and maladaptive, believed to be a result of malfunctions in the somatosensory system.[5] A malfunction of peripheral neurons is a state of inappropriate signalling that gives rise to multiple errors in both transmission and transduction, providing occasion for changes at each point of the pain pathway and ultimately contributing to central sensitization. Albeit, there is no evidence to support that central sensitization alone can maintain a state of persistent pain without the peripheral signalling.[6] The impaired

message coming from the sensory peripheral neurons is characterized by spontaneous activity and abnormal discharge behaviour. These signalling inaccuracies are well correlated to a condition known as painful neuropathy.

Among chronic pain patients, it is estimated that around 20-25% of the individuals suffer from pain with neuropathic characteristics, corresponding to 7-8% of the general population.[7] Still, as neuropathic pain has multiple aetiologies and presentations, it is difficult to establish accurate prevalence and incidence data,[8] not to mention diagnostics and efficient treatment. The fact that between the painful neuropathies only a few are yet mechanistically elucidated might well be the core of this paradox.

1.2 Painful neuropathy

Neuropathic pain can be classified as peripheral, where the primary injury is in peripheral nerves, and central, where a disease or lesion is present in the spinal cord and/or in the brain.[9] The peripheral neuropathies specifically, can be further distinguished based on the number of nerves involved, being a mononeuropathy when a single nerve is intricated and a multifocal neuropathy and polyneuropathy when multiple peripheral nerves are affected.[10]

The most common causes of neuropathic pain include diabetes, spinal cord injury, shingles, viral infection (HIV, herpes zoster), cancer, traumatic or postsurgical nerve injuries, lumbar or cervical radiculopathies (peripheral), stroke and multiple sclerosis (central).[11] Based on the many central or peripheral aetiologies of neuropathic pain, there is no consensus about the most suitable method of diagnosis and treatment. The discussion moves around classifying the pain syndrome only according to its aetiology and/or including the symptoms and somatosensory abnormalities presented by patients.[12]

The diagnosis of neuropathic pain is established mainly by quantitative sensory testing (QST) and intra-epidermal nerve fibre density abnormalities. Even if the skin biopsies assess epidermal innervation, mostly from unmyelinated C-fibre terminals and few small myelinated A-delta (Aδ), the strength of the relationship to neuropathic pain or the occurrence of such is as yet unknown.[9] The QST assesses the function of small and large neuronal fibres and tests for sensory thresholds, yet the heterogeneity of phenotypes is remarkable between the most common neuropathic pain syndromes, obscuring the diagnosis.[12]

An inaccurate diagnosis in turn influences greatly the provision of adequate treatment to those patients.[13] Thermal and mechanical hyperalgesia, hypoesthesia, hypoalgesia and allodynia are found in neuropathic patients referring to abnormalities in the somatosensory neurons.[12]

1.2.1 Cold allodynia

Allodynia is a term used to refer to a pain owed to a stimulus that usually does not evoke pain[14] and cold allodynia is characterized by a pathological state in which pain is induced by an innocuous cold stimulus.[15] The prevalence of cold allodynia in neuropathic pain patients is rather difficult to estimate, although it is mostly associated to patients suffering from diabetes and post-herpetic neuropathy.[14]

In normal conditions, mild cooling of the skin is expected to be analgesic, while only moderate to extreme cooling becomes painful.[16] Pain in response to cooling may arise from integration of nociceptive and non-nociceptive thermal inputs.[17] It has been reported before that both "silent cold-sensing neurons" and "low-threshold mechanoreceptors" respond to cold stimulus and increase their population in glabrous

(mouse hind-paw) skin in neuropathic pain models endowing the development of cold allodynia.[18]

Patients suffering from painful neuropathy not only can have a great impairment in quality of life, but may also be affected by comorbidities such as anxiety, depression, impaired cognition and sleep disturbances.[7]

Accordingly, excitability changes of somatosensory neurons could present an accurate biological marker for the occurrence of neuropathic pain, particularly by means of abnormal discharge behaviour and spontaneous activity in a particular class of unmyelinated somatosensory neurons. It is well stated that excitability changes in unmyelinated nociceptors from class C, particularly a subset of mechano-insensitive nerve fibres, are well correlated to painful neuropathy.[19,20,21]

Based on the relevance that somatosensory neurons possess in neuropathic pain, the exploration of this theme seems crucial for further understanding of its pathophysiology, and we may start by shedding some light on how the different cases of peripheral nerve fibres can be classified as follows.

1.3   Classification of peripheral nerve fibres

The nerve fibres were initially classified according to diameter and degree of myelination. These two characteristics directly influence the speed at which the impulses are conducted. Another important factor to mention is the threshold of electrical activation. As a rule, the threshold is lower the thicker the fibre, and the thicker the fibre the higher the conduction velocity (CV).[22] The classical studies of Joseph Erlanger, Herbert Gasser and David Lloyd provided us with the nerve fibre classification still in use today: A alpha (Aα) being the largest 12-20µM with a conduction velocity varying from 70-120m/s; A beta (Aβ) with a diameter of 6-12µM and a conduction velocity of 30-70m/s; A gamma (Aγ) with a diameter to 1-6µM and a conduction velocity ranging from 30-70m/s; A delta (Aδ) with a diameter less than 3µM and a conduction velocity ranging from 5 to 20m/s; and unmyelinated C-fibres with a diameter of 0.3-1.35µM and a conduction velocity of 0.5-2m/s.[23,24] In addition to this, nerve fibres are separated into "efferent" motor and "afferent" sensory neurons, among which Aβ fibres, Aδ and C-nociceptors are sensory.[25]

As expected, when recording from electrically excited peripheral sensory nerves (for instance a single fascicle), the compound action potentials (CAP's) of the recorded units will reflect the conduction velocities of the fibre classes within the fascicle. The first peak to be seen will be Aα and Aβ, followed by Aδ and lastly C-fibre compound potentials (Fig. 2).

The Aβ fibres are low threshold mechano-sensors, while Aδ are mechano-heat-nociceptors in the skin. Aβ and Aδ fibres were not a focal point of the present study. The main interest was instead in the different classes of C-nociceptors, and those fibre types were extensively explored in this work. The challenge in recording from C-fibres separately rely on the fact that those sensory neurons have ten-fold higher electric thresholds of activation when compared to A-fibres, meaning that activating them using the traditional rectangular short duration pulses also activates Aβ and Aδ fibres. Additionally, different classes among C-nociceptors also present differences in electrical thresholds of activation.[26]
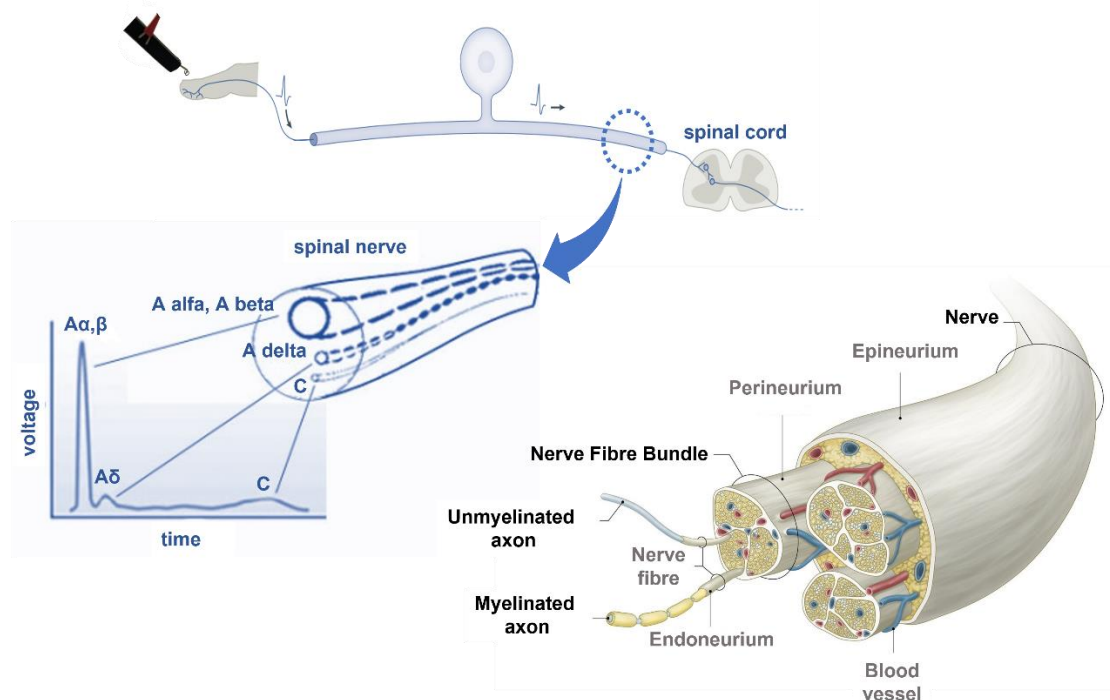
Figure 2: Nerve fibre classification: The nerve fibres are classified by diameter, myelination, and conduction velocity. Myelinated Aα and Aβ fibres conduct the electrical impulse faster compared to thinly myelinated Aδ nociceptors and unmyelinated C-nociceptors.

At the early stages of human nerve fibre recordings "*in vivo*" (microneurography) in the 70's, C polymodal nociceptors or mechano-heat nociceptors (HT) were the first fibre type to be identified and recorded from.[27] Around the same time, sympathetic C-fibres (vasoconstrictors) were also identified and differentiated from mechano-thermal-insensitive nociceptors (CMi or "silent" nociceptors).[28] The C-sympathetic fibres were also disregarded in the current study based on their non-nociceptive function.

C-polymodal nociceptors recorded from human intact skin were defined as responsive to non-painful pressure and warming. The after-stimulus discharge and reduced excitability after repeated mechanical stimulation observed in polymodal nociceptors were also highlighted by the author.[29] The very high threshold silent fibres seemed to be sensitive to chemical mediators, including inflammatory mediators. It was described that only after sensitization, those nociceptors start responding to mechanical and thermal stimuli. At that stage of research, both the very high threshold (VHT) and silent fibres were treated as a single class of C-nociceptors.[30] Based on the functional results obtained in this study, the VHT and CMi are referred to as different fibre classes.

The unmyelinated low mechano-threshold units (LT) were later differentiated from polymodal nociceptors based on higher sensitivity to mechanical-stimulus and poor to absent response to heat. These tactile C afferents were also clearly differentiated from myelinated fibres, based on a conduction velocity in the range of the C-fibre class (around 1m/s) and the "fatigue" effect after repetitive stimulus.[31]

The "fatigue" effect is an axonal property of slowing the conduction velocity upon repetitive stimulation named activity dependent slowing (ADS). The different patterns of ADS became a valuable tool to differentiate not only sub-classes of C-afferents, but also the C-fibres from C-efferents and A-fibres as mentioned above.[32]

Another class of C-fibres were brought into light as a relevant subset of mechano-insensitive nociceptors, named cold nociceptors (CN). The identification of a functional

response to noxious cold temperatures in human was initially attributed to polymodal nociceptors.[33] Indeed, a study conducted in porcine CN showed a conduction velocity in a range of mechano-responsive nociceptors and a smaller ADS compared to the silent units. Nevertheless, CN are described as unresponsive to mechanical von Frey stimulus corroborating our observations of cold units in the present study.[34]

A more recent attempt has been made to correlate single cell RNA-sequencing of dorsal root ganglion (DRG) with "*in vivo*" recordings and real time PCR expression patterns, allowing for the identification of around 10 types of DRG neurons.[35,36] The expression pattern of some DRG's were correlated with known functions of sensory neurons, but the overlay in the expression pattern of different neuron types and the difficulty to correlate the expression in the soma with the functional protein expression in the sensory endings remain a challenge to be overcome.

The development of modern genetic approaches has raised questions related to the translational value of the classification of neurons into "peptidergic" (containing neuropeptides) and "non-peptidergic". This classification is based on somatosensorial studies in rodents, and it is unclear whether this is translatable to humans. Not only fundamental differences in the expression of neuronal markers associated with pain signalling, but also in the expression of the voltage gated Na$_V$ channels (VGSC's) Na$_V$1.8 and Na$_V$1.9 in peptidergic neurons were found between mouse and human neurons. The higher expression of Na$_V$1.8 and Na$_V$1.9 in peptidergic neurons in humans for instance, renders the axons more prone to longer lasting action potentials and higher discharge frequency.[37]

To increase the translational value of the present study, the majority of the results to be presented later were investigated using *Sus Scrofa.* Pigs appear to be a highly suitable model to study human pain due to the many anatomical and physiological similarities with humans. It is known that neuronal distribution and axonal excitability are akin for humans and pigs when comparing both nociceptive and non-nociceptive fibre classes, making swine a suitable model for modulation of excitability in C-nociceptors.[38]

While more detailed and elaborate data is not available on the classification of C-fibres, we hold on to the classic classification of sensory neurons for the intent of this study and centre our focus on the abovementioned LT fibres and HT, VHT, CN and CMi nociceptors. A detailed description on how those nociceptors were differentiated from one another during the "*in vivo*" recordings with pig saphenous nerve is provided later in the *Material and Methods* section. Meanwhile one should recapitulate on what is known about VGSC's distribution amidst C-nociceptors and how their individual kinetics influence C-fibres response to noxious stimulus.

1.4   Voltage gated sodium channels

Many of the transmembrane voltage gated sodium channels are action potential generators responsible for conducting Na$^+$ currents across the membrane of axonal neurons and many excitable cells.[39,40] The nomenclature of the VGSC's relate to the chemical symbol of the permeating ion (Na$^+$), associated to the principal physiological regulator (voltage) indicated as subscript (Na$_V$), followed by the number of the gene subfamily and the number of the specific channel isoform.[40]

Na$_V$ channels consist of a pore-forming α-subunit associated with β-subunits of smaller size. The family of α-subunits are composed of around 2000 amino acids, divide into 4 domains (DI-DIV) and each domain possess 6 transmembrane segments (S1-S6), being the S1-S4 voltage sensing segments and S5-S6 pore forming segments.[2] The β-subunits comprise four subtypes (β1- β4) that influence localisation and modulate

the kinetics of VGSC. The mammalian VSGC are divided into nine isoforms (Nav1.1 to Nav1.9) expressed in different proportions among the biological tissues with a high homologous sequence in the transmembrane and extracellular domains.[2] The VSGC isoforms have distinct sensitivity to the neurotoxin tetrodotoxin (TTX) and can be separated into TTX sensitive (TTX-S) and TTX resistant (TTX-R) isoforms. The sensitivity to TTX is mainly determined by the presence of an aromatic residue (tyrosine and phenylalanine) between segments S5-S6 in domain 1, which confers an electrostatic negative potential and attracts TTX.[41] The TTX resistant VGSC have a serine or a cysteine in the same position, reducing greatly their affinity to the toxin.[42] Even if Nav channels share many similarities between the amino acid sequences, they differ when referring to channel kinetics properties. The **Table 1** provides an overview on the isoforms of VGSC localization, kinetics as well as sensitivity to TTX.[43]

It is described that small diameter dorsal root ganglia (DRG) and trigeminal ganglia (TG), which are the cell bodies of unmyelinated sensory neurons, express high levels of TTX-R VGSC Nav1.8 and 1.9 and TTX-S Nav1.7 and 1.6.[44] Nav1.1, 1.6, 1.7, 1.8 and 1.9 are expressed in primary sensory afferents at adult age.[45] The other VGSC channels Nav1.2, 1.3 and 1.5 are expressed in sensory neurons during the embryonic period but downregulated later,[46,47] with the exception of Nav1.5 (heart) and Nav1.3, the latter can be re-expressed following injury of peripheral nerves.[48] The re-expression of Nav1.3 together with the enhanced expression of Nav1.7 and Nav1.8 has also been described in patients with painful neuromas.[44] Those channels, plus Nav1.9, are thought to be the main players in nociceptive signalling.[49] The Nav1.6 is the main channel present in the nodes of Ranvier in myelinated axons,[50] although there is evidence that Nav1.6 is also expressed along the axons of unmyelinated C-fibres and contributes to action potential generation.[51,52]

Isoform	TTX sensitivity	Tissue Expression	Kinetics
Nav1.1	TTX-S	CNS neurons, PNS neurons	Fast activation, fast and slow inactivation
Nav1.2	TTX-S	CNS neurons	Slow repriming
Nav1.3	TTX-S	CNS neurons, PNS neurons (post-injury)	Fast activation, fast inactivation, rapid repriming
Nav1.4	TTX-S	Skeletal muscle	Fast inactivation
Nav1.5	TTX-R	Heart	Fast activation, fast inactivation
Nav1.6	TTX-S	CNS neurons, PNS neurons	Fast activation, fast inactivation, rapid repriming
Nav1.7	TTX-S	Large and small DRG, PNS neurons	Fast activation, fast inactivation, slow repriming
Nav1.8	TTX-R	Small DRG neurons, PNS neurons	Slow activation, slow-inactivation, rapid repriming
Nav1.9	TTX-R	DRG neurons, PNS neurons	Ultra-slow activation and inactivation, persistent currents

Table 1: The human VGSC α-subunits.[53,43,54,48,46,50,49,55,56,57,58]

Based on the afore mentioned and on the objectives of this study, a description of VGSC function is provided along these lines, together with a more detailed description on the kinetics of key VGSC isoforms enrolled in nociceptive signalling: Nav1.3, 1.6, 1.7, 1.8 and 1.9.

1.4.1 VGSC function

The Na$_V$ channels can exist in different states: "*closed*" or "inactive" during hyperpolarization, "*open active*" (1ms) during depolarization, and "*fast inactivated*" before closing again when the membrane returns to resting potential. These VGSC are also known to go into "*slow inactivation*" (tens of seconds) states when submitted to prolonged depolarization.[2] (Fig. 3)
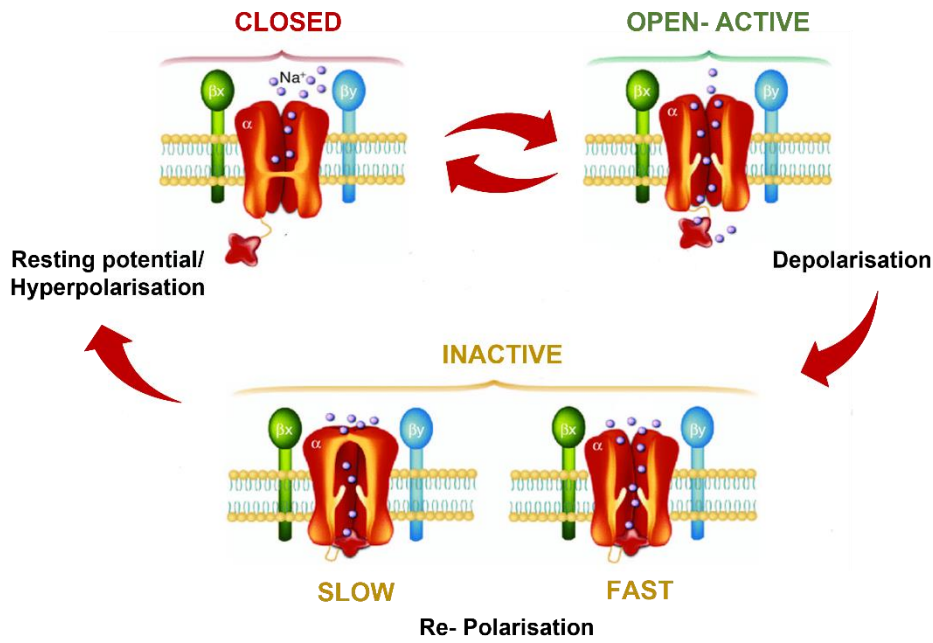
Figure 3: States of Na$_V$ channels: The sodium channels are in closed or inactive state at resting membrane potential. As depolarization of the neuronal membrane starts, the channel moves to an open state, allowing the Na$^+$ currents to move inward, according to its electrochemical gradient. Deactivation occurs when the membrane returns to the resting potential and the channel assumes a closed conformation. If depolarisation last longer, the channel can move to a fast or slow inactive state. Hyperpolarization is needed to change the conformation of the channel from inactive to closed.

At resting potential (approximately -80mV, related to outer extracellular compartment), the channel is in its closed conformation. During a depolarisation, the membrane potential move to a more positive voltage and allows for an outer change in the conformation of S4, opening the channel to inward currents of Na$^+$,[43] along their electrochemical gradient.[59] Fast inactivation occurs after few milliseconds by a change in the inner conformation of S6 in domain III and S1 in domain IV, blocking the intracellular side of the pore and consequently impeding influx of Na$^+$. When the depolarising stimulus persists longer, the slow inactivation mechanism takes place, which is thought to change the conformation of the outer side of Na$_V$ pore.[60,59] The recovery from inactivation, also known as repriming, is dependent on repolarization of the membrane potential. As hyperpolarisation progresses and the resting potential is re-established, the inactivated position returns to its closed conformation.[43,59]

The VGSC have an overall fast transient kinetic and close within milliseconds. Nevertheless, under specific circumstances fast inactivation is not completed and persistent Na$^+$ currents may occur.[49]

1.4.2 Kinetics of VGSC involved in nociception

As previously mentioned, the focus of this work in addressing C-fibres originated with the need to perceive the properties of VGSC directly involved in action potential generation and transduction in those nerve fibres.

The $Na_V1.7$ channels seems to play a great role in action potential initiation and propagation.[61] The channels have fast activation and inactivation kinetics, but are known to recover slowly from inactivation. $Na_V1.7$ is also described as a threshold channel; as it produces significant ramp currents in response to small depolarisations, facilitating neuronal discharge upon subthreshold stimuli.[49,62]

The activation of $Na_V1.8$ happens at more depolarised membrane potentials (around -35mV) than the Na1.7 isoform and is responsible for the majority of the transmembrane Na^+ current during the rising phase of the action potential.[49,54] The late activation in the human NaV1.8 combined with a more depolarised voltage to shift into inactivation allows the channel to remain open for longer periods of time compared to other VGSC. This feature allows the channel to increase the width of action potentials and modify the release of neurotransmitters from synaptic terminals. Besides that, $Na_V1.8$ has a fast recovery from inactivation, meaning that more channels are available for activation shortly after an action potential, contributing to repetitive firings at high frequencies. [54]

$Na_V1.3$ channels have similar kinetics to $Na_V1.7$ (fast activation and fast inactivation) except for a rapid repriming at hyperpolarised membrane potentials and a slow recovery from inactivation at more positive potentials. It is suggested that upon slow depolarising stimulus, the channel has a slow closed state inactivation, allowing for the generation of ramp currents.[55] This could be a reason why NaV1.3 is re-expressed in peripheral neurons at adult age after tissue injury,[44,52] because under such conditions, the capacity to recover relatively fast from inactivation of $Na_V1.3$ promotes high frequency firing in damaged tissues.[55]

$Na_V1.6$ possesses fast activation and fast inactivation kinetics with a rapid repriming time, which is tenfold faster than $Na_V1.7$ and twofold faster than $Na_V1.3$. Because the time to recovery from inactivation is directly correlated with how fast a neuron can repetitively fire, fibres with $Na_V1.6$ channels can follow much higher frequencies of stimulation compared to $Na_V1.7$. This characteristic of rapid repriming and a fast closed state inactivation makes $Na_V1.6$ very unlikely to generate ramp currents and respond to slow depolarising stimuli.[56]

$Na_V1.9$ has a low threshold of activation and can give rise to persistent Na^+ currents in sensory neurons. The channel activates at hyperpolarised potentials close to the resting potential and therefore do not participate in the generation of action potentials, but instead contribute to the maintenance of the resting membrane potential and neuronal excitability.[49]

It is known that identified mutations of the voltage-dependent $Na_V1.7$, 1.8 and 1.9 channels with an enhanced function ("gain-of-function mutation") are related to the development of painful neuropathies, even if only very few patients with painful neuropathies presented the mutations.[63] Among the most common genetic diseases of voltage-dependent $Na_V1.7$, 1.8 and 1.9 channels, we can cite paroxysmal extreme pain disorder ($Na_V1.7$), inherited erythromelalgia ($Na_V1.7$) and small-fibre neuropathy ($Na_V1.8$/sporadic mutations in $Na_V1.9$).[64,65,37] In general, gain-of-function mutations modulate "*in vitro*" excitability[66], increase discharge rate of action potentials in response to slowly depolarizing stimuli[54,65] and provoke spontaneous activity.[67]

The gain of function mutations in $Na_V1.7$ isoform, for instance, renders the channel hyperexcitable either by hyperpolarising the voltage of activation or by affecting its inactivation kinetics. The impairment of the fast inactivation causes the channel to

remain open for longer periods. The hyperpolarisation of activation makes it easier to excite and increases the frequency with which the channel is activated. As a result of a reduced activation threshold and slower closed state inactivation, its ramp currents increase. Additionally, a high firing frequency is a common trait for gain of function mutations of $Na_V1.7$.[43]

$Na_V1.8$ gain of function mutations are known to provoke a shift on the channel voltages, granting a more hyperpolarised activation threshold and a more depolarised voltage to shift into inactivation. In some cases, the inactivation is completely impaired. The consequences of those mutations are a decrease in the threshold of activation, with an increase in the discharge frequency and spontaneous firing in the absence of a stimulus. Ultimately, spontaneous firing means spontaneous pain.[54]

Lastly, $Na_V1.9$ mutations are related to modulation of gating properties, making the membrane potentials more depolarised and resulting in increased excitability of DRG neurons.[49] However, extreme depolarisation will inactivate the other Na_Vs and render the nociceptors unexcitable. Thus, extreme gain of function mutations of $Na_V1.9$ will desensitize rather than sensitize nociceptors. The clinical effect for such mutations is congenital inability to experience pain.[68]

1.4.3 SNF and CAP recordings of C-nociceptors

Neuronal excitability can be investigated using single nerve cell/fibre recordings, as well as in whole nerve fascicles comprising several axons. The main advantage of recording from single units is the possibility to differentiate and classify functional classes of C-fibres.[69,70,71,72] In general, studies on single-fibre level are conducted by performing extracellular recordings,[73] but there are also attempts to perform sensory afferent classifications by means of intracellular recordings from dorsal root ganglia "*in vivo*".[74,75,69]

The investigation of nerve excitability using nerve fascicles instead of single units generates compound potentials as a result of a summation of unitary action potentials from all the stimulated single axons. Pharmacological studies greatly benefit from the last method, as the simultaneous assessment of multiple axons become possible by this approach. The differentiation of C to A-fibres is still defined by their specific conduction velocity mentioned previously. Nevertheless, the evaluation of C-fibre subtypes is no longer attainable using compound action potentials. The neuronal excitability is assessed in compound action potentials mostly by varying the electrical stimulus amplitude and duration and observing the changes in the neuronal response. More detailed information is provided in the following *Material and Methods* section.

1.4.4 VGSC modulation with neurotoxins

Regarding neurotoxins, it is important to clarify a fundamental difference between blockers and inhibitors. Blockers physically obstruct the channel pore, impeding the flux of Na^+ currents, while inhibitors act to modulate channel function and interact with the channel domains.[43] Tetrodotoxin for instance is a pore blocker that impedes Na^+ influx by binding extracellularly to the site 1, S5 and S6 of all four domains of the VGSC.[43] The toxin is mainly present in marine species like puffer fish, blue ring octopus, some worms, shellfish and crustaceans.[49] μ-Conotoxin PIIIA is a venom extracted from a fishing hunting marine cone snail *Conus purpurascens*[76] that acts by occluding the VGSC pore and compete for TTX binding site 1 in the α-subunit.[77,78]

Xenon 907 (XEN907) is a synthetic lipophilic spirooxindole that showed high "*in vitro*" potency as a Na$_V$1.7 blocker, with an IC50 of 8nM (HEK293 cells) but poor solubility in saline (PBS).[79,80] No electrophysiological data has been generated and no information on the exact mechanism of Na$_V$1.7 blockade for XEN907 has been found.

Protoxin II (ProTx II) is a peptide extracted from the *Thrixopelma prurient* venom that selectively inhibits Na$_V$1.7 by binding to domain II S3. It has an IC50 of only 0.3nM for Na$_V$1.7, compared to 30-150nM for other isoforms of Na channels. The selectivity to Na$_V$1.7 is granted by a phenylalanine in the S3b helix of domain II. The second sodium channel mostly affected by the inhibition of ProTx II is Na$_V$1.6, where a concentration 100-fold higher seems to be necessary due to a serine in the same position. The other Na$_V$ channels have a glycine in domain II S3 rendering them even less sensitive to ProTx II. ProTx II acts by shifting the voltage-dependence of channel activation to more positive potentials. It is also worth noting that ProTx II has demonstrated a complete inhibition of C-nociceptor compound potentials in desheathed cutaneous nerves, with little effect on Aβ fibres.[81] Protoxin III is a toxin also obtained from the tarantula venom and is known to block Na$_V$1.7, Na$_V$1.6 and Na$_V$1.3. It is suggested that the toxin acts on S3-S4 domain II. ProTx III holds the channel in a closed state and does not change voltage-dependent activation or steady-state inactivation of Na$_V$1.7.[82]

1.5   Aim of this work

It was demonstrated in previous studies by using animal pilot studies (mouse and domestic pig), as well as healthy subjects and patients with neuropathic pain, that unmyelinated nociceptors can be preferentially activated by means of transcutaneously applied slow depolarization. Mechano-insensitive nociceptors (identified by the development of a flare response) and polymodal nociceptors could be activated even at current intensities as low as 0.05 mA.[26]

The preferential electrical activation of C-nociceptors could contribute immensely to the understanding of abnormalities in those afferents when testing neuropathic pain patients. However, .

The aim of the present project was to elucidate the involvement of specific voltage-dependent sodium channels (Na$_V$) in the activation of C-nociceptors by slow depolarizing electrical stimulus (SDES). The studies include the modulation of neuronal excitation on specifically identified nociceptor sub-classes with slow depolarizing electrical stimulation "*in vivo*" and "*ex vivo*" via recording anesthetized pigs and the saphenous nerve collected "*post-mortem*", respectively. Specific VGSC blockers and inhibitors were applied to clarify the role of Na$^+$ channel isoforms in the response to slow depolarising stimulus using two different electrophysiological methods: single nerve fibre recordings (SNF) "*in vivo*" and compound action potentials (CAP) "*ex vivo*".

This study also attempts to confirm previous studies in which C-nociceptors seem to be more excitable at colder temperatures, providing insights into the mechanisms of cold allodynia.

2   <u>MATERIAL AND METHODS</u>

2.1   Experimental animals

Experiments were performed in mouse and pig. Aiming to establish more translational results to humans, most of the experiments were performed in pig, as swine is a highly suitable model for pain studies based on anatomical[83] and physiological[38] characteristics, compared to humans. It is known, that major differences exist when comparing rodent and human sensory tissue, including differences in the expression and kinetics of VGSC.[37] As the purpose of this research is to understand the functional response of C-nociceptors to slow depolarizing electrical stimulation, and VGSC channels are the main targets of this approach, pigs represent a more suitable animal model. In this study, mice were used only to compare interspecies results and for establishing the final experimental protocols.

2.1.1   Pig

Male Domestic German Landrace pigs (*Sus Scrofa domesticus*) were provided by a breeder in Sommerhof, Dielheim-Unterhof, Germany. The average weight was 20-25kg, and the average age was generally 12±4 weeks. Before the experiments, the animals were acclimatized to the new environment for a period of 7 days with water *ad libitum* and fed twice a day with Muskator EM DE BW200060 (MuskatoWerke, Mannheim, Germany).[84] The studies followed the guidelines for the welfare of experimental animals as determined by the Federal Republic of Germany, obtained ethical approval for animal experimental procedures by the Ethics committee of the regional government (Karlsruhe, Baden-Wuerttemberg, Germany), approval number G-78/18, and were carried out within the Medical Faculty Mannheim of Heidelberg University.

2.1.2   Mice

C57BL/6N mice were obtained from Charles River Laboratories. Animals were housed in individually ventilated cages under 12-hour light-dark cycles and were provided with water and food *ad libitum*. Both male and female mice were randomly selected for experiments, anesthetized by Sevoflurane (Abbott, Germany), and killed by cervical dislocation after complete loss of hind paw withdrawal reflexes. The experiments were performed following ethical approval for animal experimental procedures by the Ethics committee of the regional government (Karlsruhe, Baden-Wuerttemberg, Germany), and were carried out under approval number I-19/15 within the Medical Faculty Mannheim of Heidelberg University.

2.2   Solutions

2.2.1   HEPES extracellular physiological solution

All peripheral nerves used in the "*ex vivo*" experiments were stored in HEPES extracellular physiological solution composed of (in mM): NaCl 118; KCl 3.2; HEPES 6; Na^+ gluconate 20; $CaCl_2$ 1.5; $MgCl_2$ 1.0; D-Glucose 5.55. The pH of the HEPES solution was adjusted to 7.4 by adding NaOH (1M). HEPES solution was prepared in batches of 2 liters without glucose or Ca^{++} and Mg^{++} and kept at 4°C. Glucose, Mg and

Ca were added to the solution directly prior to each experiment. Sodium chloride (S7653), potassium chloride (P9333), HEPES (H3375), D-Gluconic acid sodium salt (G9005) and D-(+)-Glucose (G8270) were purchased from Sigma-Aldrich, Germany. Calcium chloride (21114) and Magnesium chloride (63020) were purchased from Fluka, Germany.

2.2.2 Phosphate-Buffered Saline (PBS)

PBS was used to constitute the hydrophilic peptides Tetrodotoxin citrate, µ-Conotoxin PIIIa, Pro-Toxin II and Pro-Toxin III. The PBS solution was composed of (in mM) NaCl: 1037; KCl: 27; Na_2HPO_4: 100; KH_2PO_4: 18; Potassium dihydrogen phosphate (4871) and di-Natriumhydrogenphosphate (6346) were purchased from Merck, Germany. The solution was kept at a room temperature and diluted 10-fold in distilled water (Milli-Q Millipore, Merck, Germany) before use.

2.2.3 Na^+ channel blockers

Tetrodotoxin citrate (TTX) (T-550), XEN907 (X-105), 20µM µ-Conotoxin PIIIa (STC-400), 3µM Pro-Toxin II (STP-100) and 3µM Pro-Toxin III (STP-150) were purchased from ALOMONE labs®, Israel. Stock solutions of tetrodotoxin citrate, µ-Conotoxin PIIIa, Pro-Toxin II and Pro-Toxin III were diluted in phosphate buffered saline (PBS) while stock for XEN907 was prepared in DMSO (D5879, Sigma Aldrich). Stock solutions were diluted on the day of experiment in physiological solution. TTX was prepared at concentrations 10nM, 100nM and 1µM for single nerve fibre recordings (SNF) and the concentration-response curves for extracellular compound action potentials (CAP) were performed from 1pM to 10µM. XEN907 was used at 10µM in SNF, and the concentration-response curves for CAP were performed from 0.1nM to 100µM. The concentration-response curves for Pro-Toxin II and III were performed at a concentration range of 0.1nM to 10µM and 50nM to 5µM, respectively.

2.3 Compound action potential recordings *"ex vivo"*

2.3.1 Mouse sural nerve preparation

Mice were killed by cervical dislocation under general anaesthesia with Sevoflurane. The cervical dislocation was performed only after the complete loss of hind limb paw withdrawal reflex, indicating that a deep level of anaesthesia was achieved. The hind limb was shaved and disinfected with 70% alcohol solution. Mice were positioned ventrally and fixed on a flexible structure by the paws. A 1cm incision was performed proximal to the knee (Fig. 4A) and the skin retracted caudally until complete exposure of the muscles gluteus maximus, vastus lateralis and biceps femoral posterior. The gluteus maximus was reflected to expose the sciatic nerve (Fig. 4B). The sciatic nerve was cut at its proximal end and the distal portion dissected from the surrounding tissue, allowing identification of the sural nerve branch close beyond the trifurcation at/in the popliteal fossa. The sural nerve was carefully freed from the surrounding tissue up to the Achilles tendon and placed in HEPES solution with added glucose. The sural nerve was desheathed in a petri dish with a dark flexible silicone base providing better contrast under the microscope view. The nerve was pinned and desheathed by carefully removing the perineurium using scissors and needles. The cleaned nerve was cut in segments varying from 10-12mm in length to fit the organ bath.
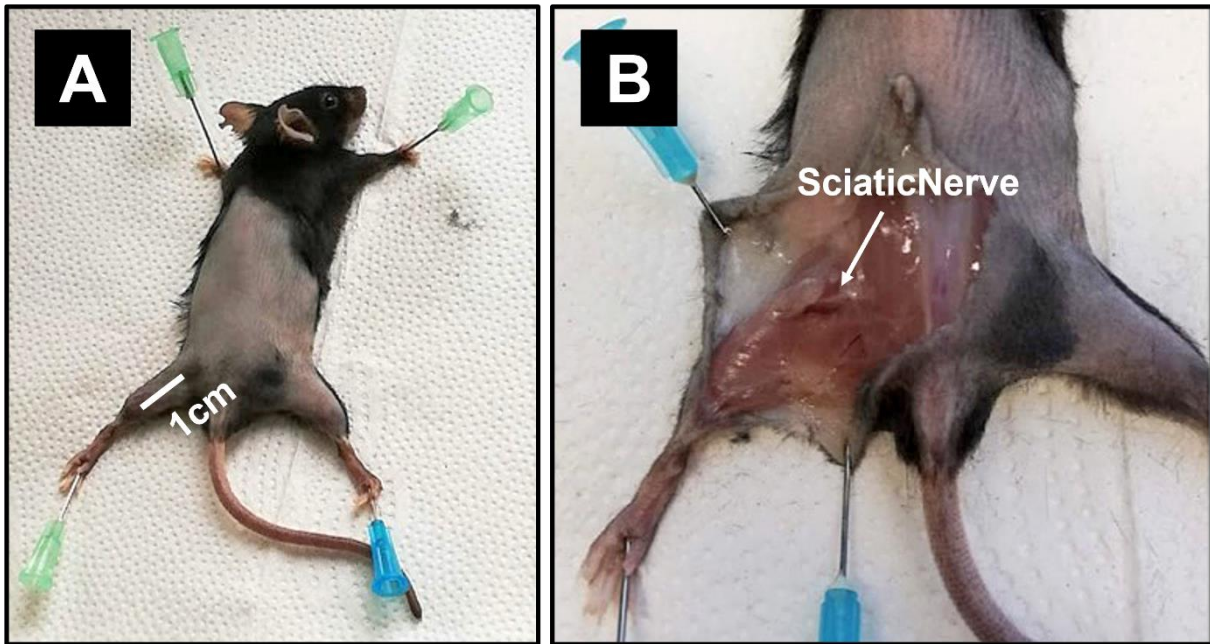
Figure 4: Mouse sural nerve preparation: Mice were positioned in ventral recumbency and fixed on a flexible structure by the paws. A 1 cm incision was performed on the proximal area of the hind limbs (**A**), the skin rebated caudally and the gluteus maximus was rebated to expose the sciatic nerve (**B**).

2.3.2 Pig Saphenous Nerve Preparation

A segment of pig saphenous nerve of approximately 3cm in length was collected from the contralateral leg from animals in which single nerve fibre recordings were performed. The nerve segment was collected under general anaesthesia and left overnight in HEPES buffer solution with glucose. The following morning, the nerve was fixed with needles to silicone-based petri dish and desheathed under the microscope. The epineurium was opened transversally, and nerve fascicles were isolated and desheathed in one movement by holding the perineurium and pulling out the nerve fascicle. The cleaned fascicles were cut into segments of 10-12mm in length and used for recording (Fig. 5).

2.3.3 Nerve Recordings

The desheathed nerves/fascicles were placed in a custom-made organ bath (volume ca. 1ml) perfused continuously with HEPES buffer solution. Nerves were drawn through a thin silicone layer inside glass pipettes on either side of the bath. The silicone layer serves as mechanical fixation and the sealing all around the nerves generated high electrical resistance. The glass pipettes were filled with HEPES buffer solution. The distance between the glass pipettes varied between 3-7mm, according to the nerve length. Electrical currents in a range of 0-50µA were delivered by a constant current electrical stimulator A395 (WPI, FL, USA) across the nerve via two silver wires, one placed inside the glass pipette and the other in the organ bath. A second pair of silver wires, one placed on the glass pipette and the other in the bath served as the recording electrodes (Fig. 5).
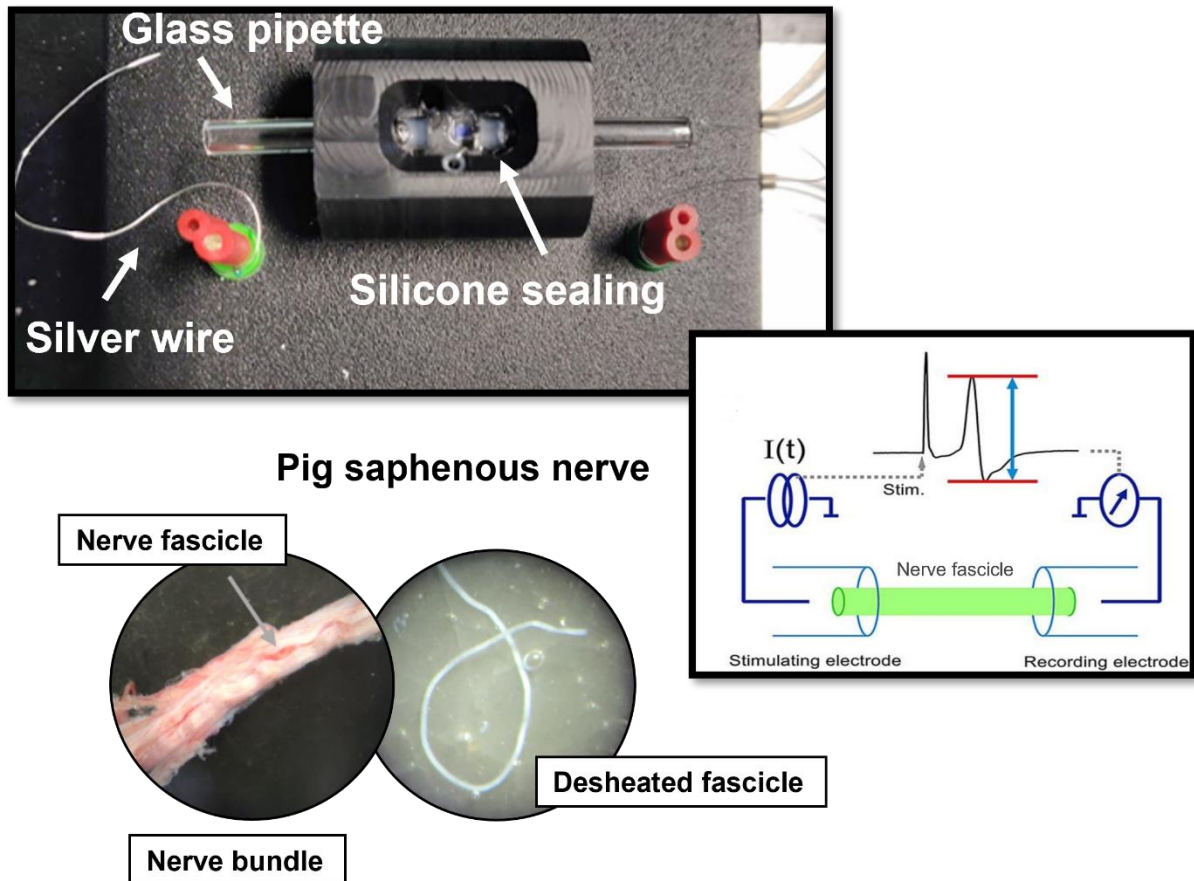
**Figure 5: Pig Saphenous nerve preparation and recording set up:** The epineurium was opened transversally, and the nerve fascicles were separated from the nerve bundle. The nerve fascicle was desheathed and the cleaned nerves were placed in a custom-made organ bath. Electrical currents were delivered via a silver wire placed on the outside silicone layer inside the glass pipette. A second silver wire placed on the contralateral glass pipette served as a recording electrode.

The HEPES buffer solution was continuously bubbled with oxygen and perfused into the organ bath in rates varying from 5-12ml*min^{-1} by a pump Watson-Marlow 502S (GEMINI, Germany). The temperature of the solution was adjusted using an inline Peltier, the current supply of which was provided by a constant current source (TDK Lambda, Germany). Bath temperature was measured by a thermistor in the organ bath (GHM Group, Germany). Using a differential amplifier NL905 (DIGITIMER, UK) the electrical signal was recorded over the sealing resistance at an amplification range varying from 2500-5000 times. A "Hum bug" (Quest Scientific, Germany) was used to filter noise frequencies (50-60Hz). The electrical stimulation and the compound action potential recordings were performed using QTRAC software (Institute of Neurology, UK). The program controls the relative timing of electrical stimuli and the acquisition of short "sweeps" of the extracellular signal and a signal proportional to temperature. The software can record the time intervals for pre-defined electrical stimulus paradigms in different channels. The recording of the different channels happens sequentially and in the same order. The number of channels recorded can be adjusted anytime by the user (select channel- "SC" function).

The induction of action potentials by electrical stimulation of the nerves resulted in a compound action potential (CAP). The amplitude of the extracellular CAP signal was tracked using QTRAC software. To delineate the C-fibre component of the CAP, a digital time window was defined manually by the user (Fig. 6) as well as the current intensity delivered by the test height command ("TH"). A list of QTRAC software

commands and corresponding functions used during the pig saphenous nerve and mouse sural nerve compound potential recordings is presented in **Table 2**.
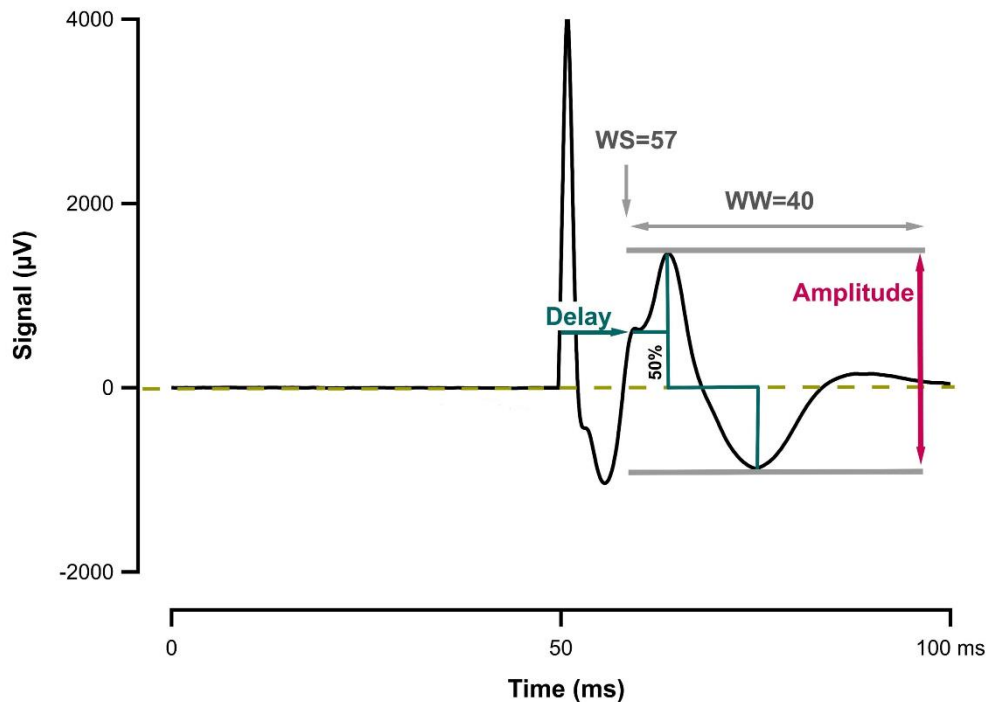
Figure 6: Recordings window: All CAPs were measured in the window set by the user with the commands Window width (WW) and Window start (WS). The signal amplitude was measured as the distance from peak to peak in µV. Latency was measured as the delay between start of the electrical stimulation at 50ms (peak stimulation artefact) and 50% of the up-rising positive peak response of stimulation.

The parameters recorded by QTRAC software for each pre-defined channel are the following:

- *Current intensity, T*: defined as the amount of current delivered at each stimulation in %, with 100% equal to 50µA. The input of the constant electrical stimulator varies from ±10V while the computer output has a limited range of ±5V, meaning that the computer can only deliver 50% of the current at each stimulation. Therefore, at a maximal 100µA current set at the stimulator, only 50µA will be delivered by the computer software.
- *Peak, P* (signal amplitude): defined as the distance from the negative to the positive peak of the signal in µV for a synchronized compound action potential in between the recording window.
- *Latency, L_R* (conduction delay): defined as the time between the start of the stimulus and a point located at 50% of the uprising CAP positive signal amplitude. The rectangular stimulus is known to evoke an action potential immediately after the initial depolarization, therefore the latency for this stimulus represents only the time needed to conduct the action potential from the stimulation to the recording site.
- *Latency, L_S*: defined as the time from the start of the sine wave stimulus to the time during the sine wave cycle when the 50% of the uprising CAP positive signal amplitude occurred.
- *Temperature, N*: defined as the temperature of the solution perfused into de organ bath measured at each time interval.

17

QTRAC Command	Function
"ML", "MH"	Pass filters for high ("MH") and low ("ML") frequencies
Test Height ("TH")	Stimulus intensity. The command "TH" is followed by the desired amount of current to be delivered (%), being the maximum TH100 = 50µA.
Select Channel ("SC")	Record the selected channels. The command "SC" is followed by the numbers of channels to be recorded separated by comma. E.g., SC1,4 records channels 1 and 4.
Display channel ("DC")	Displays the selected channels. The command "DC" is followed by the numbers of channels to be displayed on the recording screen separated by comma.
Stimulus Interval ("SI")	Define the stimulus interval between electrical stimulations. The command "SI" is followed by the number of seconds between each electrical stimulation.
"DA"	Adjust the selected axis automatically to fit the CAP occurrence.
Window Start ("WS")	Adjust the starting point of the window recording on the x-axis. The command "WS" follows the number of the channel to which the function is defined.
Window Width ("WW")	Adjust the size of the window recording on the x-axis. The command "WW" follows the number of the channel to which the function is defined.
Grabbing Traces ("GS")	Record the shape of the CAP.
Test Width ("TW")	Defines the duration of the electrical stimulus. The command "TW" follows the number of the channel to which the function is defined.
Test Start ("TS")	Defines the starting point of the stimulus on the x-axis. The command "TS" follows the number of the channel to which the function is defined.
Test Period ("TP")	Defines the period of the stimulus. The command "TS" follows the number of the channel to which the function is defined.
"SS"	Stop/Start the stimulation.
File save ("FS")	Saves the recording file.
File close ("FC")	Closes the recording file.

Table 2: QTRAC commands and its respective functions.

2.3.4 *Experimental protocols*

For the compound potential recordings two types of stimulus paradigm were applied: rectangular stimulation and sinusoidal 4Hz stimulation. Constant current rectangular stimuli were delivered in the different experiments at 0.1 or 1ms duration. The sinusoidal stimulus was delivered at 250ms duration. The compound action potential signals were filtered by an 800Hz low pass and by a 30-800Hz bypass bandwidth filter. The CAP generated by C-fibres (C-CAP) were differentiated from the CAP of A-fibres based on the conduction delay. Stimulus-response curves of C-fibres signals were done by increasing the stimulus intensity from 0 to 50µA for rectangular stimulation or until a maximum CAP amplitude was induced (approximately 20-30µA). Stimulus

response curves were constructed by plotting peak to peak CAP amplitude (µV) versus stimulus current (µA). The resulting data were fitted with Igor Pro 7.1 software package (Wavemetrics, Lake Oswego, USA) using a sigmoidal function of the form

$$f(x) = A + \frac{B}{1 + exp\left(\frac{xhalf - x}{rate}\right)}$$

where *A*= offset, *B*= maximum amplitude, and *x-half*, and *rate* values signify the half-maximal stimulus current (equivalent to EC50) and potency respectively.

Comparisons were made between these values at two different temperatures, 20 and 26°C, before and after the administration of VGSC toxins (Fig. 7). For some substances, the perfusion pump was stopped, and the peptides were added directly into the recording bath.
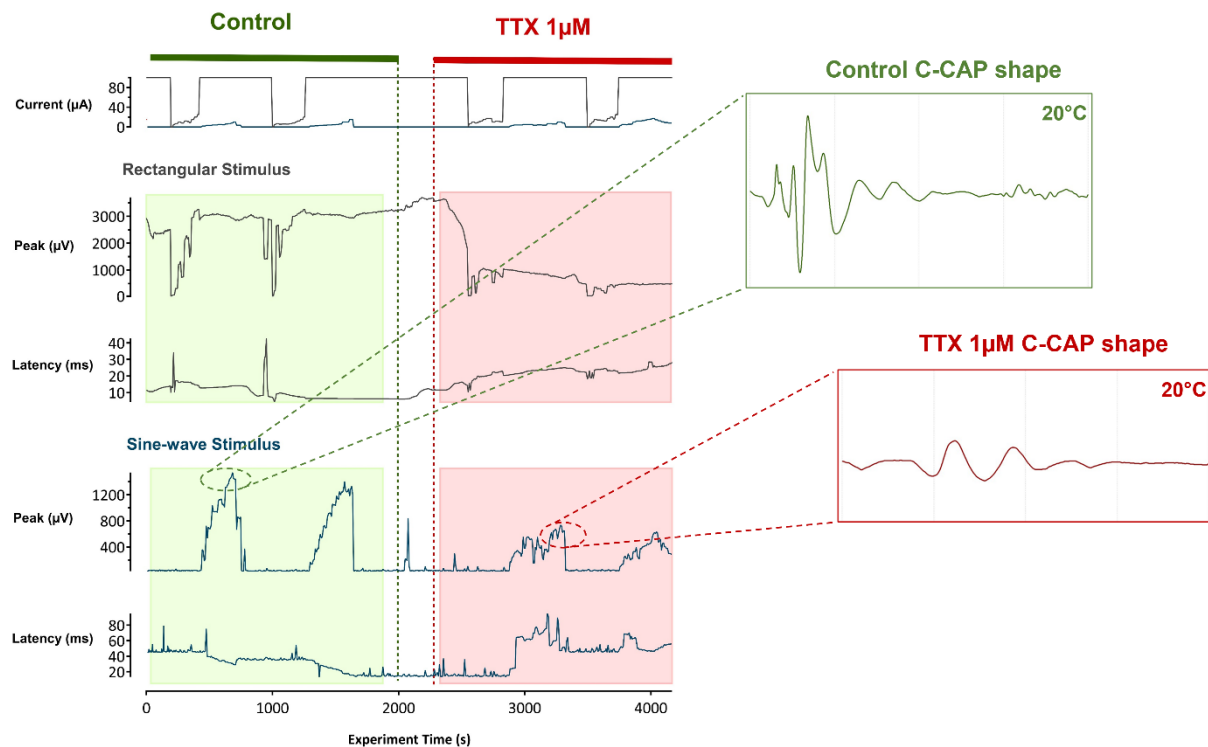
Figure 7: QTRAC recording overview: The peak (µV) and current (µA) obtained from QTRAC software provided triplicate values for the generation of stimulus-response curves for both, rectangular and sine wave stimuli. Latency (ms) QTRAC values were obtained for both stimulation profiles. The results of the recordings at 20°C were used to establish a comparison between the two electrical stimulus profiles.

The amplitude of the C-CAP induced by a supra-maximal 50µA rectangular stimulation was considered maximal, and thus its latency (L_R) to be the minimum conduction time of C-fibres from the stimulation to the recording site of the recording bath (conduction delay). The values of C-CAP latency (ms) in response to a sine wave stimulus (L_S) were used to estimate the time point during the sine wave cycle at which the CAP was initiated. To determine the exact time of initiation of the sine C-CAP, the minimum conduction delay to a maximum rectangular stimulation (L_R) was subtracted from the L_S and thereby arrives at a corrected initiation latency (corLs) (Fig. 8).
Latency values were then used to determine the amount of electrical charge (current integrated over time) delivered by both stimuli. Charge was calculated for rectangular pulses (q_R) as stimulus intensity multiplied by 1ms duration (Fig. 8A) and sine wave

stimulation charge (q_S) calculated based on the values of initiation latency (corLs) (Fig. 8B). The general form for determining the charge that applies during a sinusoidal current profile is given by:

$$q(t) = \int_0^{t_c} A.\sin(w.t)$$

Where q is the charge delivered from the beginning of the sine wave current profile up to the initiation of the action potentials t_c. In this case we substituted corLs values in for t to determine the charge delivered up to the point of CAP initiation; A is sine profile amplitude; and w equals 2*π*f, with f being the designating frequency.
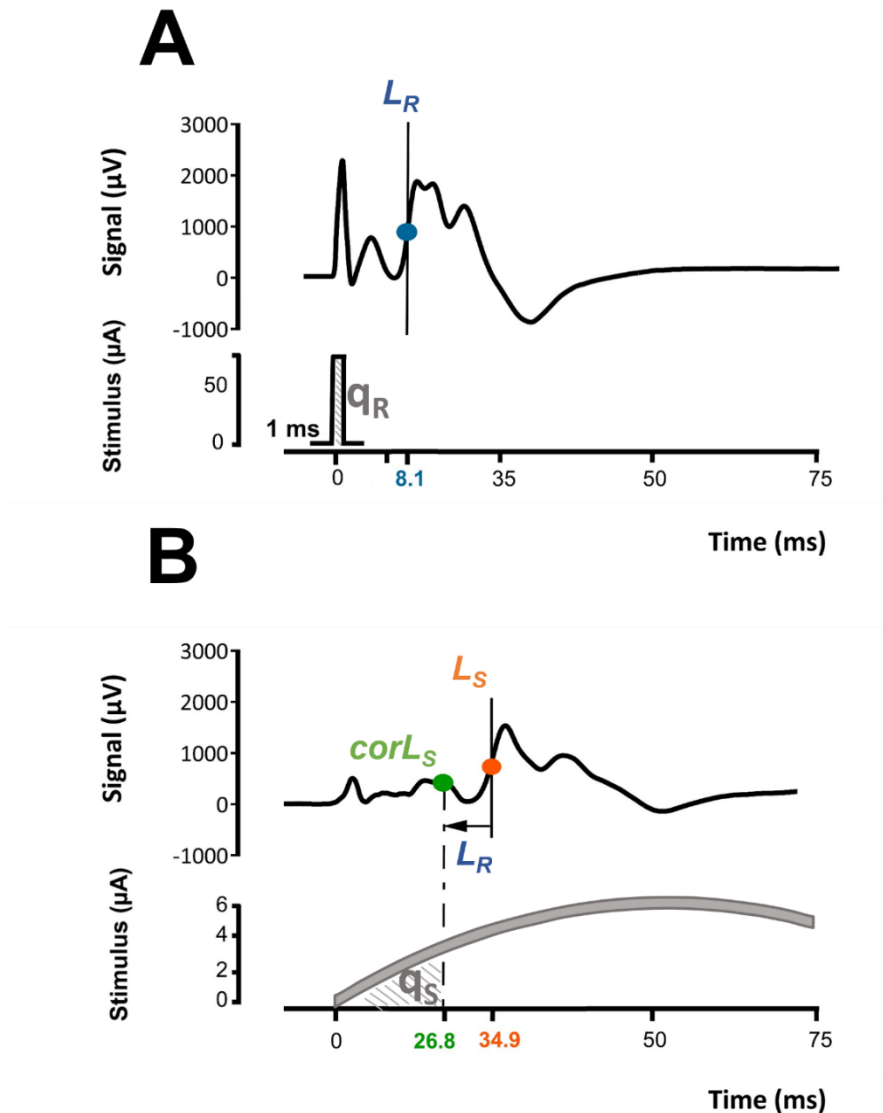
Figure 8: Latencies and charge: The C-CAP induced by a supra-maximal 50µA rectangular stimulation latency (L_R) is the conduction time of C-fibres from the stimulation to the recording site of the recording bath (conduction delay). Charge for rectangular stimulus (q_R) was calculated by the multiplication of stimulus duration and stimulus intensity (**A**). The latency of sinusoidal C-CAPs (L_S) was corrected by subtracting the conduction delay, providing the value of corrected latency (corLs) used for data comparison (e.g. between VGSC toxins). The value of corLs was used as the corrected time of stimulus duration to calculate charge for sine wave stimulation (q_S) (**B**).

The average conduction velocity of C-fibre axons was estimated by dividing the nerve segment length between stimulation and recording electrodes, by latency of the C-CAP to supra-maximal stimulation.

2.4 Extracellular single nerve fibre recordings "*in vivo*"

2.4.1 Anaesthesia and pig nerve preparation

Pigs were submitted to a fasting period of 6h prior to anaesthesia. A dose of 1mg/kg of Dormicum® (Midazolam, Roche, Switzerland) associated with 5mg/kg of Stresnil® (Azaperone, Jannsen Pharmaceutica, Belgium) was injected intramuscularly into the trapezius for premedication. After a sedation period of 10-15 minutes, the hair was removed from the medial portion of both hind legs and the ventral cervical area. An intravenous access was performed with a 22G infusion cannula (Vasofix, B. Braun, Germany) into the lateral ear vein and Propofol 1-1,5mg/kg (Fresenius, Germany) was administered for the induction of anaesthesia. The animals were intubated with an endotracheal tube number 6.5 (Rusch, Germany) using a 28mm blade laryngoscopy (HUM®, Germany). Volume-controlled mechanical ventilation adjusted at a tidal volume varying between 5-10ml/kg and a maximum airway pressure of $20cmH_2O$ was performed with a (Primus®, Dräger, Germany) in a mixture of compressed air and oxygen (O_2: 50-62%) adjusted to maintain normocapnia (end-tidal CO_2 concentration) at 40-45mmHg.[85,86] A central access into the jugular vein was placed for administration of Narcoren® (Pentobarbital-Natrium, Rhone Merieux, Germany) in a bolus of 15mg/kg followed by continuous intravenous anaesthesia (CRI) at a rate of 15-20mg/kg/h using a syringe pump TE311 (Terumo, Germany). Ringer Acetate (Deltajoin®, AlleMan Pharma, Germany) was also infused at an infusion rate of 3ml/kg/h. Animals were monitored during anaesthesia using an electrocardiogram (ECG) and temperature monitor Sirecust 404-1A (Siemens, Germany), an oxygen saturation (SPO_2) monitor (Henry Schein®, USA) and a non-invasive blood pressure (NIBP) controller (cuff neonate 6-11cm and C08A-VET, CONTEC, China). End tidal carbon dioxide $EtCO_2$ values were provided by the ventilator (Primus®, Dräger, Germany).
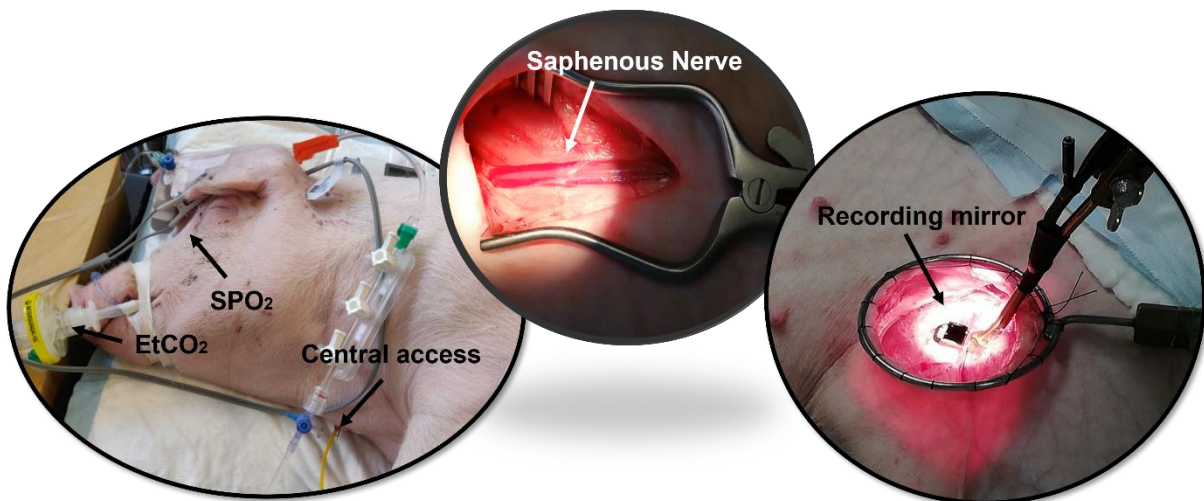
Figure 9: Anaesthesia and pig nerve preparation: Pigs were intubated and monitored during the whole anaesthesia for ECG, temperature, SPO_2, $EtCO_2$ and NIBP. The saphenous nerve was dissected from the connective tissue and placed into a grove of a recording mirror.

A rocuronium (Esmeron®, Organon International, The Netherlands) CRI was administered when further muscle relaxation was necessary in a bolus of 1mg/kg followed by a rate of 2mg/kg/h. The depth of anaesthesia was monitored by the heart rate and palpebral reflexes and the phenobarbital CRI adjusted accordingly. Body temperature was maintained during the whole anaesthesia above 36ºC and below

39.5°C (normal, 38–39.5°C)[85] with the help of a water mattress (Bronsom++, Germany) and a TP700 pump (Stryker Medical, USA).

Animals were positioned in a lateral recumbency and both hind limbs were fixed to expose and allow free access to the medial part of the hind limb used for recordings. After cleaning and disinfection, an incision of 7cm was made with an electrical cutter Radiotom 804 (Siemens, Germany) at the mid-tight and 6cm of the saphenous nerve completely dissected from the contiguous connective tissue and exposed. The subcutaneous tissue was rebated, and the skin flap was sutured in a metal ring to form a pool. The pool was filled with paraffin oil (ROTH, Germany) for electrical insulation and the saphenous nerve placed into a grove of the recording mirror positioned inside the paraffin pool (Fig. 9). Approximately 1cm of a fascicle was carefully separated from the Saphenous Nerve under a microscope (LEICA M320 Full HD, Germany), cut proximally and placed on top of the recording mirror for further desheathing and removal of the epi- and perineurium. After desheathing, fine strands suitable for a single unit recording were splatted from the nerve fascicle with an ultra-fine forceps (Moria MC40, Fine Science Tools FST, Heidelberg Germany) following the teased fibre technique.[34,87]

Euthanasia was performed at the end of every experiment with deepening the level of anaesthesia with an extra bolus of phenobarbital 30mg/kg followed by a dose of 1ml/kg of supersaturated potassium chloride solution (Sigma-Aldrich, Germany) administered intravenously in the jugular vein.

2.4.2 Nerve Recordings

The nerve filaments were put on a golden wire magnetically attached to the recording mirror, which was attached to a Low-Noise Voltage Preamplifier (Model 5113 Ametek Inc., USA). The receptive field of the afferent nerve fibres was localized upon scratching and squeezing slightly the hind limb skin, evoking a C-fibre characteristic discharge. Within this receptive field, 2 non-insulated microneurography electrodes (FHC Inc., USA) delivered electrical search stimuli to the skin with an intensity of 20mA, a pulse width of 0.5ms, and at 0.25Hz using a constant current stimulator (DS7A, DIGITIMER Ltd., UK). The electrodes were then inserted intradermally at a site where a single action potential was elicited and appear repeatedly in the recording window with a fixed time (time-locked action potential). The pre-amplified signals were amplified and filtered (bandwidth 100 to 3000 Hz, Model 3364, Krohn-Hite Corp., Brockton, USA) and audio monitored.

DAPSYS 8.0 software package was used to display and record action potentials in real-time and allowed for window discrimination and latency measurements. The discrimination of action potentials performed online during the recording could also be further refined offline using DAPSYS by manual deletion of signals other than the action potential of the unit under study. The time of the occurrence of action potentials stored by DAPSYS could also be compared offline with the trigger time of a certain stimulus allowing for direct correlation between them (Fig. 10).
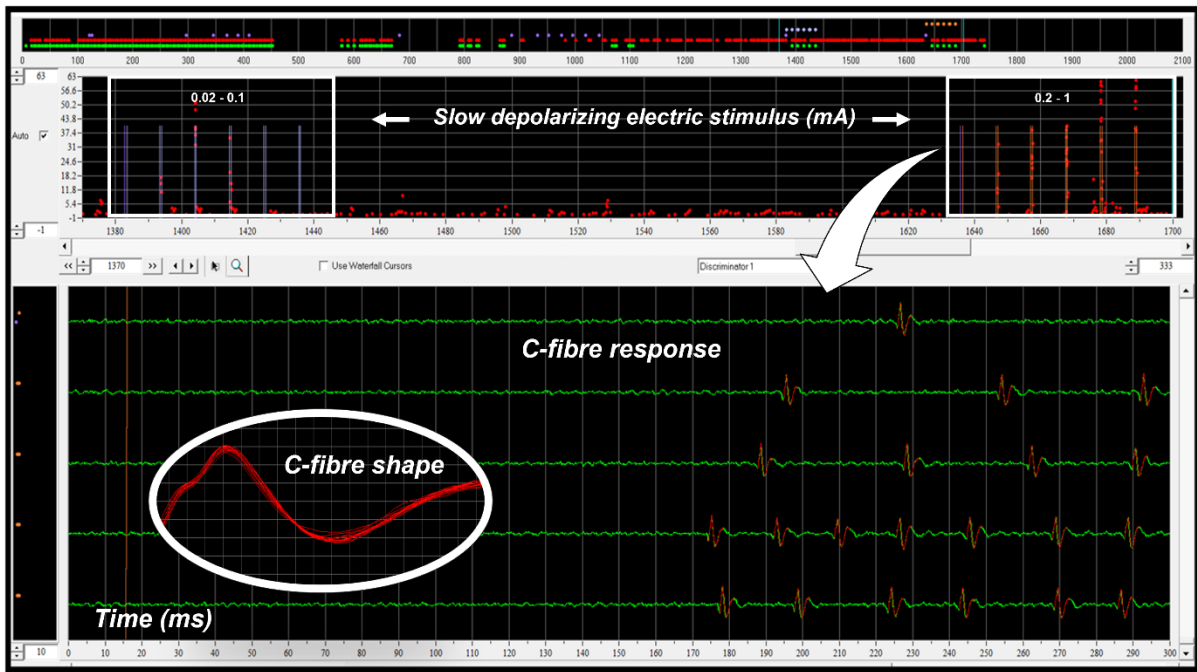
Figure 10: Dapsys recording window: Dapsys allows for displaying, recording, and storing the firing frequency of action potentials in response to different stimulus paradigms. The example shows 5 traces (bottom) of recorded action potentials (red, inlet particular shape) evoked in response to slow depolarizing half-sine wave stimuli (middle) of 0.2 – 1 mA intensity. The discrimination of action potentials is performed by manual deletion of non-shaped compatible signal responses.

2.4.3 Experimental Protocol

Once a time-locked action potential was discriminated, the stimulus threshold I_R was defined for a rectangular stimulus. A threshold was considered the minimum current intensity at which the nerve fibre responded consistently, and the stimulation intensity for monitoring the fibre was set at 2-fold the threshold at 0.5ms pulse duration. This ensured activation of the fibre despite possible small fluctuations in absolute threshold. The latency L_R was defined as the time (ms) between stimulus onset in the skin and the time at which the response at the recording electrode was observed. The shortest distance between the most distal recording electrode and the transcutaneous needles was measured and divided by the latency (recorded after a 2-min interval without stimulation) to estimate the resting conduction velocity (CV) in meters per second (m/s). Charge q_R was calculated as stimulus intensity (µA) times 1ms (duration of the rectangular stimulus) given in µC.

Electrical current profiles at 1Hz delivered as a half-sine wave of 500ms duration and at intensities ranging from 0.05-10mA were used together with sine wave stimulation of 250ms duration (4Hz) pulses at intensities ranging from 0.05 – 1.2mA and applied using a constant current stimulator (A395, WPI, US) and a pulse generator (NI USB-6221, National Instruments, USA), the latter controlled by DAPSYS 8.0. The stimulus was delivered via a pair of transcutaneous L-shaped blunted bipolar platinum-iridium electrodes, with a diameter of 0.4mm separated by 2mm (Cephalon, Netherlands) placed on the area of the receptive field (Fig. 11). For action potential recordings, single 1Hz half-sine wave pulses applied at incrementally increasing intensities were delivered at 10s intervals.

The threshold I_S (mA) for 1Hz half-sine wave stimulus was considered the minimum stimulus intensity to generate at least three action potentials per pulse. Conduction

delay (L_R) was the minimum time needed for an action potential to travel from the receptive field (where a suprathreshold rectangular pulse was delivered) to the recording electrode localized close to the dissected saphenous nerve. Latency (corL$_S$) (ms) was defined as the time of the 1st AP responding to a stimulus intensity in which at least 3 APs were evoked by the half-sine wave cycle, and it was corrected to the conduction delay.
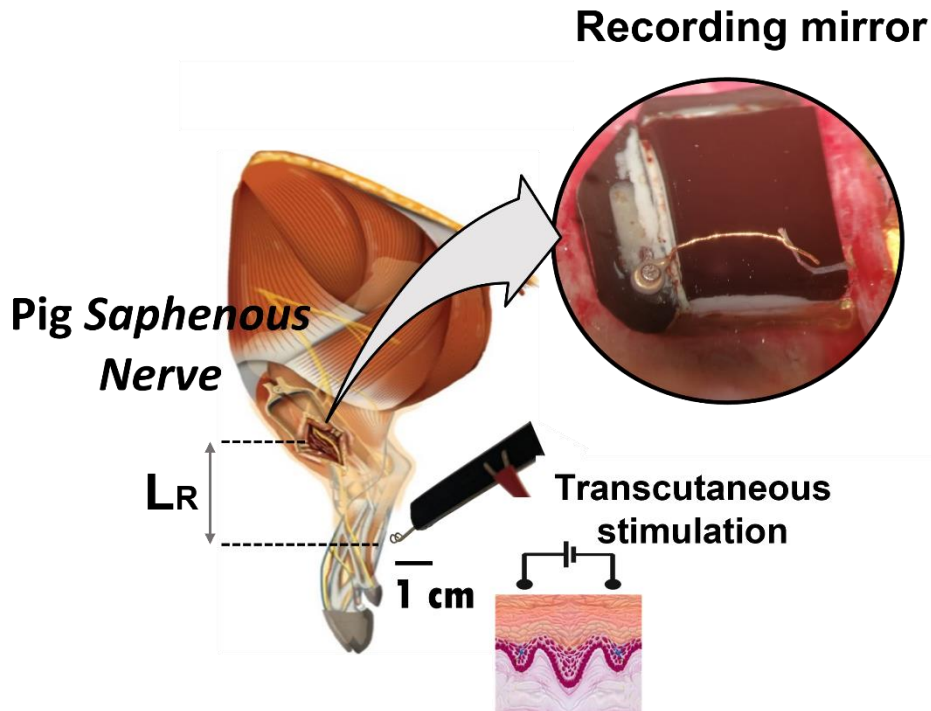
Figure 11: Nerve recordings: The nerve filaments were put on a golden wire, magnetically attached to the recording mirror. The receptive field of the afferent nerve fibres was localized, and 2 transcutaneous electrodes delivered electrical stimulus to the receptive field on the skin. L_R or conduction delay (dashed lines) stands for the minimum time the action potential required for travelling from the stimulation site in the skin to the recording electrode following a rectangular stimulus.

Charge q$_S$ for half-sine was considered the amount of accumulated charge needed to generate the first action potential for stimulus intensities that evoked at least 3 APs. The equation used to calculate charge for half-sine wave stimulation was:

$$q(t) = \int_0^{t_c} A.\sin(w.t)$$

Where q defines the charge of half-sine stimulus; t_c was replaced by the corrected latency for half-sine stimulus (corL$_S$) to determine the charge delivered up to the point of first action potential at threshold intensity; A the threshold current to generate at least three action potentials; *and* w equals 2π*f, with f the designating frequency of 1Hz.

The number of action potentials in response to half-sine wave stimulation was determined for each of the three stimulus intensity ranges: from (I) 0.02-0.1mA, (II) 0.2-1mA and from (III) 2-10mA. When a certain range of stimulus was not tested, a carry backwards and a carry forward technique were used to allocate the response of the recorded unit to the missing ranges. The carry backwards technique consisted of allocating a response value of zero to all intensities in the smaller non-tested ranges, when the unit did not respond to the lowest tested range. The carry forward technique

consisted of allocating a response values equivalent to the maximum number of action potentials in response to the intensities higher than the tested range.

A single 1Hz half-sine wave pulse induced (if current was sufficiently high) a burst of action potentials. The highest, second highest and third highest action potential peak frequencies (Hz) for the action potential burst during the half-sine wave stimulus were averaged and grouped according to the stimulus intensity ranges described above (0.02-0.1mA, 0.2-1mA and 2-10mA). The number and average peak frequency of action potentials evoked by 1Hz half-sine wave stimulation were compared between fibre types and within fibre types, before, and after, the intradermal injection into the receptive field of specific VGSC blockers.

Regarding to sine wave stimulation, 4Hz sinusoidal pulses were applied continuously for 1-minute and data analysed for the phase at which the first action potential occurred in response to the continuous 4Hz stimulus determined for each stimulus intensity (0.05, 0.1, 0.2, 0.4, 0.8 and 1.2mA). The median of the phase and the median of the charge (µC) were calculated across all stimulus intensities among the same fibre type. Charge for sine wave stimulus was calculated using the same formula above mentioned in the charge calculation for half-sine wave stimulus, being t_c the time from the beginning of the stimulation up to the time of the occurrence of the first action potential, also corrected to conduction delay. The number of action potentials in response to the 4Hz sine wave were binned into 60 segments of 1 second bins and corresponding numbers averaged for each stimulus intensity in all tested units of the same fibre type. The parameters analysed for sine wave stimulation at 4Hz were also compared between fibre type, and for the same fibre type before and after the intradermal administration of VGSC blockers.

2.4.4 Nerve Fibre classification

The single nerve fibres with a time-locked response and a clear discrimination from other afferents in DAPSYS, were classified either online or offline into Aβ- fibres, Aδ-nociceptors, sympathetic efferent fibres, low-threshold mechano-sensitive C-fibres ("touch" fibres, LT), high-threshold mechano-thermal-sensitive C-nociceptors ("polymodal" nociceptors, HT), very high-threshold mechano-thermal-sensitive C-nociceptors ("polymodal" nociceptors, VHT), mechano-insensitive nociceptors ("silent fibres", CMi) and cold nociceptors (CN).

The Aβ- fibres, Aδ-nociceptors were classified based on their low-latencies (±15-30ms) and high conduction velocities (>2m/s) but not included in the analyses of recordings. Sympathetic efferent fibres were also excluded from this study, and they were classified according to their activity dependant slowing (>10%) and the response to a twin-pulse electrical stimulus as described before.[88] The ADS pattern of sympathetic fibres is also clearly marked by a delayed onset and reversal of their conduction slowing during 2Hz stimulation.[89]

The different C-fibre classes were classified according to their responsiveness to mechanical, heat and electrical stimulation. The LT fibres are sensitive to light brush, can fire in response to 100Hz electrical stimulation and do not respond to heat stimuli. HT and VHT also respond to 100Hz electrical stimulation. HT and VHT can be differentiated based on their mechanical thresholds using a set of Semmes-Weinstein monofilaments (North Coast Medical Inc., CA, US) and their response to heat stimulation as previously described.[90] Cold nociceptors (CN) cannot be activated by mechanical stimuli, can follow 100Hz electrical stimulation, and they are activated by application of ice on the receptive field. The mechano-insensitive fibres (CMi) were classified based on their mechano-insensitivity and their intense slowing of conduction to 5Hz electrical stimulation.[27]

2.5   Data and statistical analysis

2.5.1   CAP recordings

Stimulus-response curve fitting, averaging, and filtering were performed in Igor Pro 7 (WaveMetrics, Lake Oswego, OR, US). Statistical analyses were performed in Prism 9.3.1. Bonferroni post-hoc tests were used in multifactorial repeated measures ANOVA and *p<0.05* indicated statistical significance. The comparison between control conditions and treatments were performed by two tailed t-test. Group data is presented as mean ± standard deviation (SD).

2.5.2   SNF recordings

Single fibre data were acquired and analysed using DAPSYS 8.0 software (DAPSYS; Brian Turnquist; see {"http://www.dapsys.net"}). Statistical analyses were performed in Prism 9.3.1. Bonferroni post-hoc tests were used in multifactorial repeated measures ANOVA and *p<0.05* was considered statistically significant. The comparison between control conditions and treatments were performed by two tailed t-test. Group data is presented as mean ± standard deviation (SD).

2.6   Summary of methods

Protocols were designed to determining activation of unmyelinated C-fibres by slow sinusoidal current and to examine the role of ion channels involved in the generation of action potentials during slow (low frequency) current stimulation.

- **Compound action potentials** of isolated nerve fascicles "*ex vivo*" (Pigs and Mice): The excitation pattern of unmyelinated afferents "*ex vivo*" is compared with identical stimulation protocols delivered "*in vivo*" and the role of subgroups of sodium channels are analysed after addition of the VGCS blockers TTX (leaving Nav1.8 and Nav1.9 conducting); XEN907 or ProTx II (Nav1.7 blockers); and μ-conotoxin PIIIa (Nav1.6 blocker) in the perfusion and recording bath.

- **Single nerve fibre recordings** "*in vivo*" (Pigs): The excitability parameters of classified C-nociceptors (LT, HT, VHT, CN and CMi) are determined on slow depolarization electrical stimulation protocols comprising a single 500ms half-sine wave pulse and 4Hz sine wave stimuli delivered for 1min. The modulation of stimulus-induced neuronal discharge is investigated by intradermal injection of 100μl of a specific VGSC blocker at a predefined concentration.

3 <u>RESULTS</u>

3.1 Compound action potentials (CAP)

Mainly pig saphenous nerve fascicles were used to record compound potentials, but some experiments were also performed in mouse sural nerve as previously mentioned. The working hypothesis was that TTX sensitive (TTX-S) voltage-dependent sodium (NaV) currents plays a crucial role in the response of C-fibres to slow depolarising sine wave stimuli. The CAP recordings were initially performed at two different temperatures (20 and 26°C) comparing the traditional rectangular stimulation to sine wave 4Hz stimulus before and after the addition of TTX 1µM. The maximum amplitude in µV; the current to generate a half-maximum C-fibre CAP in µA; the latency (conduction delay/L_R and corrected latency corL_S) in ms; the conduction velocity in m/s; and the charge in nC were used as parameters of nerve fibre excitability. Experiments using $Na_V1.7$ and $Na_V1.6$ blockers were performed to investigate the specific role of these VGSC in the electrically induced C-CAP excitability using the same stimulus parameters above mentioned. XEN907, ProTx II and ProTx III were used to block $Na_V1.7$ channels and µ- conotoxin PIIIA was used as $Na_V1.6$ blocker.

First of all, concentration-response curves (CRC) were performed at concentrations ranging from 1 pM-10µM for TTX, 0.1nM-200µM for XEN907, 0.1nM-10µM for ProTx II and 50nM-5µM for ProTx III. µ-conotoxin PIIIA was used at a concentration of 20µM based on the results of previously performed proof-of-concept experiments (data not shown). The C-CAP signals were analysed, and triplicates of maximum amplitudes (µV) were collected for each concentration tested. The curves were fitted with a sigmoidal fit and the x-half value considered as the concentration to inhibit 50% of the response (IC50). In total, 7 CRC were performed for TTX, 7 for XEN907, 11 for ProTx II and 5 for ProTx III. The IC50 values were averaged and presented in µM as mean ± SD (Table 3).

Toxin	VGSC	n	IC50 (µM)
TTX	TTX-S ($Na_V1.1$, 1.2, 1.3, 1.4, 1.6, 1.7)	7	0.12±0.12
XEN907	$Na_V1.7$	7	10.82±4.68
ProTx II	$Na_V1.7$	11	2.24±2.37
ProTx III	$Na_V1.7$	5	2.7±2.14

Table 3: IC50 values of VGSC blockers: The values were obtained by plotting triplicates of C-CAP maximum amplitude versus the concentrations of the toxins and fitting it into a sigmoidal fit. The IC50 was considered the concentration of the toxin to determine 50% reduction on maximum amplitude. The values are presented as mean ± SD.

All toxins, except XEN907, were applied to the bath during the nerve recordings in concentrations varying from 2 to 9-fold the IC50. XEN907 was applied at 10µM concentration diluted in di-methyl sulfoxide (DMSO). Aiming to exclude any effect of DMSO in the nerve fibre excitability, DMSO alone was tested before XEN907. A concentration of 0.25µL of DMSO was applied directly into the recording bath and left in contact with the nerve fascicle for a minimum of 3 minutes. Similar to all other recordings, triplicates of the maximum amplitude (µV) were collected before (2443.18±616.68) and after the addition of 0.25µL DMSO (2375.77±614.61). There was no effect of DMSO on C-CAP maximum amplitude for rectangular stimulation ("two-tailed paired t-test", n=9, *p=0.26*).

3.1.1 Influence of cooling on C-fibre activation

It is known that temperature modulates different factors of neuronal activity. Previous results obtained in mice indicated that cooling increases C-CAP maximum amplitude and less current is needed to generate neuronal responses to sine wave stimulation. This preliminary observation appears contradictory when considering the analgesic effects of cooling traditionally used to attenuate acute pain. On the other hand, if confirmed, this phenomenon could provide insights on cold allodynia, reported by chronic pain patients. To confirm the early experiments in mice, 25 fascicles of pig saphenous nerve were recorded, and excitability parameters compared before (26±1°C) and after cooling (20±1°C) the circulating buffer solution of the recording bath. The recordings were performed for both rectangular and sine wave stimulus paradigms.

3.1.1.1 Maximum amplitude (µV)

The effect of temperature on maximum amplitude (recorded voltage from peak to peak of C-CAP signal) was compared before (26°C) and after cooling (20°C) between rectangular and sine wave stimulus paradigms. The means ± SD of maximum C-CAP amplitudes induced by supra-maximal rectangular stimulation at 50µA were 1490±672.6 µV at 26°C and 1621±732.6 µV at 20°C (″two-tailed paired t-test″, n=25, *p=0.0001*) (Fig. 12A). The means ± SD of max. C-CAP amplitudes evoked by sine wave stimulation were 830.5±454.9 µV at 26°C and 1115±604.5 µV at 20°C *(p<0.0001)*. (Fig. 12B). Cooling increased the maximal C-CAP amplitudes for both rectangular and sine wave stimulus (Fig. 12C).
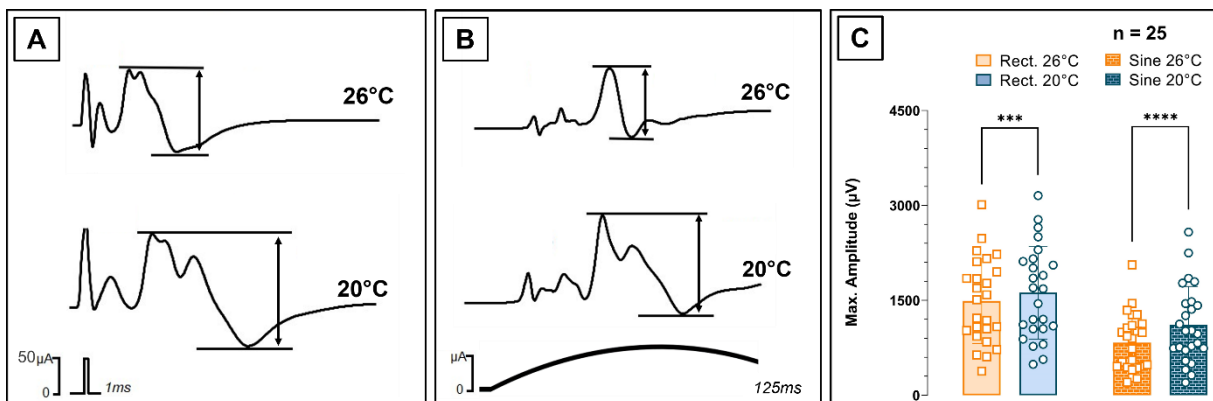
Figure 12: Cooling effect on maximum amplitude: Comparison of C-CAP signal evoked by rectangular stimulus at supra-maximal 50µA intensity (**A**) and by sine wave stimulus 4Hz (**B**) at tested temperatures (26°C and 20°C). The arrows point to the measurement of signal amplitude from the positive peak to the negative peak in µV. The pooled data of maximum C-CAP amplitude from both stimulus paradigms is presented as means ± SD (**C**) (″two-tailed paired t-test″, **** meaning p<0.0001 and *** *p=0.0001*). Cooling the recording bath from 26°C to 20°C increased maximum amplitude for both rectangular and sine wave stimulus.

3.1.1.2 Stimulus intensity (µA)

The stimulus intensity to generate a 50% maximal C-CAP amplitude was extracted from stimulus-response curves at 26°C and 20°C. The stimulus intensities tested varied from 0µA to the supra-maximal 50µA for rectangular and from 0µA to 30±5µA for sine wave stimulation. For each tested intensity, corresponding C-CAP amplitudes (µV) were collected in triplicates and normalized to the maximum C-CAP value of the corresponding fitted curve. Data points were fitted using a sigmoidal fit in IGOR Pro

7.1. The means ± SD of current intensities to generate a 50% C-CAP amplitude induced by a rectangular stimulus were 7.08±3.09 µA at 26°C and 7.50±3.04 µA at 20°C ("two-tailed paired t-test", n=24, *p=0.0086)* (fig. 13A). The means ± SD of current intensities to generate a half-maximum C-CAP amplitude evoked by sine wave stimulus were 3.72±1.67 µA at 26°C and 2.25±0.64 µA at 20°C (*p=0.0002*) (fig. 13B). The results indicate that cooling increased the current needed to generate a half-maximum C-CAP response for rectangular stimulation, but unexpectedly, the opposite was observed for the sine wave stimulus. The current needed to elicit a half-maximum C-CAP amplitude under sine wave stimulation decreased by cooling from 26°C to 20°C (Fig. 13C).
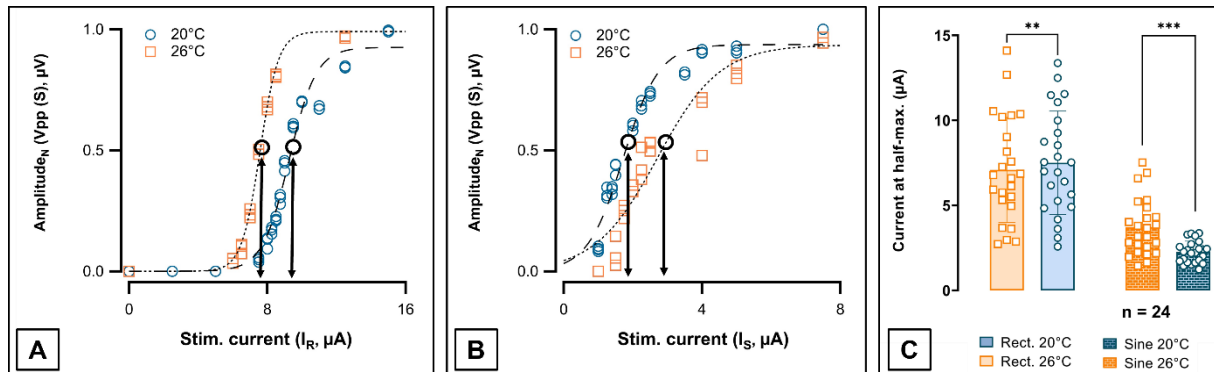
Figure 13: Cooling effect on excitability: Comparison of stimulus-response curves of C-CAP amplitude elicited by rectangular stimulus (**A**) and by sine wave stimulus (**B**) for two temperatures (26°C (depicted in orange) and 20°C (depicted in blue). The arrows point to the measurement of current intensity needed to generate a 50% C-CAP amplitude (µV) for both temperatures at rectangular (I_R, µA) and sine wave (I_S, µA) stimulus paradigms. C-CAP amplitudes were normalized to the maximum value of amplitude (100%, 1.0) for each curve. The pooled data of current intensity to generate a half-maximum response for both stimulus paradigms is presented as means ± SD (**C**) ("two-tailed paired t-test", ***p=0.0086* and ****p=0.0002*). Cooling the recording solution increased the required current to generate a half-maximum C-CAP response for rectangular stimulation but decreased it for sine wave stimulation.

3.1.1.3 Latency (ms)

The values of conduction delay (L_R) for rectangular pulses and corrected latency (corL_S) for sine wave stimuli were compared before (26°C) and after cooling (20°C) the recording bath solution. For rectangular pulses there is no relationship between stimulus intensity and conduction delay. As expected, the time to generate a compound potential remains similar for different stimulation intensities (Fig. 14A). Unsurprisingly, cooling clearly increases both L_R and corL_S. The means ± SD for conduction delay under rectangular stimulation were 8.44±1.31 ms at 26°C and 12.54±3.86 ms at 20°C ("two-tailed paired t-test", n=25, *p<0.0001)*. The means ± SD of corrected latency for sine wave stimulus were 31.18±5.64 ms at 26°C and 39.72±6.11 ms at 20°C (*p=0.0013*) (Fig. 14B). In contrast, latencies (L_S and corL_S) for sine wave increase with lower stimulus intensity (Fig. 14C). Moreover, this effect was more pronounced at lower temperatures as shown in the specimen (Fig. 14D). The very long latencies for action potential generation by sine wave stimuli at low stimulus intensities were intriguing and suggested that the cell membrane can accumulate charge for longer periods of time and that cooling can even facilitate such accumulation.
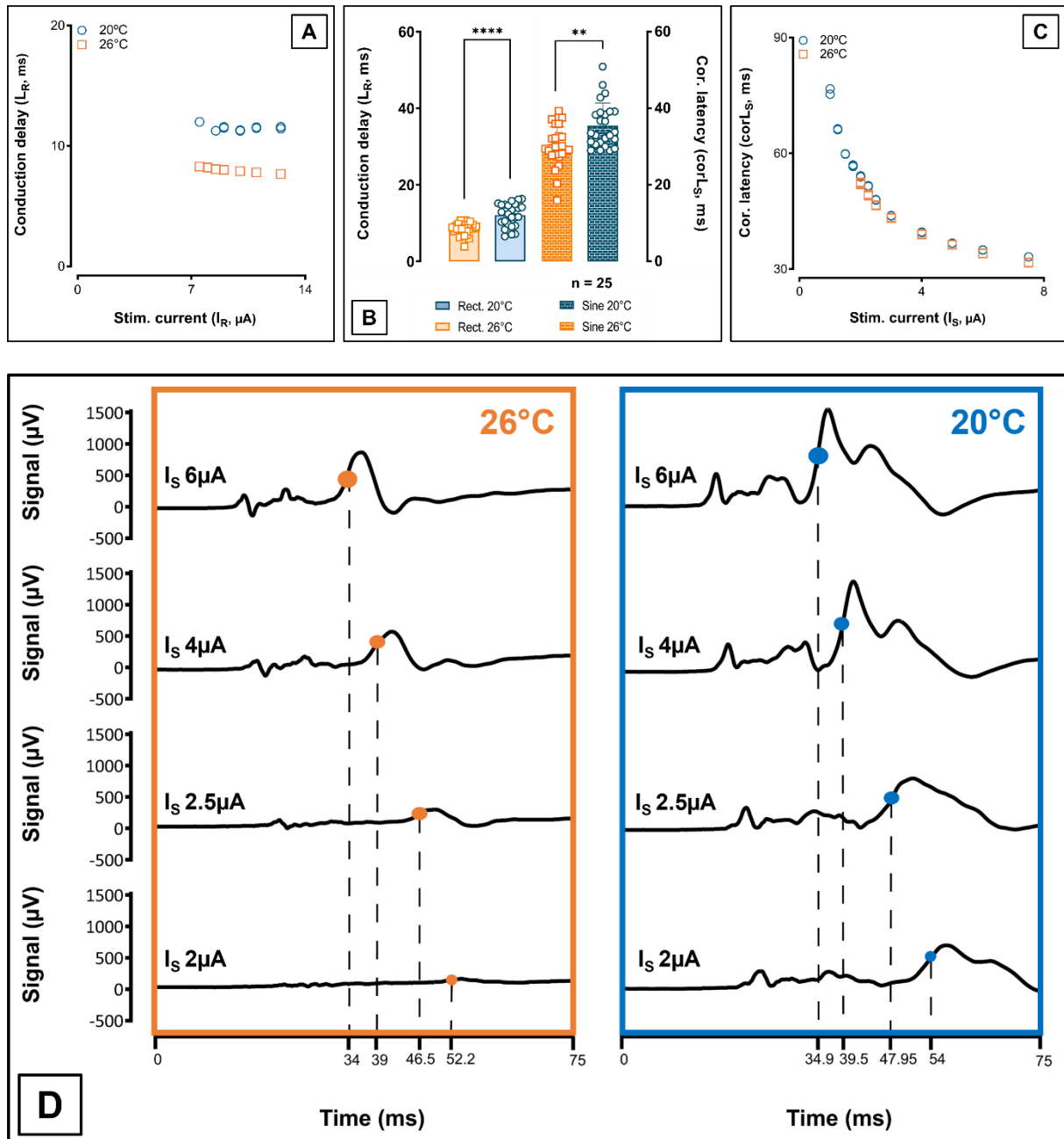
Figure 14: Cooling effect on latencies: For rectangular stimuli, conduction delay is independent of stimulus intensity (**A**) but there is a clear increase in conduction delay and corrected latency after cooling the recording bath from 26°C to 20°C. The pooled values of conduction delay and corrected latency are presented as means ± SD (**B**) ("two-tailed paired t-test", n=25, ****$p<0.0001$ and ** $p=0.0013$). For sine wave stimuli, corrected latencies increase for lower stimulus intensities (**C**). Two Specimen of C-CAP recordings evoked by rectangular (left panel) sine wave stimuli (right panel) at 6, 4, 2.5 and 2µA and 26°C (left orange) and 20°C (right blue) show that the increase of corrected latency at low stimulus intensity is more evident at 20°C than 26°C for sine wave stimulus (**D**).

3.1.1.4 Charge (nC)

The charge delivered by a rectangular stimulus (q_R) is calculated by stimulus duration times current intensity and equals stimulus intensity when the duration is 1ms. When plotting q_R versus C-CAP amplitudes and fitting it into sigmoidal fit, there was an evident increase in signal amplitude as charge increased (Fig. 15A). The charge required to evoke a half-maximum response by rectangular stimulus increased by cooling. The means ± SD of charge at 50% C-CAP were 7.08±3.0 nC at 26°C and

7.50±3.038 nC at 20°C ("two-tailed paired t-test", n=24, *p=0.0086).* In contrast, the half maximum charge did not significantly change by cooling when sinusoidal stimulation was used. The means ± SD of charge at 50% C-CAP were 41.95±14.61 nC at 26°C and 39.38±12.17 nC at 20°C for sine wave stimulus (Fig. 15B).

The charge delivered by sine wave stimulus was calculated by integration of the sinusoidal stimulus profile over time up to the time of C-CAP initiation (corrected latency). When plotting charge and C-CAP amplitudes for sine wave stimulus, there was no evident correlation between the two parameters (and thus, no sigmoidal fit possible as done for rectangular pulses in **Figure 15A**). The data suggested that a constant amount of charge is needed to evoke the compound potentials by slow depolarisation (Fig. 15C).
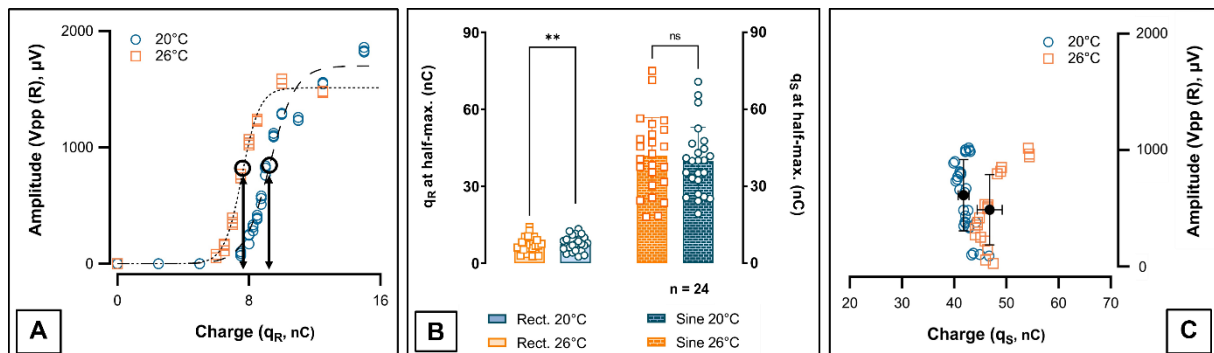
Figure 15: Cooling effect on charge vs. amplitude: The plot of charge versus maximum amplitude shows that cooling increased the amount of charge to elicit a half-max. C-CAP for rectangular stimuli (**A**). The arrows indicate the measurement of charge (q_R, nC) needed to generate a 50% C-CAP amplitude (μV) for the rectangular stimulus. Pooled data is presented as mean ± SD and shows that the increase in charge observed for rectangular is not observed for sine wave stimulus (**B**) ("two-tailed paired t-test", n=24, **p=0.0086, ns= p>0.05*). There is no effect of cooling on the amount of charge required to elicit a sine wave 50% C-CAP (**C**). Besides the lack of effect of cooling, the results suggested that a constant amount of charge is needed to induce a 50% C-CAP for sine wave stimulus.

3.1.2 Role of TTX-S currents on sine wave evoked C-CAP

To investigate the hypothesis that TTX sensitive (TTX-S) currents play a crucial role in the response of C-fibres to ramp currents, 9 experiments were performed to analyse the excitability parameters of pig saphenous nerve fascicles. The maximum amplitude in μV, stimulus intensity in μA, latencies (conduction delay and corrected latency) in ms, charge in nC and conduction velocity in m/s were used as excitability parameters. The excitability parameters were extracted in triplicates and compared between rectangular and sine wave stimulus at 20±2°C, before and after the addition of 1μM TTX to the recording bath. The temperature of 20±2°C was used based on the previous results (see 3.1.1.1 – 3.1.1.4) that indicate a more prominent compound potential at this temperature range allowing for a better signal to establish a comparison before and after TTX.

3.1.2.1 Maximum amplitude (μV)

The blockade of TTX-S currents reduced maximal C-CAP amplitude and increased the stimulation intensity to induce a half-maximum response. These effects are reflected in a downward and leftward shift of the stimulus-response curves for both, rectangular (Fig. 16A) and sine wave stimuli (Fig. 16B). The means ± SD of maximal C-CAP amplitude evoked by supra-maximal 50μA rectangular stimuli were 1414±622.5 μV before TTX and 319.3±186.8 μV after TTX ("two-tailed paired t-test", n=9, *p=0.0001).*

The means of maximal C-CAP amplitude evoked by sine wave stimuli were 1023±602 µV before TTX and 208±154.5 µV after TTX *(p=0.0015)* (Fig. 16C)*.*
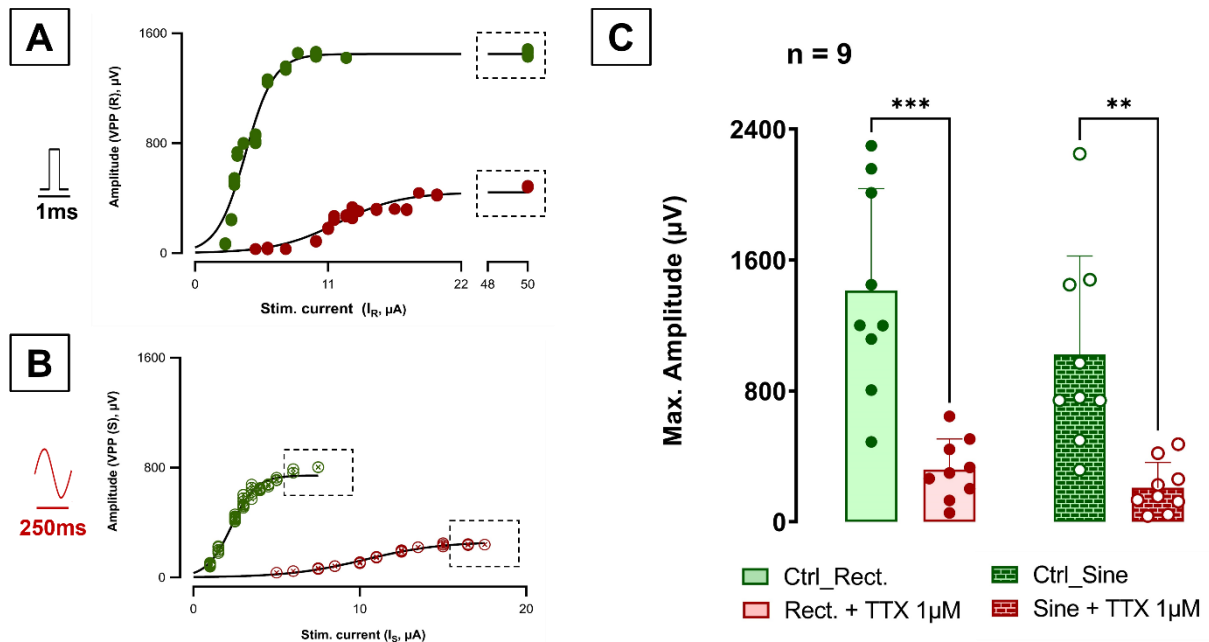
Figure 16: TTX effect on max. amplitude: The stimulus-response curves were generated for each recorded fascicle of pig saphenous nerve. The maximum C-CAP amplitudes were obtained at supra-maximal stimulus intensity for both rectangular (**A**, dashed square) and sine wave stimulus (**B**, dashed lines) before and after the addition of TTX 1µM into the recording bath. The pooled data shows a reduction of maximum C-CAP amplitudes after TTX (**C**). The maximum amplitudes are presented as mean ± SD (″two-tailed paired t-test″, n=9, ****p=0.0001 and* ***p=0.0015*).
.

3.1.2.2 Stimulus Intensity (µA) and charge (nC)

The blockade of TTX-S currents increased the current to generate a half-maximum C-CAP for both sine wave and rectangular stimulation (Fig. 17A).
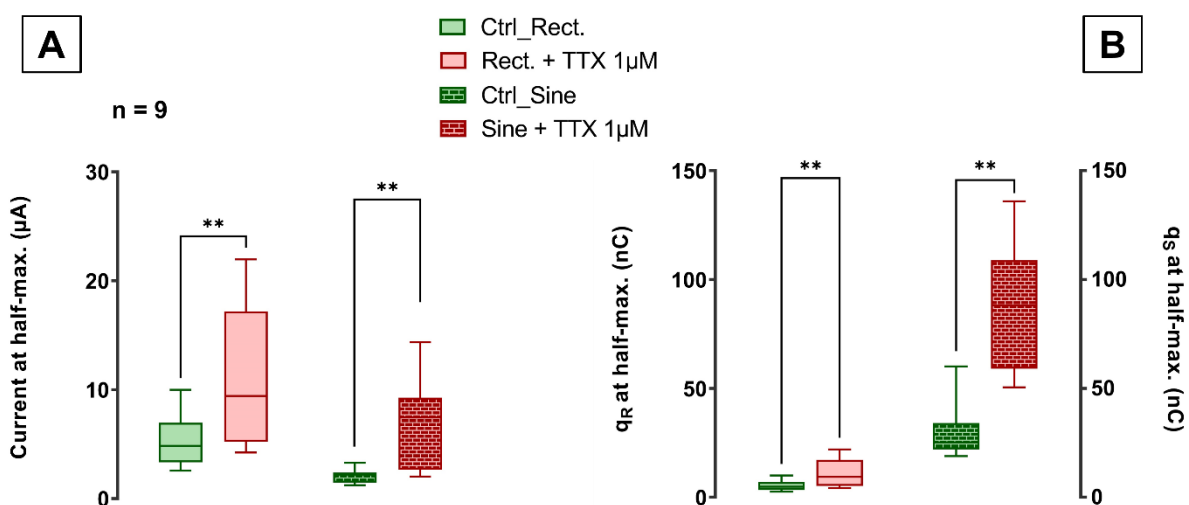
Figure 17: TTX effect on current (µA) and charge (nC): The blockade of TTX-S currents (depicted in red) increased the current (**A**) and the amount of charge (**B**) to generate a half-maximum C-CAP for both sine wave and rectangular stimulation. The values of stimulus intensity and charge are presented as mean ± SD (″two-tailed paired t-test″, n=9, *p<0.01*).

The means ± SD of rectangular constant current to evoke 50% C-CAP response were 5.28±2.37 mA before and 11.12±6.36 mA after TTX ("two-tailed paired t-test", n=9, *p=0.0037*). The means ± SD of sinusoidal constant currents to evoke half-maximal peak-peak C-CAP amplitude was 2.08±0.63 mA before and 6.65±4.12 mA after TTX (*p=0.0080*). The amount of charge at half-maximum response also increased for both stimulus paradigms (Fig. 17B). The means ± SD of rectangular q_R at half-maximum amplitude were 5.28±2.37 nC before and 11.12±6.36 nC after TTX ("two-tailed paired t-test", n=9, *p=0.0037*). The sinusoidal q_S to evoke half-maximal C-CAP amplitude were 29.65±15.13 nC before and 87.43±30.36 nC after TTX (n=6, *p=0.0014*).

3.1.2.3 Latencies (ms) and conduction velocity (m/s)

Similar to the cooling effect (see **Figure 14A**), TTX increased the conduction delay and the stimulus intensity required to induce C-CAPs for rectangular stimuli and the conduction delay was independent of stimulus intensity for rectangular stimuli (Fig. 18A). For sinusoidal stimulation, a similar increase of corrected latency at low stimulus intensities was found (Fig. 18B) as already shown for cooling (see **Figure 14C**). However, current intensities required to induce C-CAPs increased after TTX contrasting the lower thresholds after cooling. Notably, even after TTX very long latencies were observed in response to low stimulus intensities indicating that TTX-S currents nevertheless are not necessary to induced C-fibre compound potentials.
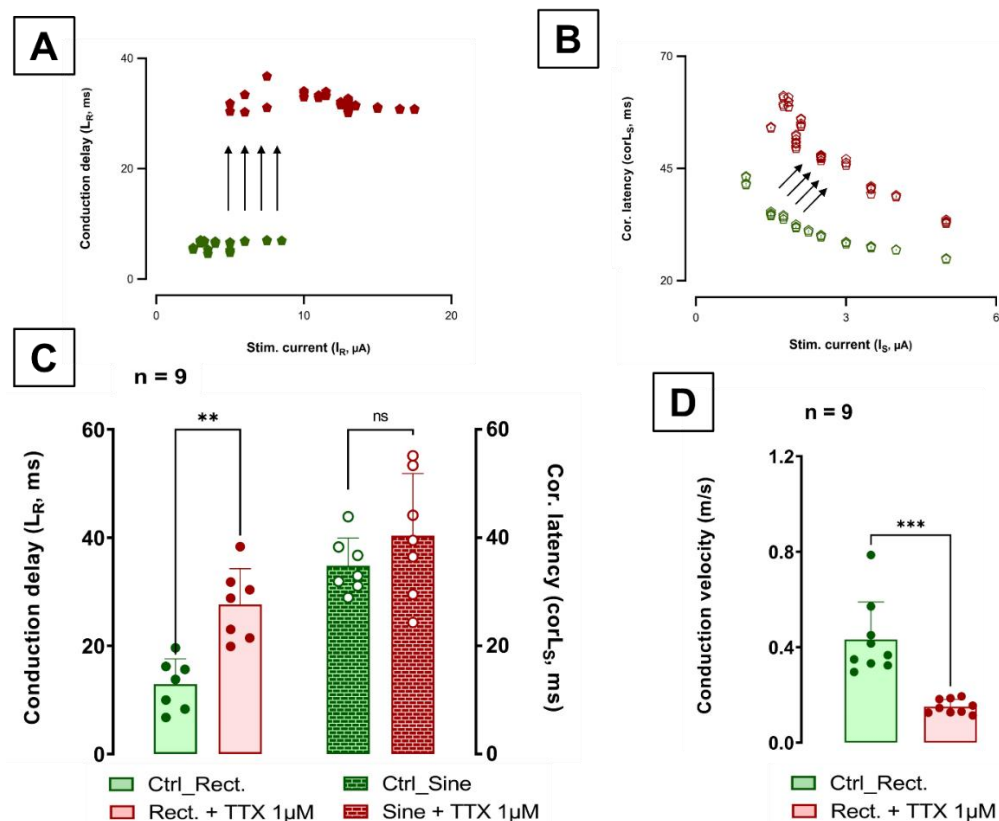
Figure 18: TTX 1µM slows C-CAP: Conduction delay is plotted versus stimulus intensity for rectangular (**A**) and sine wave stimuli (**B**). Conduction delay is increased for both stimulation profiles (arrows). Cumulative data indicate that TTX increased conduction delay significantly for rectangular stimulation, but the increase of corrected latency for sinusoidal stimulation is not significant (**C**). The TTX slowing effect is also observed by the reduction in rectangular stimulus evoked C-CAP conduction velocity (**D**). The values of conduction delay, corrected latency and conduction velocity are presented as mean ± SD ("two-tailed paired t-test", **p=0.0049, ***p=0.0009, ns= p>0.05).

TTX clearly increased conduction delay for rectangular stimulus from 12.91±4.69 ms to 27.67±6.59 ms ("two-tailed paired t-test", n=9, *p=0.0049*), but not the for sine wave stimulus. Beyond the expected increase in latency (L$_S$) after blocking TTX-S currents (data not shown) there was no additional slowing of action potential generation by the sinusoidal stimulus as measured by the corrected latency (Fig. 18C). The means of corrected latency for sine wave stimulus were 34.82±5.14 ms before and 40.36±11.5 ms after TTX.

The slowing effect of TTX on the C-CAP responses to rectangular stimulus is reflected by a massive reduction in conduction velocity (Fig. 18D). The means of conduction velocity were 0.43±0.16 m/s before and 0.15±0.03 m/s after TTX ("two-tailed paired t-test", n=9, *p=0.0009*).

Based on the effects observed after TTX-S currents blockade in nerve fibre excitability, i.e. reducing maximum amplitude and conduction velocity, increasing current and charge to generate a half-maximum C-CAP; the experiments proceeded by blocking Na$_V$1.7 and Na$_V$1.6 separately. The idea was to observe if the TTX-S effect in C-fibres excitability could be attributed to one VGSC or the other.

3.1.3 Na$_V$1.6 and Na$_V$1.7 blockade

3.1.3.1 XEN907

XEN907 is a synthetic pentacyclic spirooxindole and it was selected to be used as a Na$_V$1.7 inhibitor based on its specificity, low molecular weight (351.1Da) and a high potency "*in vitro*".[80] Initial experiments were preformed using XEN907 at 10µM based on the mean ± SD of IC50 values obtained from pig saphenous nerve.

The addition of XEN907 to the recording bath only partially reflected the results obtained with TTX 1µM. In agreement with previous results obtained for TTX, XEN907 at 10µM showed a significant reduction of maximum C-CAP amplitude (Fig. 19A) for both, pig and mice nerve recordings and for both, rectangular and sine wave stimuli ("two-tailed paired t-test", pig n=10, mice n=7, *p<0.05*). An increase in stimulation current (Fig. 19B) and in charge (Fig. 19C) for both rectangular and sine wave stimulation at half-maximum C-CAP after XEN907, as observed after TTX blockade (see **Figure 17**), was recorded only in pig experiments (mice data not shown). XEN907 reduced conduction velocity (Fig. 19D), similar to TTX, yet observed again only for pig recordings (mice not shown). Differently to TTX results, there was no significant increase in conduction delay for rectangular stimulus (see Figure18C) when comparing to both pig and mouse. Moreover, the results showed a significant decrease in corrected latency for sine wave stimulus in both mouse and pig nerve recordings (Fig. 19E). The excitability parameters are presented as means ± SD in **Table 4** and organised by species and stimulus paradigm.

The comparison of XEN907 to TTX results abovementioned, especially regarding conduction delay and corrected latency, were the motivation to perform further compound recordings in mouse sural nerve. As experiments were initially performed only in pig saphenous nerve, the CAP recordings were repeated in mouse sural nerve, not only to exclude any species specificity of XEN907, but also to rule out the possibility that diffusion barriers might prevent XEN907 from reaching its binding site. The results comparing mouse and pig recordings (shown partially in **Figures 19A** and **E**) were similar between the two species and therefore excluded the hypothesis that XEN907 had no effect on pig saphenous nerve or that the results were affected by diffusion barriers. A few more experiments were repeated increasing the concentrations of

XEN907 up to 100µM, to exclude that the differences observed in relation to TTX were due to the use of a sub-optimal concentration. Even at 100µM concentration the reduction on C-CAP maximum amplitude evoked by supra-maximal 50µA rectangular stimulus was only 50% (Fig. 19F) compared to the 80% reduction of TTX 1µM on maximum amplitude.

The obtained XEN907 results raised two hypotheses: 1. The blockade of $Na_v1.7$ by XEN907 was effective and $Na_v1.7$ does not facilitate action potential initiation by slow sine wave stimulus. 2. XEN907 is not an ideal inhibitor for $Na_v1.7$, the blockade was only partial and/or not selective to $Na_v1.7$.

To rule out the second hypotheses, the experiments were repeated using Protoxin II (ProTx II) and Protoxin III (ProTx III), two other specific $Na_v1.7$ blockers. In addition, µ-conotoxin PIIIA was added to the protocol to block $Na_v1.6$ in order to observe the effect of $Na_v1.6$ on C-CAP excitability. IC50 values of ProTx II (2.7±2.14µM) and III (2.24±2.37µM) for the pig saphenous nerve preparation did not differ significantly. The overall results obtained from the blockade of $Na_v1.7$ using ProTx III were very similar to the results obtained with tetrodotoxin and thus could not provide us with additional information (results not shown). Two assumptions raised from3 these observations: either all the effect observed in the blockade of TTX-sensitive currents can be attributed to $Na_v1.7$, and the ProTx III is the most specific peptide to block $Na_v1.7$; or ProTx III is not selective to $Na_v1.7$ and other VGSC channels were also blocked (like for TTX) as already suggested for $Na_v1.6$ and $Na_v1.3$.[82] Further tests using ProTx III seemed obsolete and the use of ProTx III was discontinued.
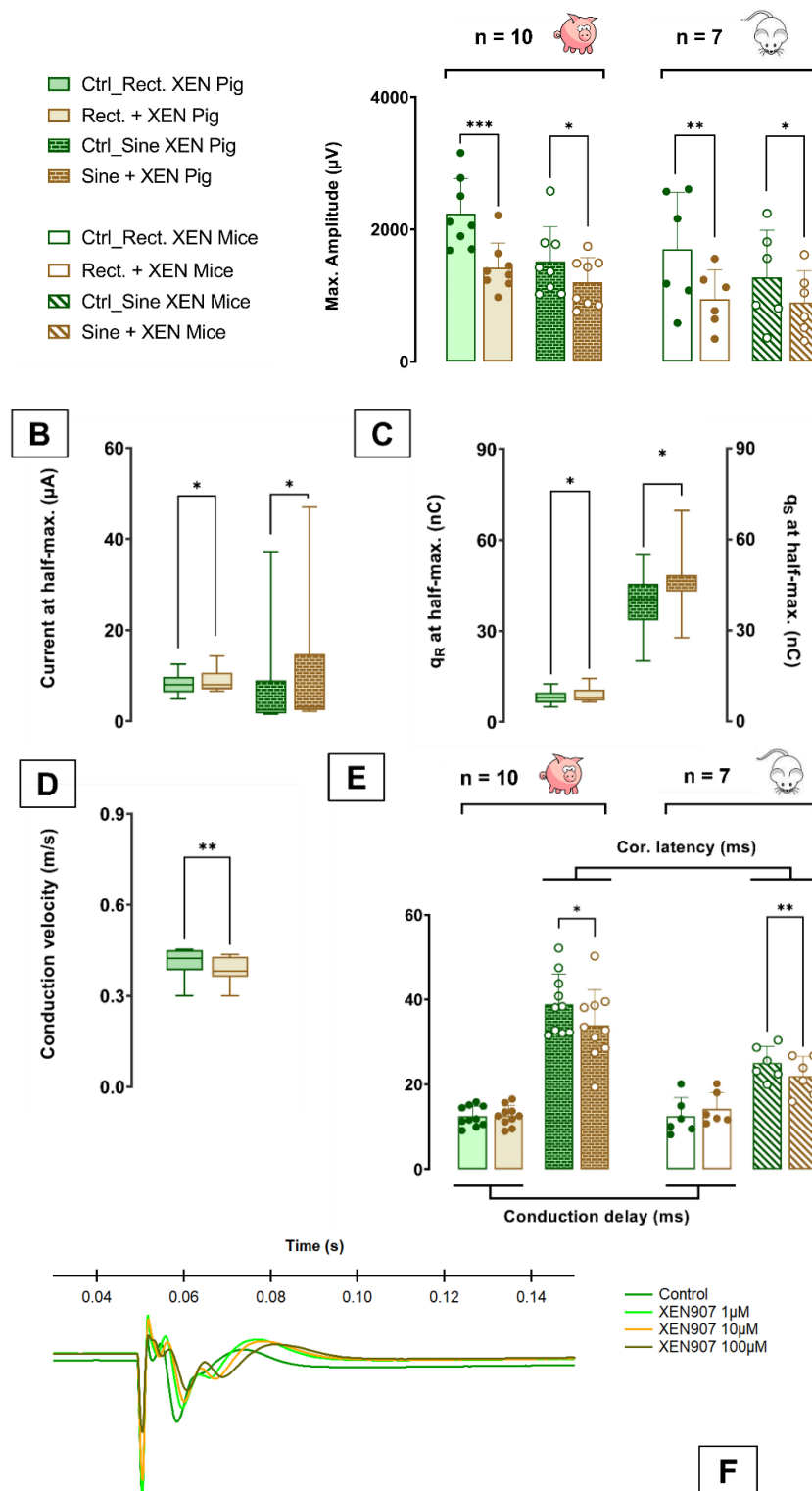
Figure 19: Effect of XEN907 on pig and mice nerve excitability parameters: XEN907 reduced maximal amplitude for rectangular (″two-tailed paired t-test″, pig n=10, *p=0.0004* and mice n=7, *p=0.0091)* and sine wave stimulus in pig (*p=0.0496*) and mice recordings (*p=0.0124)* (**A**). In pig saphenous fascicles there was a significant effect in increasing stimulation current (**B**) and charge (**C**) at half-maximum C-CAP (*p<0.05*) and in reducing conduction velocity (p=0.0022) (**D**). The contradictory effect of XEN907 in reducing corrected latency for sine wave stimulus was observed in both, pigs and mice nerves. There was no significant effect of XEN907 in increasing conduction delay for rectangular stimulus in both species (**E**). The blockade of 100µM XEN907 did not reduce maximal amplitude for rectangular stimulus on pig C-CAP signal as much as TTX blockade did (**F**). Data is presented as means ± SD (″two-tailed paired t-test″, *p<0.05*).

		Rectangular stimulus		Sine wave stimulus	
		Control	XEN907	Control	XEN907
Pig	Max. Amp.	2235.31±495.48	1419.64±349.81***	1511.61±493.58	1199.11±352.22*
	Current	8.19±2.29	9.04±2.34*	2.22±0.56	3.85±2.22*
	Charge	8.19±2.29	9.04±2.34*	39.41±9.98	46.46±10.9*
	CV	0.41±0.05	0.38±0.04**	-	-
	Cond. delay	12.46±2.29	12.60±2.29	-	-
	Cor. latency	-	-	38.94±6.78	33.92±7.94*
Mice	Max. Amp.	1695.15±785.44	944.26±402.87**	1271.47±650.29	890.24±439.38*
	Current	4.14±0.48	4.26±0.72	2.61±1.21	3.1±2.14
	Charge	4.14±0.48	4.26±0.72	21.28±3.72	18.67±6.78
	CV	0.39±0.13	0.31±0.08	-	-
	Cond. delay	12.44±4.03	14.24±3.47	-	-
	Cor. latency	-	-	25.03±3.62	21.98±4.59

Table 4: Effect of XEN907 on pig and mice nerve excitability parameters to rectangular and sine wave stimulation: Data is presented for both rectangular and sine wave stimulus as mean ± SD ("two-tailed paired t-test", * $p<0.05$, ** $p<0.01$ and *** $p<0.001$). Note that charge for a 1ms rectangular stimulus is identical to current.

3.1.3.2 Protoxin II and µ-conotoxin PIIIA

The blockade of TTX-S channels caused an increase in conduction delay that was not reproduced by the results of XEN907 in pig saphenous nerve, as mentioned before. To confirm XEN907 results, the blockade of $Na_V1.7$ was repeated using ProTx II, a $Na_V1.7$ blocker with high selectivity. ProTx II is a gate modifier and interacts mainly with binding site 4 of the channel domain II. The toxin causes a positive shift on the threshold of $Na_V1.7$ activation and subsequently blockade of the channel.[43] The blockade of $Na_V1.6$ was implemented by adding µ-conotoxin PIIIA (CTX) at 20µM concentration to the experimental protocol. The µ-conotoxin is a pore blocker that acts on binding site 1 of the VGSC.[77] The A-fibres compound (A-CAP) is highly dependent on $Na_V1.6$ currents and therefore blockade of A-CAP served as positive control for the effect of µ-conotoxin PIIIA (Fig. 20A, top panel).
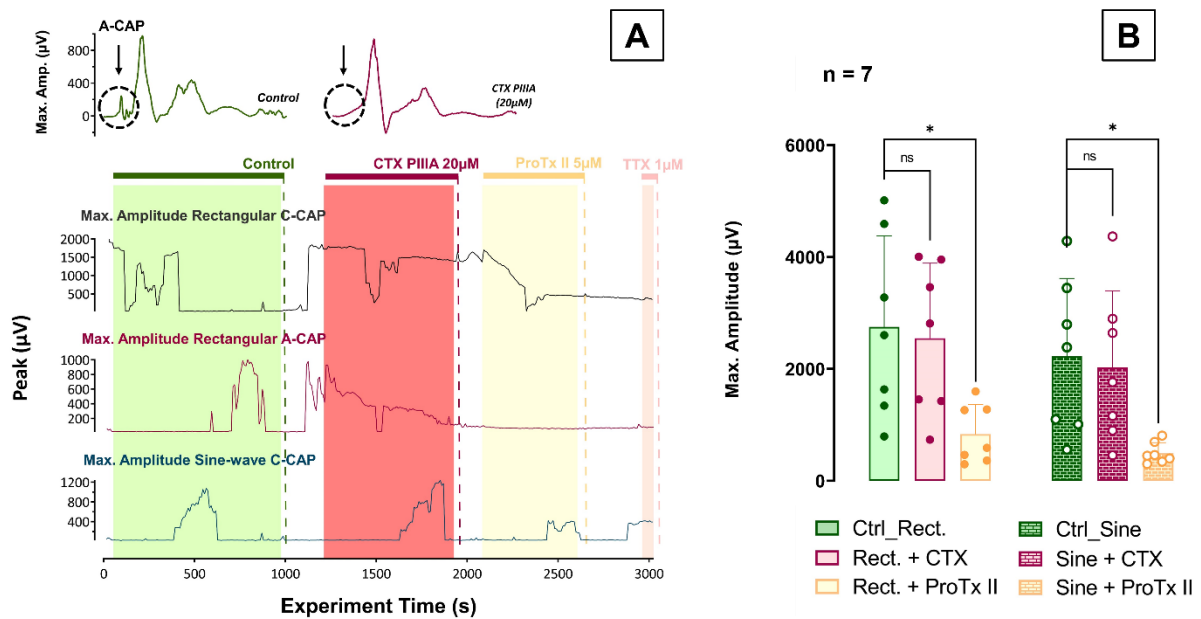
Figure 20: Effects of NaV1.6 and 1.7 blockers on A- and C-CAP: Effects of Na$_V$1.6 blocker μ-conotoxin PIIIA at 20μM and Na$_V$1.7 blocker Pro-Toxin II at 5μM are shown. TTX at 1μM was used at the end of the protocol as positive control. Specimen for the blockade of Na$_V$1.6 abolishing the A-CAP but leaving C-CAP amplitude unchanged (**A**, top panel). Time course of peak CAP levels are shown for rectangular and sine wave stimulation (**A**, bottom panel). Note, that TTX 1μM did not further reduce sine wave induced C-CAP amplitude. Cumulative data depicting that ProTx II (**B**) reduces C-CAP maximal amplitude for both rectangular (left) and sine wave (right) stimuli. The data is presented as means ± SD ("two-tailed paired t-test", *p=0.01).

A rectangular stimulation with 0.1ms duration was applied to evoke A-CAP in pig fascicles. 20μM μ-conotoxin PIIIA was added to the recording bath and left in contact with the nerve for 10-30 minutes. Only when the A-CAP signal was completely or mostly inhibited, ProTx II at 5μM was added to the recording bath for about 3-5 minutes. Tetrodotoxin at 1μM was used as positive control at the end of each experiment. There was no perfusion (wash-out) of the recording bath in between toxins (Fig. 20A, bottom panel). Stimulus- response curves were generated before and after the addition of each VGSC blocker at 20±1°C.

The blockade of Na$_V$1.6 abolished the A-Fibre signal but did not affect C-CAP maximum amplitude (Fig. 20A, top panel). The means ± SD of maximal C-CAP amplitude evoked by supra-maximal 50μA rectangular stimuli were 2751.95±1506.12 μV before and 2550.91±1239.28 μV after μ-conotoxin. The means ± SD of sine wave induced maximum amplitudes were 2226.27±1289.27 μV before and 2027.38±1264.21 μV after μ-conotoxin ("two-tailed paired t-test", n=7, p>0.05). ProTx II reduced the C-CAP amplitude for both rectangular and sine wave stimulation (Fig. 20B). The average of maximal C-CAP amplitude evoked by rectangular stimuli was 836.02±488.42 μV (*p=0.01*) and 494.26±174.15 μV (*p=0.0154*) for sine wave after ProTx II. The subsequent blockade by TTX did not further reduce the maximal amplitude of the sine wave C-CAP, therefore one may assume that the decrease in maximal amplitude by ProTx II is mainly related to the blockade of Na$_V$1.7 currents.

When looking into the latencies of C-CAP traces, the blockade of Na$_V$1.6 did not alter conduction delay for rectangular stimuli or corrected latency for sinusoidal stimulation. ProTx II reduced conduction delay (Fig. 21A) but did not consistently increase corrected latency (Fig. 21B). The values of conduction delay were 20.47±2.40 ms before, 18.69±2.78 ms after μ-conotoxin and 34.98±19.44 ms after ProTx II. The

values of corrected latency were 31.89±5.61 ms before, 32.18±5.63 ms after μ-conotoxin and 42.12± 9.30 ms after ProTx II ("two-tailed paired t-test", *p>0.05*).

The results obtained were very similar to previous results with TTX and the increase in corrected latency for the sinusoidal stimulation did not reach a statistically significant level. The exponential increase of corrected latency at low stimulus intensities seen for sine wave stimulation (see **Figure 18B**) was conserved in ProTx II experiments (data not shown). To further investigate the effect of Na$_V$1.7 blockade in the corrected latency, the exponential function generated by plotting corrected latency versus stimulus intensity was converted into a linear function by plotting latency against the reciprocal of stimulus intensity. This approach facilitates comparisons, in particular for conditions with different stimulus intensities. Moreover, it allowed to check for excitability changes occurring specifically at low or high stimulus intensities. Since Na$_V$1.7 can hypothetically act as an amplifier for weak depolarization, one might expect blockade of Na$_V$1.7 to be particularly effective for such stimuli. Accordingly, at low stimulus intensities, the blockade Na$_V$1.7 should increase the time needed to initiate an action potential under slow depolarizing sine wave stimuli (Fig. 21C). Thus, one would expect that Na$_V$1.7 block increases the latency for weak sinusoidal stimulation that is on right side of the reciprocal axis in **Figure 21C** and thereby the linear fit should be steeper. However, no significant difference between the slope of the linear fit before and after the addition of μ-conotoxin and ProTx II was found. The slope values were 41.21±19.37 before, 46.09±15.48 after μ-conotoxin and 52.67±23.15 after ProTx II ("two-tailed paired t-test", *p>0.05*). In contrast, there was a significant increase on the intercept values after the addition of ProTx II ("two-tailed paired t-test", n=6, *p=0.0415*) when comparing with the linear functions before and after μ-conotoxin (Fig. 21D). The values of intercept were 15.24±4.61 before, 14.54±3.83 after μ-conotoxin and 22.54±6.46 after ProTx II. The intercept reflects the minimum delay for supra-threshold intensities. Our results therefore suggest that Na$_V$1.7 accelerates the initiation of action potentials for sinusoidal stimulation at higher stimulus intensities.

There was no effect of μ-conotoxin on stimulus intensity, charge, or conduction velocity, when comparing with the control condition (Table 5). ProTx II increased the amount of current and charge to generate a half-maximum C-CAP for rectangular ("two-tailed paired t-test", n=7, *p=0.0487*), but not for sine wave stimulus (*p=0.8904*). In contrast to the XEN907 and TTX results, half-maximum current was not increased by ProTx II for sine wave stimulus (see **Figure 19B** and **C**) yet charge at half-maximum amplitude appeared increased albeit with high variability (*p=0.074*). In agreement with XEN907 and TTX results, ProTx II reduced conduction velocity of pig saphenous nerve (*p=0.0129*). The conduction velocity, stimulus intensity and charge at 50% C-CAP for rectangular and sine wave stimulation are presented as mean ± SD (Table 5).
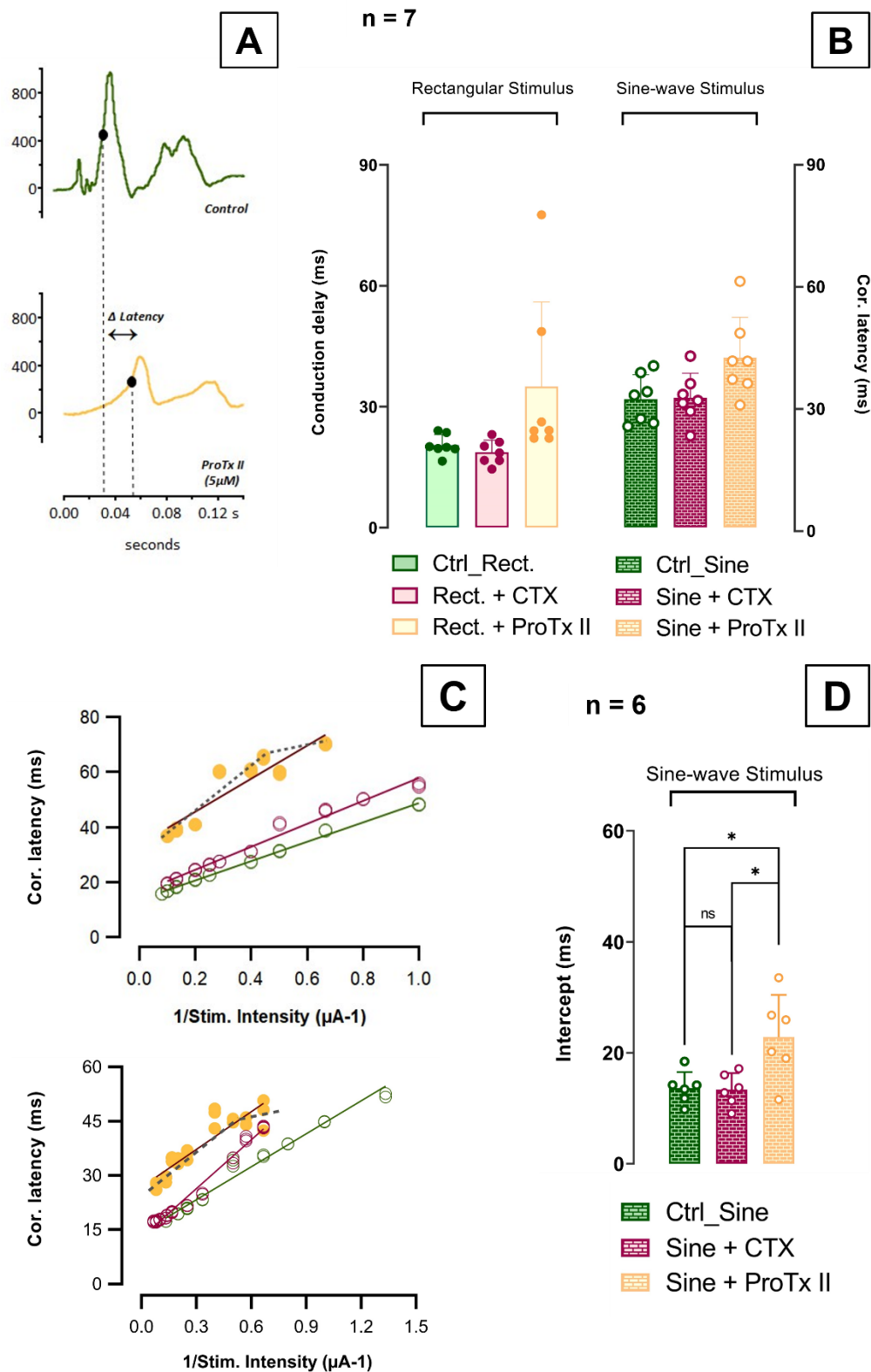
Figure 21: Effect of CTX and ProTx II on pig saphenous nerve latencies: The blockade of $Na_V1.6$ (CTX) did not affect either conduction delay (LR) or corrected latency (corLs), but the C-CAP signal dislocate to the right after ProTx II as seen in the specimen of a C compound (**A**). Even though, no overall effect in increasing conduction delay and corrected latency was observed by the blockade of $Na_V1.7$ (ProTx II) (**B**). There was a tendency of increasing corrected latency at lowest stimulus intensities (high reciprocal values) after $Na_V1.7$ blockade (yellow), but this was only present for some but not all C-fibre compound potentials recorded (**C**). The intercept was consistently higher after the addition of ProTx II at 5 µM to the recording bath (**D**). The values of conduction delay, corrected latency and intercept are presented as mean ± SD ("two-tailed paired t-test", *p<0.05*).

Pig Saphenous Nerve				
		Control	μ-conotoxin PIIIA	ProTx II
Rectangular	Current	5.28±2.54	5.24±1.49	7.80±1.95*
	Charge	5.28±2.54	5.24±1.49	7.80±1.95*
	CV	0.28±0.04	0.28±0.06	0.18±0.06*
Sine wave	Current	2.81±0.86	3.1±0.20	2.89±1.32
	Charge	32.90±10.91	34.87±6.30	55.49±23.65

Table 5: **Excitability parameters before and after μ-conotoxin and ProTx II:** Conduction velocity, the amount of current and charge to generate a 50% C-CAP are listed for both rectangular and sine wave electrical stimulus and compared to the values obtained after the addition of 20μM μ-conotoxin and 5 μM ProTx II to the recording chamber. Excitability parameters are presented as mean ± SD ("two-tailed paired t-test", *$p<0.05$).
.

The disparity of the TTX, XEN907 and ProTx II results might be linked to the differences in their specificity of VGSC blockade or could be related to limitations of our approach to analyse excitability parameters. Supposing that the main function of $Na_V1.7$ is amplifying weak depolarisations and thereby facilitating action potential initiation, the basic parameters of latency, stimulus intensity and charge at half-maximal response might not be optimal. Instead, analysis of these parameters at threshold, when a small but clear C-CAP signal was first recorded, might be more sensitive to detect effects of specific $Na_V1.7$ blockers and are depicted in **Figure 22**.
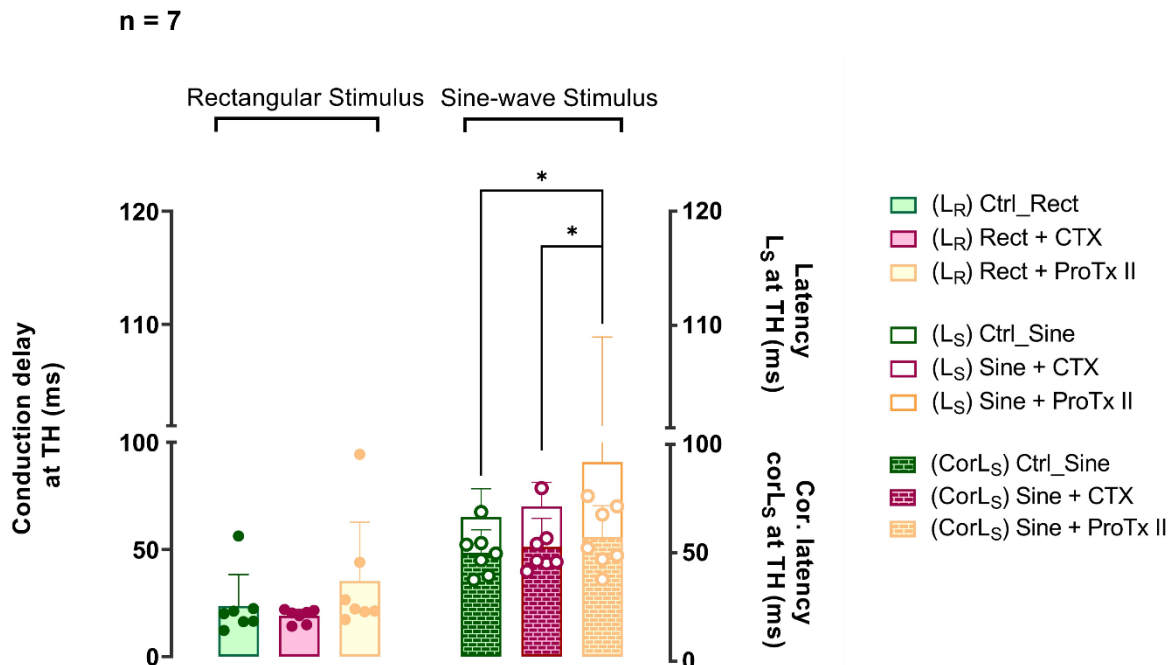
Figure 22: Effect of ProTx II on pig saphenous nerve latencies at threshold: The blockade of $Na_V1.6$ by μ-conotoxin and $Na_V1.7$ by ProTx II did not affect conduction delay for rectangular stimulus (L_R) at threshold. ProTx II increased latency for sine wave stimulus (Ls) at threshold stimulus intensity comparing to control condition and after the addition of μ-conotoxin to the recording bath. When correcting the latency values for sine wave stimuli to L_R conduction delay, no significant change was induced by μ-conotoxin and ProTx II. Data is presented as means ± SD (asterisks indicate *$p<0.05$* for Ls; "two-tailed paired t-test").

As observed at half-maximum response, when looking into the conduction delay at threshold intensity for C-CAP response to rectangular stimuli, there was no significant difference before and after the addition of µ-conotoxin. ProTx II increased conduction delay for rectangular stimulation, but this effect was not statistically significant. The means ± SD of conduction delay were 23.48±14.82 ms before, 18.87±3.15 ms after µ-conotoxin and 35.14±27.51 ms after ProTx II ("two-tailed paired t-test", n=7, *p>0.05*). The latency of the C-CAP initiated by sinusoidal stimulation increased following ProTx II compared to control condition and the C-CAP after µ-conotoxin (*p=0.0267*). The means of latency ± SD for sine wave were 65.20±13.20 ms before, 70.02±11.33 ms after µ-conotoxin and 90.81±18.07 ms after ProTx II. However, when corrected to conduction delay, no statistically significant differences were found. The means of corrected latency ± SD for sine wave were 48.40±10.67 ms before, 51.13±13.24 ms after µ-conotoxin and 55.71±14.62 ms after ProTx II (Fig. 22) ("two-tailed paired t-test", n=7, *p>0.05*).

Based on the results obtained it is possible to assume that the blockade of $Na_V1.6$ and $Na_V1.7$ does not increase the time to initiate an electrically evoked response to the sine wave stimulus (at both threshold and 50% half max intensities). When the TTX-S VGSC were blocked by TTX, there was an increase in conduction delay that, however, could not be reproduced as a significant augment by blocking $Na_V1.6$ and $Na_V1.7$ separately. It is not possible to exclude that other TTX-S channels were blocked by TTX and contributed to the increase in conduction delay observed initially, for instance $Na_V1.3$.

Therefore, an attempt to block $Na_V1.3$ was made during the compound action potential recordings using ICA121431, but the substance showed problems with solubility. ICA121431 was partially diluted in DMSO, but the substance precipitated in the stock solution and particularly later when added to the water-soluble HEPES buffer into the recording bath. The experiments were set aside, and no results are presented in this work regarding the blockade of $Na_V1.3$.

Another possible explanation for the discrepancy among results of TTX, XEN907 and ProTx II related to conduction delay for rectangular stimulus could be the low number of experiments to point out such differences. What is possible to conclude -- based on all experiments performed using TTX, XEN907 and ProTx II -- is that the blockade of $Na_V1.7$ did not affect corrected latency for sine wave stimulation.

3.1.4 Summary of Compound Action Potentials

Based on the results observed in "*ex vivo*" recordings, the following conclusions were inferred:

- Cooling the recording bath temperature from 26° to 20°C increased the amount of current and charge required for CAP generation under rectangular 1ms electrical stimulus paradigm. In contrast, less current was required to evoke a C-CAP using sinusoidal 125ms stimuli. There was no difference in the amount of charge to generate a sine wave evoked response by cooling as the time to induce an action potential increased. The experiments demonstrated that cooling facilitates accumulation of depolarizing charge during sine wave stimulation. The closure of cold-sensitive K^+ channels, reducing leak currents and additionally increasing the membrane resistance might explain this phenomenon.
- The blockade of TTX-S currents reduced the maximum amplitude, increased the amount of current and charge to generate a half-maximum compound action

potential, increased conduction delay and reduced conduction velocity for all the pig saphenous nerve fascicles tested. No significant difference in corrected latency of sine wave induced C-CAPs was observed before and after TTX.

- The Na$_V$1.7 blockade affected sine wave evoked C-CAP maximal amplitude, but the results related to stimulus intensity, charge and latencies were not consistent when comparing the data obtained from the two Na$_V$1.7 inhibitors tested (XEN907 and ProTx II). Overall, the data suggests that specific blockade of Na$_V$1.7 did not alter the amount of current and charge needed to generate a compound action potential in pig saphenous nerve both by sinusoidal stimulation at threshold and at half-maximum amplitude. It seems that the blockade of Na$_V$1.7 alone was also not sufficient to increase the time the C-fibres needed to respond to both rectangular and sine wave stimuli. The results of XEN907 even show an opposite result, with a significant reduction in corrected latency after the blockade of Na$_V$1.7.

- The additional Na$_V$1.6 blockade abolished the response of A-fibres to electrical rectangular 0.1ms stimulation, but as expected, there was no effect on C-Fibres excitability parameters analysed for all nerve fascicles tested.

3.2   Single nerve fibre recordings (SNF)

In total, 80 fibres were analysed for sine wave 4Hz stimulation: 27 C-touch fibres (LT), 34 polymodal nociceptors (HT), 8 very-high threshold nociceptors (VHT), 7 silent nociceptors (CMi), and 3 cold nociceptors (CN). The C-fibre responses to sine wave stimulus were compared between fibre types for number of action potentials, phase (π) and charge (μC). Due to the low number of CN tested for sine wave, the results for this fibre type were excluded from the analysis. The number of action potentials would be equivalent to the result of maximum amplitude and the phase the equivalent of latency obtained before on compound action potential recordings.

The half-sine wave stimulus was tested in 96 fibres, 29 LT fibres, 36 HT, 13 VHT, 6 CN and 12 CMi nociceptors. The half-sine wave response was compared to the traditional rectangular 1ms duration stimuli. The C-nociceptors response to half-sine wave were compared between fibre types for number of action potentials, peak frequency (H), stimulus intensity (mA), charge (μC), action potential latencies (ms) and conduction velocity (m/s).

All the tested fibres were submitted to the injection of TTX 100 μL at a concentration of 1μM on the receptive field. It was expected that the injection of TTX would affect C-fibres excitability in a similar fashion obtained in the "*ex vivo*" recordings. Compared to CAP recordings, the single nerve fibre recordings could also provide us with additional information on how specific fibre types respond to ramp currents and possible further clarify some mechanisms involved in this response.

The "*in vivo*" recordings using pig saphenous nerve applied rectangular, sine wave and half-sine wave stimulus, but the results are organised by type of electrical depolarising stimulus. The response of different fibre types to the low depolarising stimuli were analysed, followed by the comparison of response before and after TTX. Sine wave results are presented first as it allows for a direct comparison to CAP recordings. Following, the result on half-sine wave stimulus paradigm is presented, and it is compared with the traditional rectangular stimulus.

3.2.1 Sine wave 4Hz 1-minute

    3.2.1.1 Number of action potentials and stimulus intensity

The overall number of action potentials in response to sine wave 4Hz across 60 seconds for all stimulus intensities tested and for each specimen was compared between the different fibre types. The sine wave 4Hz 1-minute was applied at six current intensities: 0.05, 0.1, 0.2, 0.4, 0.8 and 1.2mA. The stimulus intensities were increased step by step from a point in which small or no response was obtained to a point in which a vigorous response in each specimen was observed.

In general, higher currents were needed to activate VHT and CMI compared to LT fibres and HT nociceptors. Within the same fibre type, an intensity-dependent response was observed, with more action potentials for higher stimulus intensities.
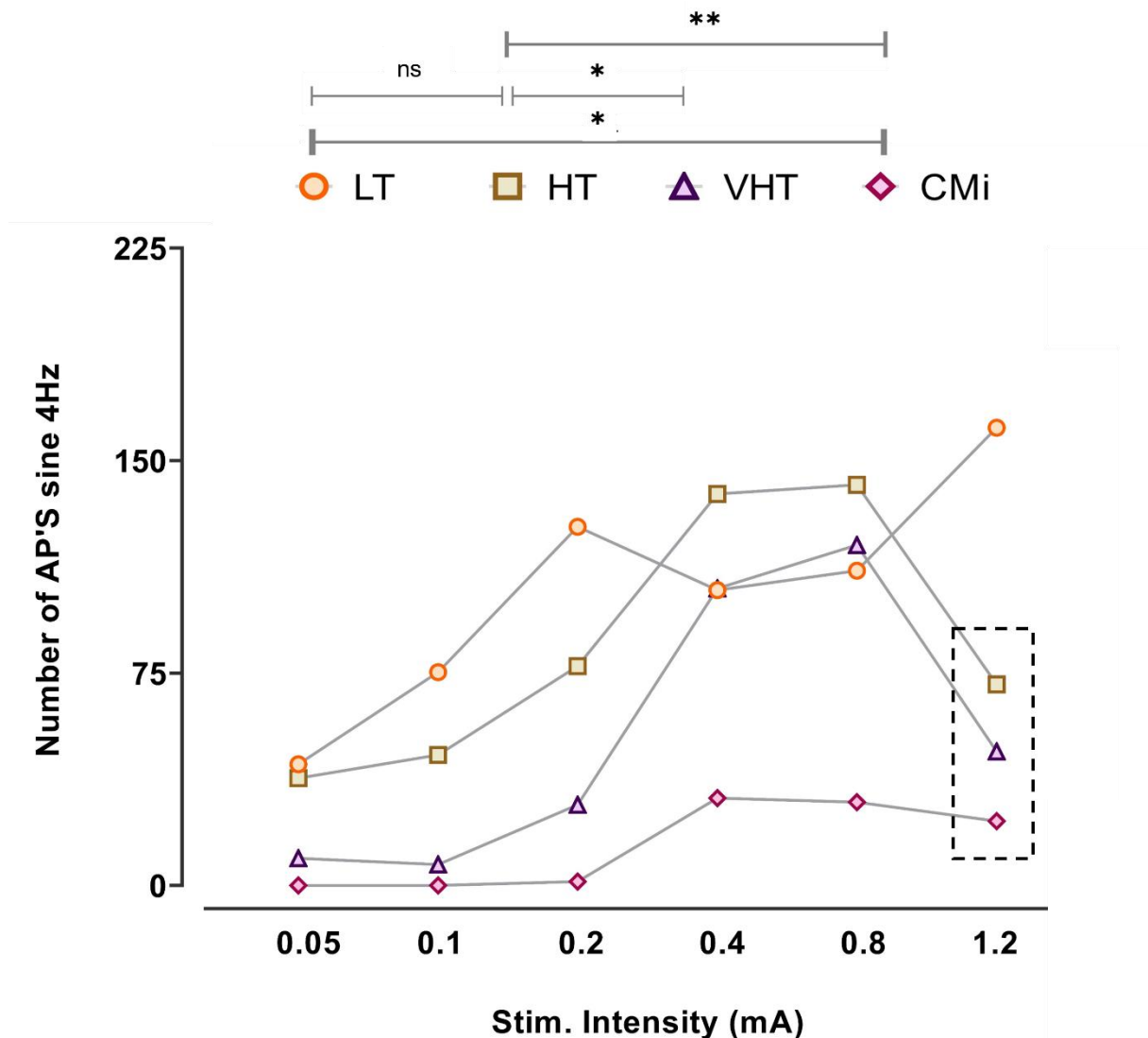
Figure 23: Intensity-dependant response to sine wave: An intensity-dependent response from all C-fibre types was observed to sine wave stimulus. The higher the stimulus intensity, the higher the number of generated action potentials. The number of action potentials are presented as means. Note that 1.2 mA was only tested for very few fibres (particularly HT n= 3, VHT n=2 and CMi n=2, indicated by the dashed square) as those did not respond to lower intensities.

The average numbers of action potentials across all stimulus intensities did not differ significantly between LT fibres and HT nociceptors. HT and LT fibres produced more action potentials as compared to CMi nociceptors (Repeated measures one-way ANOVA, Bonferroni post-hoc test). The means ± SD of action potentials across all intensities were 103.6±41.11 for LT (*p<0.01*), 85.35±44.72 *and* for HT (*p<0.05)*, and

14.07±15.15 for CMi. Also, the average number of action potentials of VHT 52.99±48.5 was significantly smaller (*p<0.05)* when compared to HT nociceptors (Fig. 23).

We also analysed the time course of activation during the 4Hz 1-minute stimulus for all fibre classes (Fig. 24). The number of action potentials per second was averaged for all fibre types. This analysis not only shows the number of action potentials for each fibre type in response to sine wave 4Hz 1-minute, but also provides us with an overall idea of which fibre types show an accommodation pattern of the response during the continuous 60 second stimulation. In general, fibres reveal most prominent response within the first 10 seconds, followed by a plateau in the remaining 50 seconds.

The results showed that LT, most HT and some VHT nociceptors start responding at current intensities as low as 0.05mA. At 0.1mA, a very modest response was observed for VHT, and CMi nociceptors did not respond. The firing of VHT nociceptors at 0.05 and 0.1mA is not consistent along the 60 seconds of stimulation. The best intensities to make a comparison between all the fibre types are 0.2mA and 0.4mA, once most of the fibres responded at these current intensities. At 0.2mA, LT and HT nociceptors showed a clear response while VHT and CMi nociceptors responded in a modest fashion. At 0.4mA, CMi start responding to sine wave 4Hz and VHT increase its response further. LT and HT C-nociceptors kept responding in a similar fashion. The stimulus intensities of 0.8mA and 1.2mA appear to be supra-threshold for all fibre types and were tested only occasionally. Besides this, an accommodation pattern was observed along the 60 seconds for all fibres at supra-threshold current intensities. At 0.05mA and 0.1mA the accommodation is already evident for LT fibres and HT and became even clearer for current intensities above 0.2mA. The accommodation is clear for VHT above 0.2mA and for CMI nociceptors above 0.4mA intensity. The results for LT, HT, VHT and CMi are in accordance with the accommodation pattern described previously in human microneurography[91,92] and the pain accommodation phenomenon reported in human psychophysics.[26] In these studies, the highest pain ratings occurred in the initial 10 seconds of stimulation, similar to our findings in single nerve fibre recordings, where the most vigorous response seems to happen during this time window.
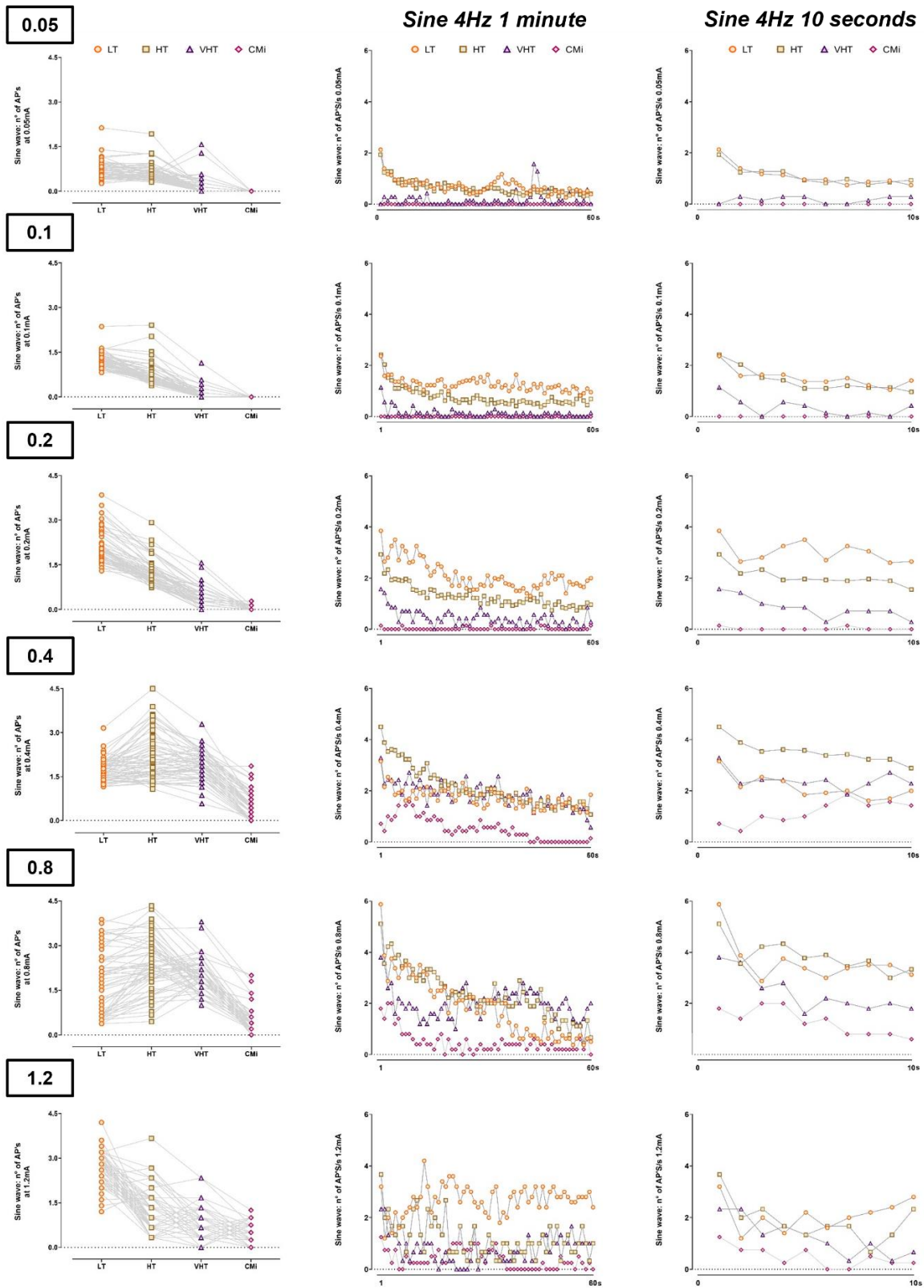
Figure 24: Fibres response (AP numbers/sec) to sine wave stimulation: While LT and HT start responding to sine wave current intensities as low as 0.05mA and 0.1mA, the responses of VHT is only clear after 0.2mA and the responses of CMi is only clear after 0.4mA. The intensities of 0.8mA and 1.2mA are supra-threshold for all fibre types and a clear response was observed for all fibre types (left panel). The accommodation pattern of the response during 1min stimulation (middle) is evident for LT and HT even at currents as low as 0.05mA. From intensities above 0.2mA for VHT and 0.4 for CMI nociceptors the accommodation pattern became evident with a prominent response in the first 10 (right panel) seconds followed by a plateau-like response. The number of action potentials are presented as means.

3.2.1.2 Phase

Typically, the 4 Hz sinusoidal stimulation provoked one action potential per complete sine, i.e. 4 action potentials per second when each stimulation was successful. Based on the results obtained for latency in CAP experiments, it would be interesting to analyse at which time of the sinusoidal cycle ("phase") the fibres were activated and if an increase in stimulus intensity would reduce this time. To calculate this, the time at which the first AP occurred (provided by Dapsys software) was collected for each specimen at all intensities and converted into the correspondent phase on the positive sine wave cycle (1π) after subtracting the conduction delay. The value of phase was averaged for all observations of the occurrence of the first action potential within the same fibre type at a certain stimulus intensity. The results pointed to an overall tendency in decreasing the phase when the stimulus intensity increases (Fig. 25A). This tendency is clearly seen in HT, VHT and CMi nociceptors, but not in LT fibres. When the median value of phase from all action potentials at a certain stimulus intensity was calculated for each fibre type, this tendency become evident even for LT fibres (Fig. 25B). It was observed that median phase is reduced when stimulus intensity increases. Those results agree with those observed in "*ex vivo*" CAP recordings in pig saphenous nerve, where latency decreases with stronger stimulation when sine wave was applied.
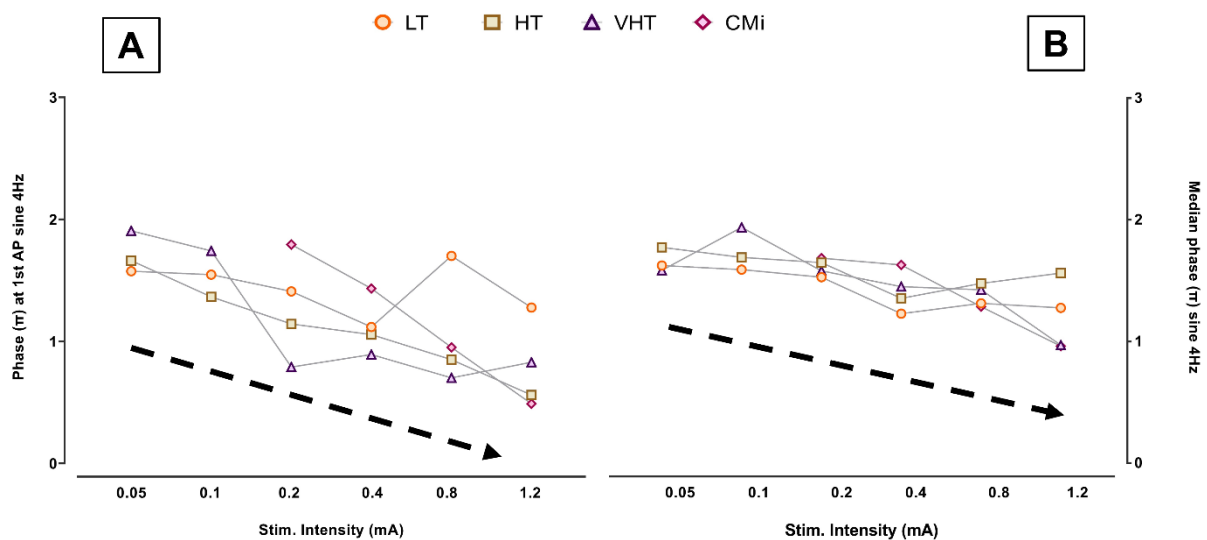
Figure 25: Occurrence of AP during phase of sine wave: It is observed an overall tendency to reduce the phase of the occurrence of the first action potential (**A**) as stimulus intensity increases for HT, VHT and CMi nociceptors. When focussing on the median phase of all action potentials at a certain stimulus intensity (**B**), the tendency to have a decrease in phase as stimulus intensity increases become more evident, across all fibre types including LT fibres.

3.2.1.3 Charge

Based on previous CAP recordings, it was expected that the amount of charge at the first action potential would remain constant, as the phase is reduced when the stimulus intensity increases. The relative increase of charge was calculated in relation to the previous stimulation intensity by division. In total, 24 LT, 28 HT, 8 VHT and 4 CMi were analysed, excluding a specimen when only one stimulus intensity was recorded. The results show a more or less constant value of charge for all fibre types (Fig. 26A). There

was no significant difference in fold charge above 1 across stimulus intensity (Repeated measures one-way ANOVA, Bonferroni post-hoc test, *p>0.05*).
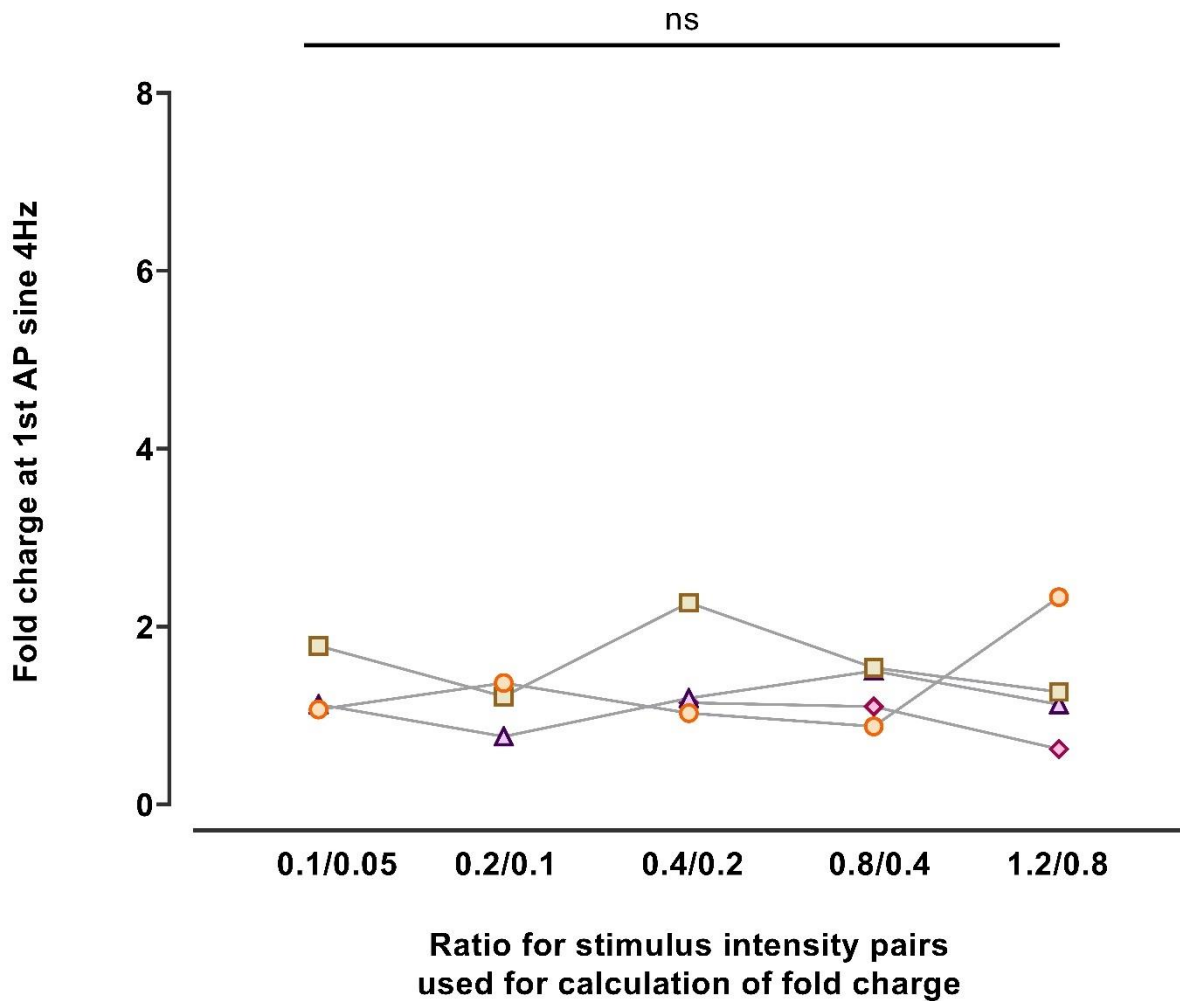
Figure 26: Fold-change of charge applied to initiate first action potential by sine wave stimulation: charge required to initiate the first action potential was in general constant even with the increase in stimulus intensity for each fibre type. There was no significant difference above 1 across stimulus intensities (Repeated measures one-way ANOVA, Bonferroni post-hoc test, *p>0.05)*. Fold-changes of charge are presented as means.

3.2.1.4 TTX effect on C-nociceptor responses to sine wave stimulation

Similar to what was presented above for sine wave induced responses in C-fibres when performing "*in vivo*" recordings, the number of action potentials, median phase and charge were compared before and after the injection of TTX 1µM into the receptive field of the recorded units. Of note, there was no observation of the effect of TTX in the parameters of CMi excitability possible, as these nociceptors stopped responding to sine wave stimulation after blockade of TTX-S currents.

When TTX 1µM was injected into the receptive field, there was a significant reduction in the number of action potentials in response to sine wave for LT fibres ("two-tailed paired t-test", *p=0.0043*), HT (*p=0.0058*) and VHT nociceptors (*p=0.0415*) (Fig. 27). The means ± SD of action potentials across all intensities after TTX were significantly reduced to 22.32±15.43 for LT, 14.82±10.37 for HT and 1.81±3.22 for VHT when compared to control condition.
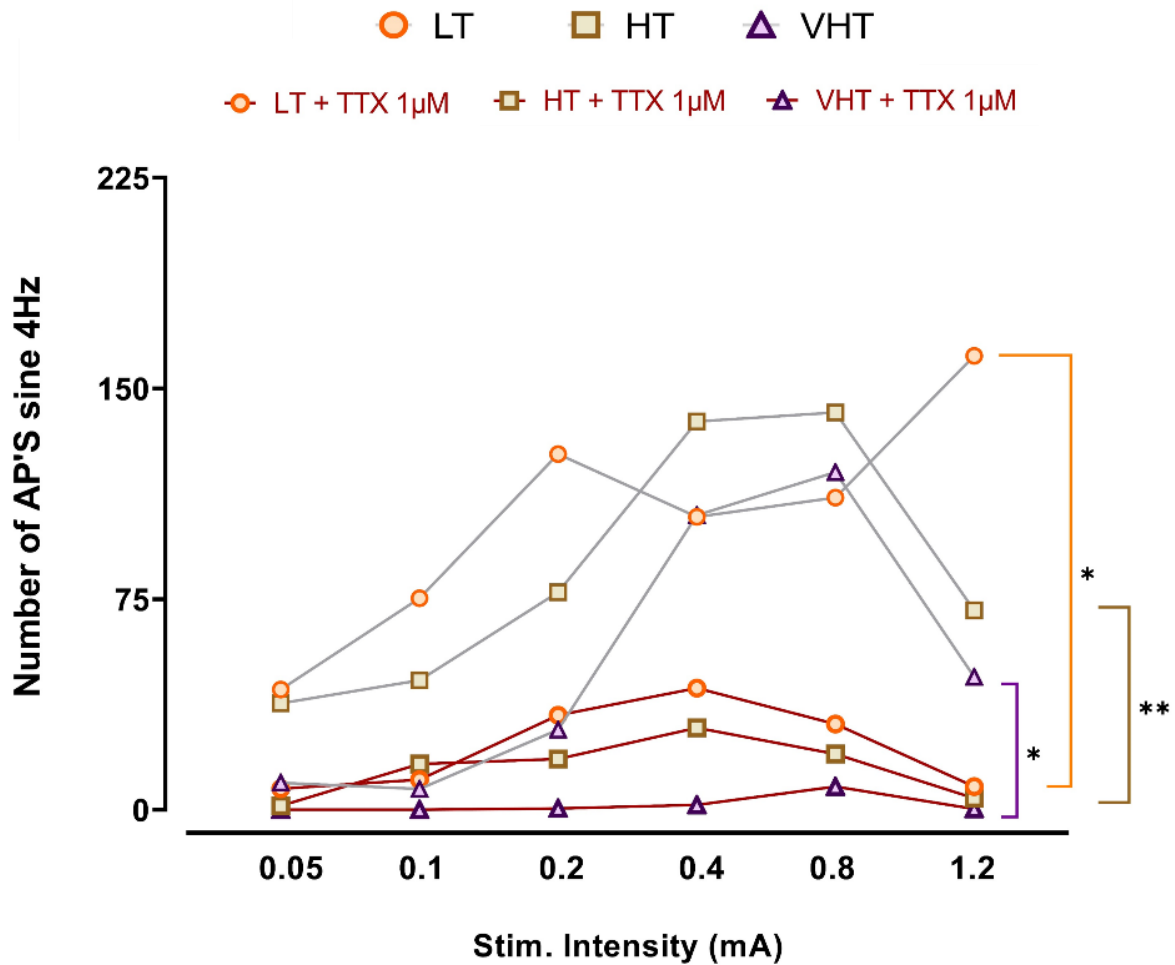
Figure 27: Effect of TTX on number of action potentials: After TTX was injected into the receptive field, there was a reduction in the overall number of action potentials across all stimulus intensities of sine wave 4Hz 1-minute for LT fibres, HT and VHT nociceptors (red lines) when compared to the AP numbers prior to injection (grey lines). There was no response of CMi nociceptors after TTX. The number of action potentials are presented as means ("two-tailed paired t-test", *p<0.05*).

The results of median phase, obtained after TTX was injected into the receptive field, show that there was an increase on phase for LT fibres across all intensities ("two-tailed paired t-test", *p=0.0463*), but not for HT and VHT nociceptors. In total, 7 LT's, 9 HT's and 2 VHT's were still responding after TTX (Fig. 28).
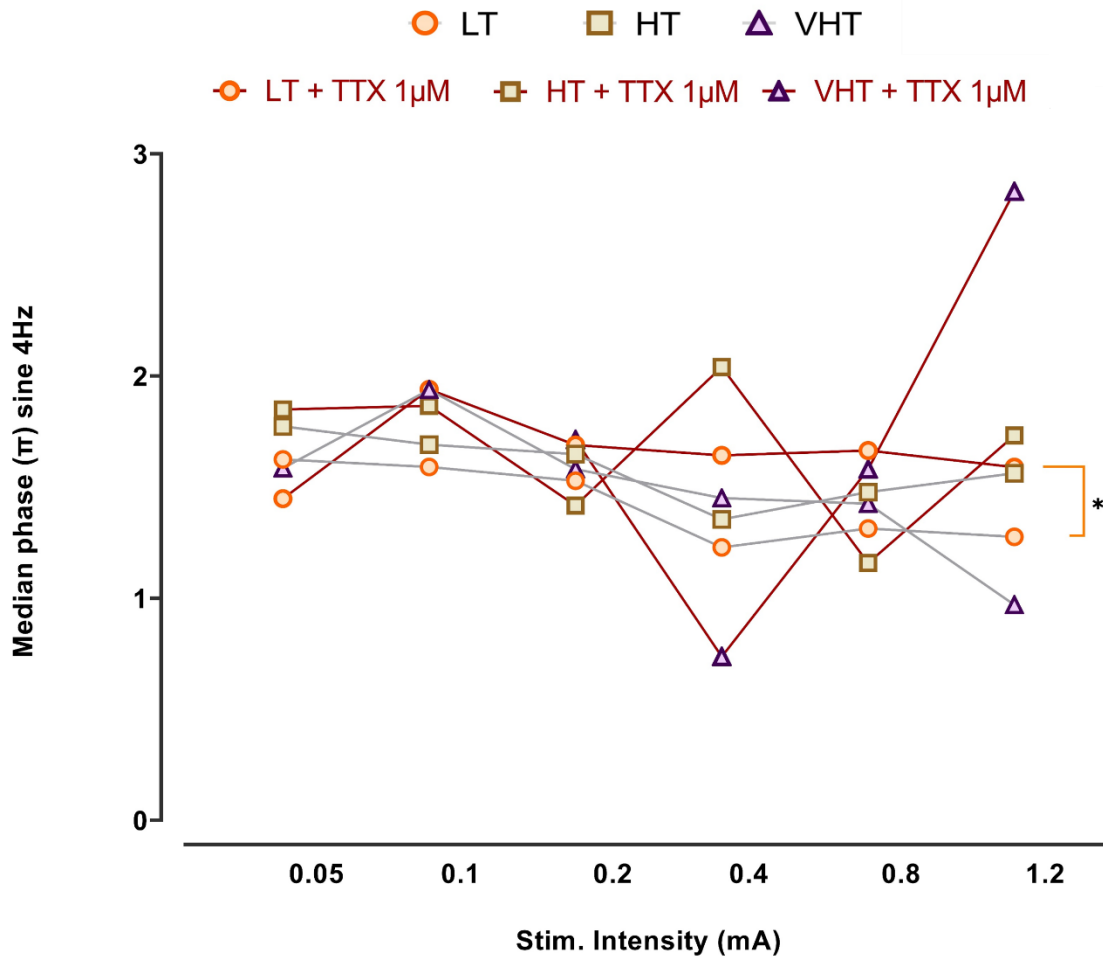
Figure 28: TTX on median phase of the action potentials: There was an increase on the median phase of action potentials across all stimulus intensities for LT fibres after TTX injection into the receptive field. This result was not observed for HT and VHT nociceptors. The median phase is presented as means ("two-tailed paired t-test", LT n=7, HT n=9 and VHT n=2, *p<0.05*).

The results obtained for median phase are consistent with the lack of effect of TTX in increasing corrected latency for sine wave stimulus in CAP recordings (see **Figure 18C**).

Based on the results obtained previously "*in vitro*", it was also expected that the injection of TTX 1μM in the receptive field in pig skin "*in vivo*" would increase the amount of charge needed to generate the first action potential (see **Figure 17B**). However, there was no difference comparing the fold charge across stimulus intensities in those specimen that responded before and after TTX 1μM (Two tailed paired t test, *p>0.05*), but the number of observations was low for all fibre classes (LT (n=5), HT (n=5), especially for VHT (n=1) and CMi, in which no comparison was possible (Fig. 29). It is noteworthy that fibres that stopped responding after TTX were disregarded in this comparison, and also those that had been tested for only one stimulus intensity had to be omitted.
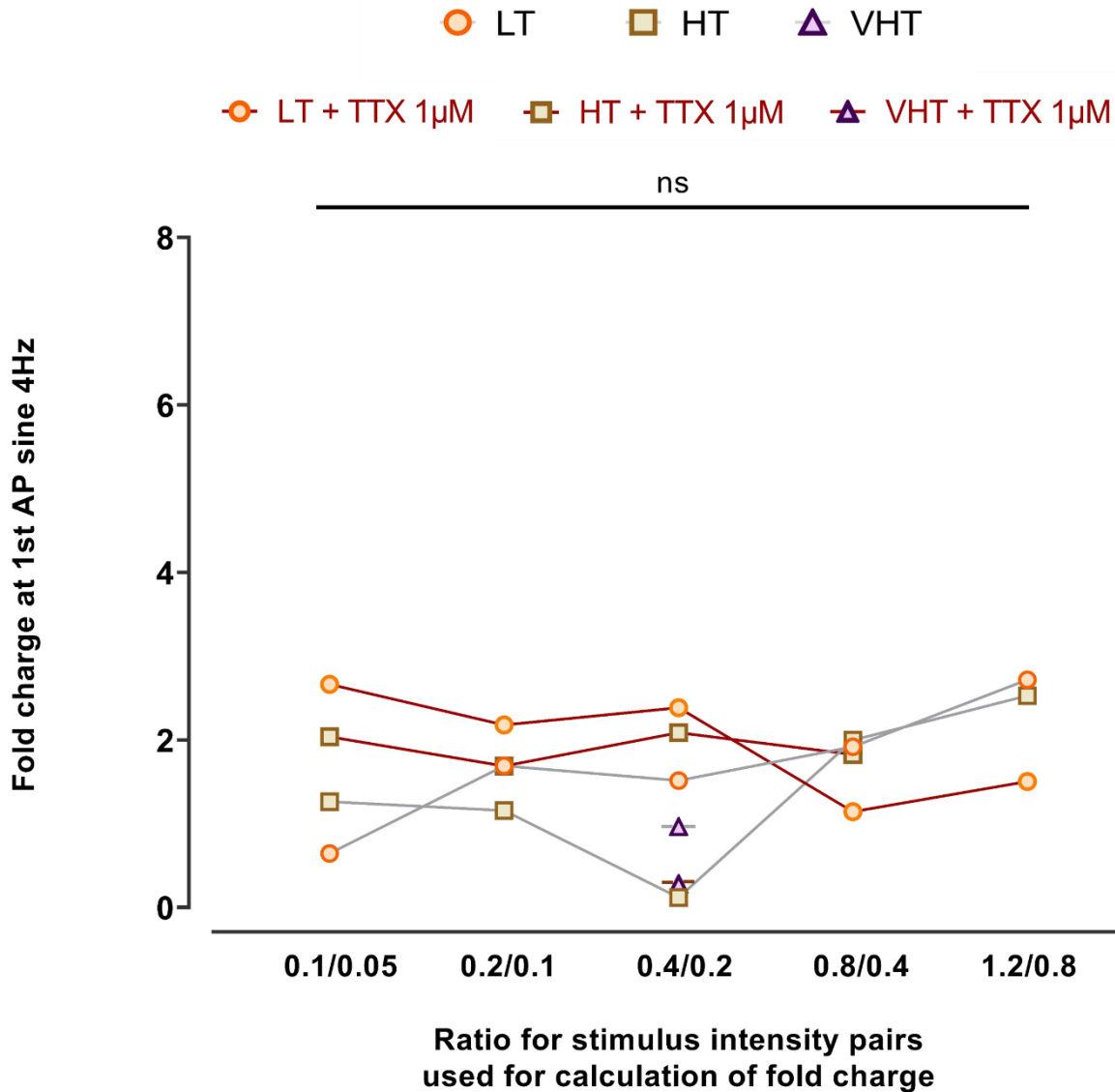
Figure 29: TTX on charge of the first sine wave induced AP: There was no difference comparing the fold charge across intensities to induce an action potential by sine wave 4Hz stimulation before and after TTX 1µM for LT, HT and VHT's. The fold charge is presented as means and only for responding fibres (LT n=5, HT n=5 and VHT n=1, "two-tailed paired t-test", *p<0.05*).

As mentioned previously, all fibre types were also submitted to half-sine wave electrical stimulation. The results of half-sine wave stimulus in single nerve fibre recordings were used to establish a direct comparison to electrical rectangular stimulation and are presented below.

3.2.2 Half-sine wave stimulation

3.2.2.1 Number of action potentials and stimulus intensity

Instead of provoking one action potential per sinusoidal stimulation, the long-lasting half-sine stimulation (500ms) typically induced a burst of action potentials. The number of action potentials per half-sine stimulation were compared for each fibre type in three ranges of stimulus intensities: (**low**) 0.02 to 0.1mA, (**medium**) 0.2 to 1mA and (**high**) 2-10mA. As mentioned previously, cold nociceptors or CN are included in the analysis

of half-sine wave. The number of action potentials were also compared between different fibre types and at the three stimulus intensity ranges (Fig. 30).

In the low 0.02-0.1 and middle 0.2-1mA intensity ranges, there is no difference in the number of action potentials fired by LT and HT upon half-sine wave stimulus. Only at the highest range, 2-10mA, the number of action potentials is higher for LT fibres compared to HT nociceptors (Repeated measures one-way ANOVA, Bonferroni post-hoc test, LT n=29, HT n=36, *p = 0.0123*). The number of action potentials of LT fibres was also higher than VHT (VHT n=13, *p=0.0015*), CMi (CMi n=12, *p<0.0001*) and CN nociceptors (CN n=6, *p=0.0408*) at 0.2-1mA and CMi at 2-10mA (*p<0.0001*). Also, the number of action potentials of HT was higher than CMi at middle (*p=0.0003*) and higher ranges of stimulus intensity (*p<0.0001*). There were no differences in the half-sine induced action potentials for VHT, CN and CMi at all stimulation ranges.
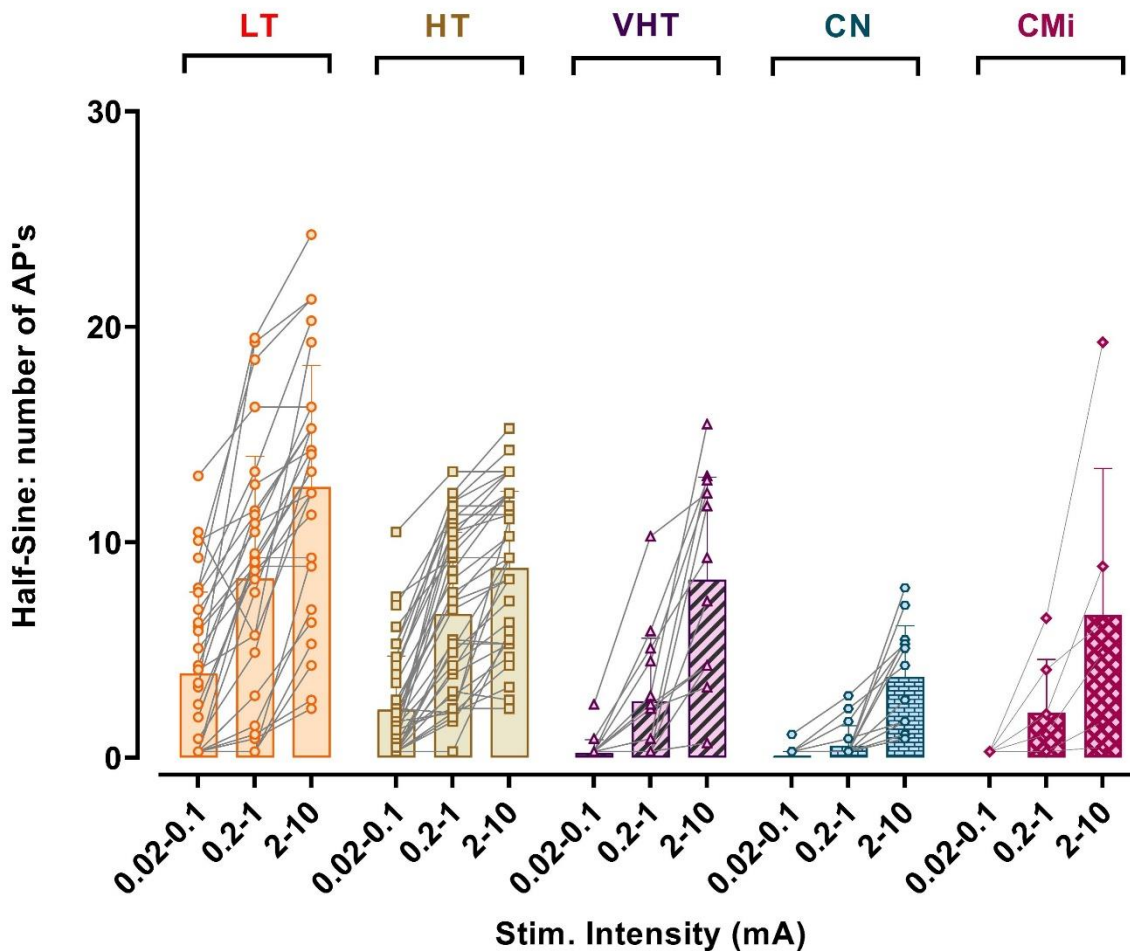
Figure 30: Half-Sine number of action potentials: LT fibres and HT nociceptors start responding to half-sine wave stimulus at the lowest intensity range (0.02-0.1mA) while VHT, CN and CMi nociceptors only showed a prominent response at the highest stimulus intensity range (2-10mA). The number of action potentials are presented as mean ± SD (columns) along with each individual recording (symbols).

The number of action potentials for current intensity range of half-sine wave pulses are summarized as means ± SD for all fibre types in **Table 6**. LT and HT nociceptors have shown an increase in the number of action potentials when comparing 0.02-0.1 to 0.2-1mA (Repeated measures one-way ANOVA, Bonferroni post-hoc test, LT *p=0.020* and HT *p=0.0002*) and 0.02-0.1 to 2-10mA (*p<0.0001*). LT fibres have also shown a significant increase in the number of action potentials when comparing 0.2-1 to 2-10mA (LT *p=0.0038*). VHT nociceptors also presented a current intensity dependent increase

in the number of action potentials when comparing 0.02-0.1 to 2-10mA (*p<0.0001*) and 0.2-1mA to 2-10mA (*p=0.0245*). There is no evidence of such intensity-dependent firing for CN and CMi nociceptors as no difference in the number of action potentials was seen when comparing low, medium and high intensity ranges.

Half-sine: Number of action potentials		
0.02-0.1mA	0.2-1mA	2-10mA
LT 3.90±3.78	8.31±5.67**	12.57±5.64****
HT 2.23±2.48	2.61±2.93***	8.80±3.56****
VHT 0.21±0.62	0.28±0.06	8.26±4.76****
CN 0.07±0.23	0.55±0.93	3.75±2.37
CMi 0.00±0.00	2.09±2.46	6.63±6.78

Table 6: Number of action potentials: Mean±SD of number of action potentials for each fibre type tested at half-sine wave intensity ranges of 0.02 to 0.1mA (low), 0.2 to 1mA (medium) and 2-10mA (high) (Repeated measures one-way ANOVA, Bonferroni post-hoc test, LT n=29, HT n=36, VHT = 13, CMi = 12, CN =6, ***p=0.002*, ****p=0.0002*, *****p<0.0001*).

These results obtained upon half-sine wave stimulation confirm what was previously observed for sine wave 4Hz with respect to LT and HT that responded vigorously at low intensity ranges and VHT and CMi that needed higher stimulus intensities to respond. When analysing the current intensity required to generate a minimum response of 3 action potentials (which is defined here as "threshold" intensity to evoke a response), LT fibres start responding at 0.69±1.42 mA, HT 0.40±1.02 mA, VHT 1.56±1.77 mA, CN 2.44±3.16 mA and CMi 4.75±3.58 mA. There is no significant difference in the half-sine threshold comparing LT, HT and VHT fibres (Repeated measures one-way ANOVA, Bonferroni post-hoc test, *p<0.05*), yet LT (*p<0.0001*), HT (*p<0.0001*) and VHT (*p=0.0009*) thresholds of activation were significantly lower than CMi nociceptors.

As mentioned before, in many experiments LT fibres and HT nociceptors were not tested for higher stimulus ranges, as soon as they responded already vigorously to stimuli of lower intensity. In these cases, the "carry-forward" technique was applied to allow valid comparison between LT and HT with other fibre types responding only at those high stimulus intensities. For the same reason, the "carry backwards" technique was performed for some specimen of VHT, CN and CMi responding at high current intensities only, as explained previously.

3.2.2.2 Peak Frequency

The peak frequency was calculated by Dapsys software, based on the occurrence of action potentials ("burst") during the 500ms half-sine wave cycle, and it is presented as a harmonic mean (**H**) in Hz within the same fibre type into a certain intensity range (Fig. 31A). Obviously, the results presented here did not include the carry forward and carry backwards techniques used for the number of action potentials, as a peak frequency cannot be assumed to stimulus intensities that had not been tested or during which conduction block occurred. This can be seen clearly when looking into the highest intensity range (2-10mA), where the harmonic means of peak frequencies in LT fibres and HT nociceptors are smaller than the medium stimulus intensity (0.2-1mA). In this case, the reduction is due to the fact that only a few LT and HT fibres were tested at the highest intensity range, in particular those with absent or mild responses to weaker stimuli. The same can be seen for VHT, CN and CMi at the lowest

intensity range (0.02-0.1mA), but this had a lower impact on the results, as very few VHT, CN and CMi nociceptors responded to these intensities anyway. Overall, the middle range provides the most accurate comparison between all fibre types, since all fibres were tested with this intensity range. Peak frequencies at 0.2-1mA are 35.54±26.88 Hz (harmonic mean ± SD) for LT fibres, 23.22±19.19 Hz for HT, 4.54±11.26 Hz for VHT, 0.15±0.03 Hz for CN and 0.12±0.15 Hz for CMi nociceptors. The peak frequency of LT is significantly higher than VHT for the middle half-sine intensity range (Repeated measures one-way ANOVA, Bonferroni post-hoc test, *p=0.0151*), but not different compared to all other fibre types. There is no difference in peak frequency among the different fibre types for the lowest and highest intensity ranges. There was also no difference between the peak frequency when comparing the different intensity ranges within the same fibre type.
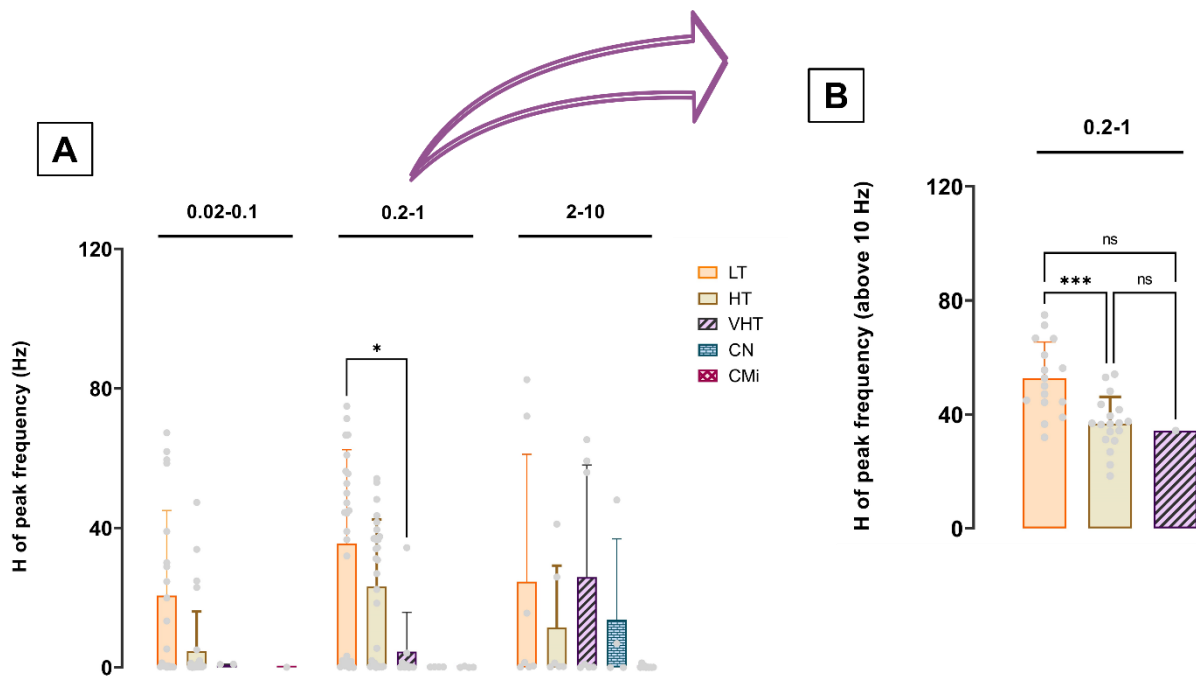
Figure 31: Peak frequency to half-sine wave stimulation: The harmonic mean (**H**) of the peak frequency of LT fibres is significantly higher than VHT nociceptors at 0.2-1mA, but not different to all other fibre types (**A**). There was no difference in peak frequency among the different fibre types for the lowest (0.02-0.1mA) and highest (2-10mA) intensity ranges and when comparing the different intensity ranges for the same fibre type. If only specimens with discharge frequencies above 10 Hz are compared, LT fibres have a higher discharge frequency than HT fibres at middle intensity range of stimulus (**B**). Peak frequencies are presented as mean ± SD (dots indicate individual recordings).

Comparisons were made also at middle intensity range for fibres only with harmonic mean discharge frequencies above 10 Hz (Fig. 31B). Thereby, LT fibres have a higher discharge frequency than HT fibres at 0.2-1mA. Also, the difference among LT and VHT became non-significant, once only one VHT has a discharge frequency above 10 Hz at this middle intensity range ("two-tailed paired t-test", LT n= 16, HT = 18, VHT = 1, *p=0.0002*).

3.2.2.3 Threshold and charge

The half-sine current intensity at threshold was compared with the amount of current needed to generate a time-locked response evoked by a supra-threshold rectangular 1ms duration stimulus. As defined above, half-sine wave threshold was considered the amount of current needed to generate a minimum number of three action potentials.

Thresholds for half-sine stimulation were lower than thresholds of rectangular stimuli for HT units ("two-tailed paired t-test", *p=0.0004*), but higher for half-sine compared to rectangular stimuli for CMi nociceptors (*p=0.0366*). No significant differences were observed for VHT, CN and CMi units (Table 7).

	Thresholds of fibre types [mA]	
	Rectangular 1ms	**500ms Half-sine wave**
LT	1.04±0.7	0.69±1.42
HT	1.37±1.02	0.40±1.02***
VHT	1.87±0.86	1.56±1.77
CN	2.88±2.95	2.44±3.16
CMi	2.06±1.22	4.75±3.58*

Table 7: Nerve fibre activation thresholds for rectangular and half-sine wave stimulus: Mean ± SD of stimulus intensity thresholds for each fibre type tested across all intensity ranges ("two-tailed paired t-test", *p=0.0366, ***p=0.0004*).

When analysing the thresholds of different fibre types, it was noticed that more current is needed to activate CMi nociceptors compared to LT (Repeated measures one-way ANOVA, Bonferroni post-hoc test, *p=0.0011*) and HT (*p=0.0059*) using rectangular stimuli (Fig. 32A).
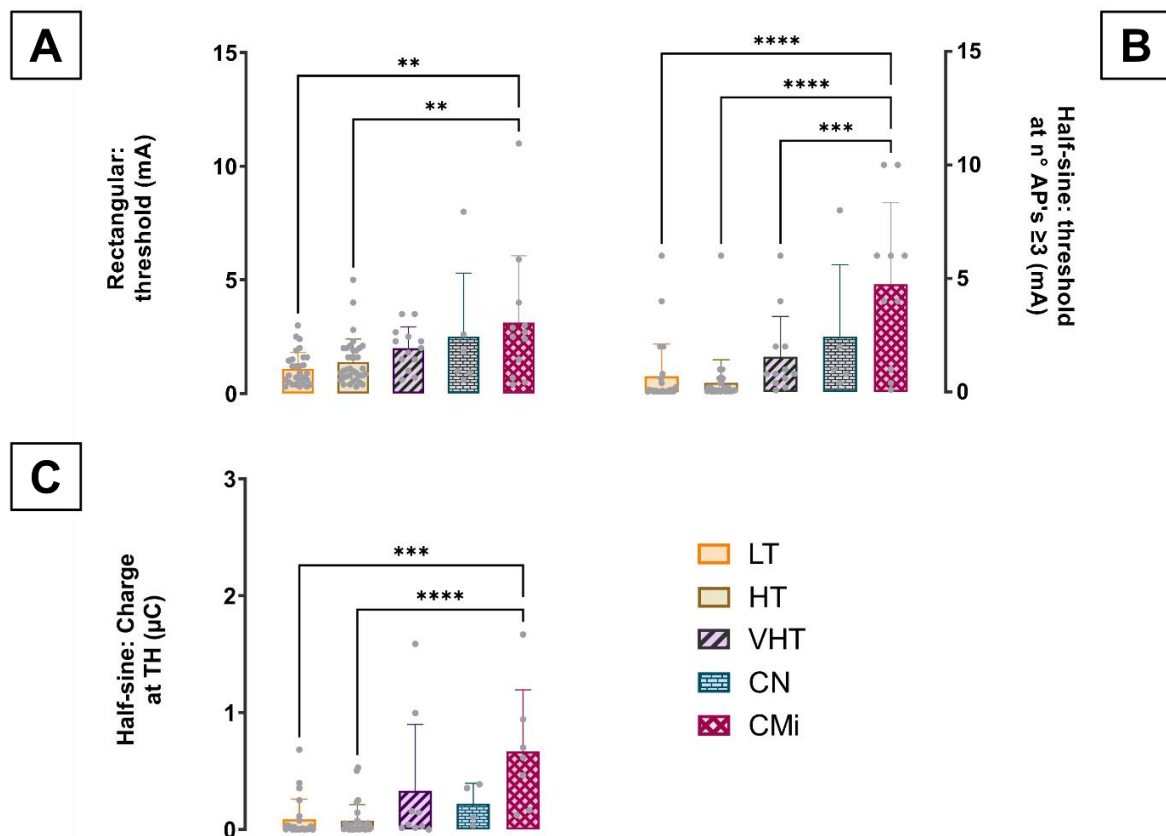
Figure 32: AP activation threshold and charge for half-sine wave stimuli: More current is needed to generate CMi action potentials in comparison to LT and HT for rectangular pulses (**A**); and similarly, more current is needed to activate CMi when comparing with LT, HT and VHT thresholds for half-sine wave stimulus (**B**). The amount of charge to initiate a response in CMi upon a half-sine wave stimulus is bigger comparing to LT and HT (**C**). The values of threshold and charge are presented as mean ± SD (Repeated measures one-way ANOVA, Bonferroni post-hoc test, **p<0.01, ***p<0.001, ****p<0.0001*).

Similarly, regarding to half-sine wave stimulation, more current is needed to activate CMi nociceptors compared to LT (Repeated measures one-way ANOVA, Bonferroni post-hoc test, *p<0.0001*), HT (*p<0.0001*) and VHT nociceptors (*p=0.0009*) (Fig. 32B). There was no difference in the thresholds of CN and CMi for both electrical stimulation paradigms. One possible explanation for the differences in threshold could be the different depths of the fibre types in the skin, an issue that will be further explored in the discussion section.

The values of charge for a rectangular stimulus are equal to stimulus intensity, once the rectangular stimulation has 1ms duration. In general, more charge was needed to initiate a response from CMi nociceptors compared to LT and HT. For half-sine wave stimulation, it was also observed that more charge is needed to initiate a response from CMi in comparison to LT (Repeated measures one-way ANOVA, Bonferroni post-hoc test, *p=0.0001*) and HT (*p<0.0001*) (Fig. 32C). The means ± SD of charge were 0.09±0.17 µC for LT, 0.07±0.14 µC for HT, 0.33±0.57 µC for VHT, 0.22±0.18 µC for CN and 0.67±0.53 µC for CMi nociceptors.

3.2.3.4 Latency and conduction velocity

The latencies for rectangular and half-sine wave stimuli, as well as the conduction velocity for rectangular stimulus, were analysed and compared between all tested fibre types. The latency for 1ms rectangular stimulation (conduction delay) was considered as the time from the stimulation of the unit within the receptive field to the time of the recording of the action potentials, which was calculated by Dapsys in (ms) once a time-locked response was observed for each fibre type. The corresponding conduction velocity (m/s) was calculated considering the distance between the receptive field stimulation and the recording electrode divided by the latency. Like CAP recordings, the time needed from the electrical stimulation to travel from the receptive field on the distal hind limb to the recording site (conduction delay) was subtracted from the latency of the half-sine stimulus at threshold. Therefore, the latency of the half-sine wave stimulus (corrected latency) was the difference between the time when the 500ms electrical stimulation was triggered to the time when the first of three or more action potentials were recorded. No difference between the fibre types in this conduction delay was observed for rectangular or corrected latency for half-sine wave stimulus paradigm. The means ± SD of conduction delay (rectangular pulses) were 89.21±28.31 ms for LT, 109.7±30.86 ms for HT, 110.3±39.40 ms for VHT, 107.5±50.32 ms for CN and 97.39±52.70 ms for CMi (Fig. 33A). The means ± SD of corrected latency for half-sine wave stimuli were 99.21±72.72 ms for LT, 115.9±101.7 ms for HT, 117.6±108.6 ms for VHT, 108.9±41.08 ms for CN and 101.3±71.53 ms for CMi (Fig. 33B).

The results also show that the conduction velocity (assessed upon rectangular stimulation) is higher for LT fibres when compared to HT (Repeated measures one-way ANOVA, Bonferroni post-hoc test, *p=0.0035*) and VHT nociceptors (*p=0.0148*). The other fibre types tested seem to have a similar conduction velocity (Fig. 33C). The means ± SD of conduction velocity were 1.25±0.51 m/s for LT, 0.88±0.20 m/s for HT, 0.92±0.42 m/s for VHT, 1.20±0.44 m/s for CN and 0.95±0.42 m/s for CMi.
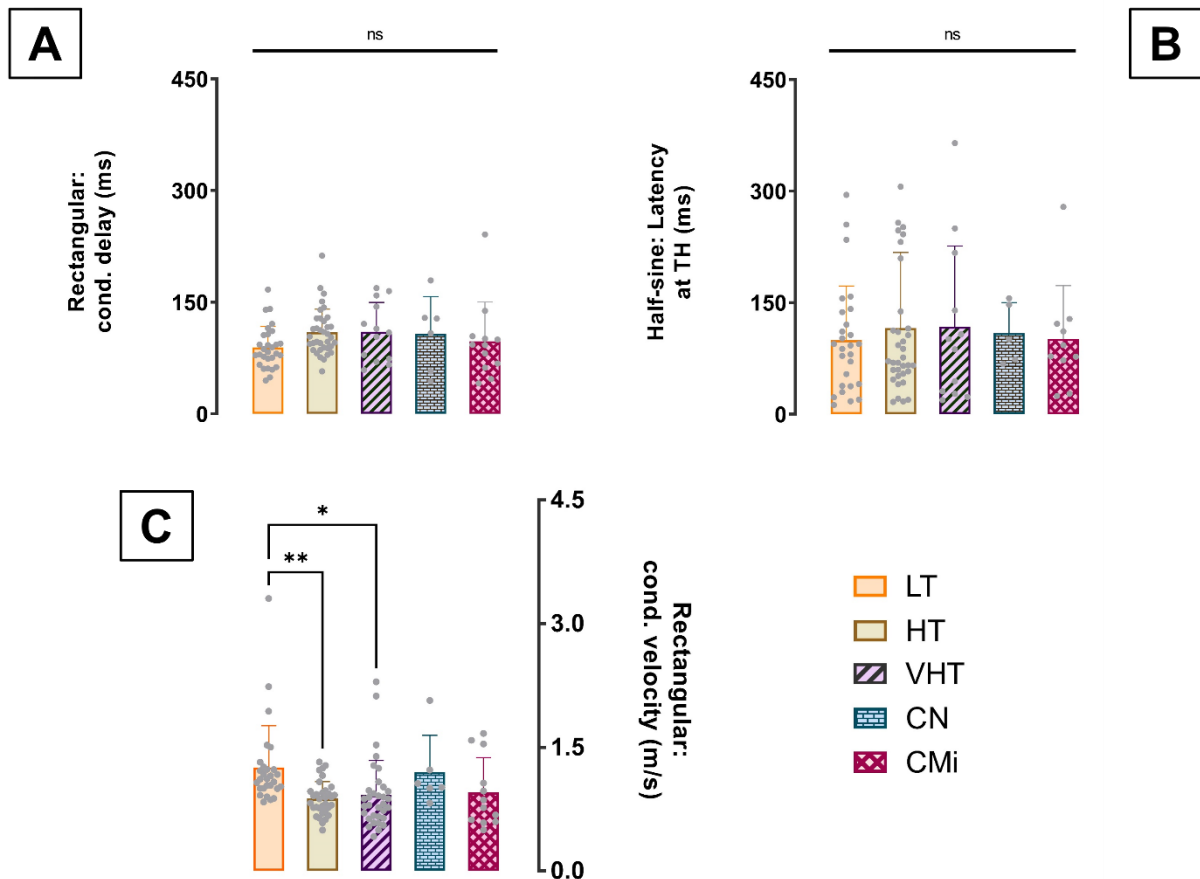
Figure 33: Response latency for rectangular and half-sine wave stimulation: There was no difference in conduction delay for rectangular stimuli (**A**) and initiation delay (latency) for half-sine pulses at thresholds (**B**) between the different fibre types. (**C**) The conduction velocity of LT fibres is higher compared to HT and VHT nociceptors (Repeated measures one-way ANOVA, Bonferroni post-hoc test, ***p=0.0035* and **p=0.0148*). The values of latency and conduction velocity are presented as mean ± SD.

The fact that the conduction velocity is higher for LT fibres and the observation that this fibre type is abundant and occasionally most prevalent in the nerve fascicle could allow for one hypothesis regarding the C-CAP signal in compound recordings: it suggests that LT dominates the initial part of the C-CAP positive rising peak. The implications of this will be later discussed.

3.2.3.5 TTX effect on C-nociceptor responses to half-sine wave stimulation

After the injection of TTX 1µM into the receptive field, a total of 12 LT fibres, 17 HT, 9 VHT, 4 CN and 2 CMi nociceptors were still responding to rectangular electrical stimulation delivered with intracutaneous needle electrodes. This observation most likely is due to the fact that stimulus intensity could be increased until action potentials were elicited even more proximally potentially skipping the TTX block. The number of action potentials evoked by half-sine wave stimulation after the blockade of TTX-S currents are presented for each intensity range (0.02-0.1, 0.2-1 and 2-10mA) before and after the injection of TTX (Fig. 34).
One relevant point to the results obtained here, is the fact that at the lowest intensity range, VHT, CN and CMi responded scarcely to half-sine wave at control condition. As expected, those responses were even more scarce after the blockade of TTX-S currents. Moreover, responses of LT and HT fibres are virtually abolished for

stimulation intensities up to 1mA, but not for very strong stimulation (10mA) that might excite axons proximal of the TTX block.
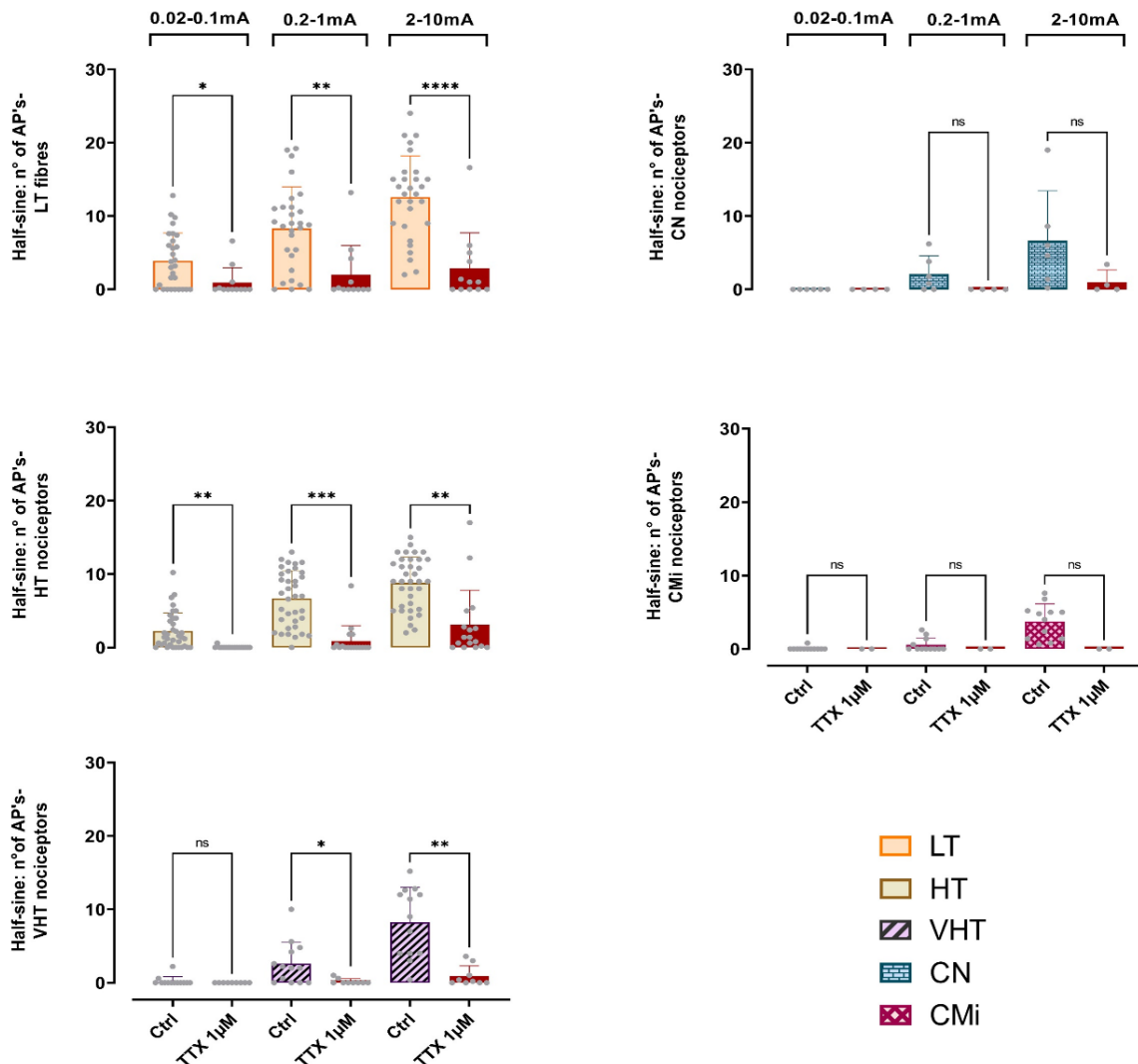
Figure 34: C-fibres responses to half-sine wave stimulation: LT fibres and HT nociceptors start responding to half-sine wave stimulus at the lowest intensity range (0.02-0.1mA) while VHT, CN and CMi nociceptors only showed a prominent response at the highest stimulus intensity range (2-10mA) under control condition prior to TTX injection (Ctrl). After TTX 1µM the number of APs significantly reduced for all C-fibre types analysed, being completely abolished for VHT, CN and CMi nociceptors. TTX reduced the number of action potentials for LT fibres and HT nociceptors at all intensity ranges; and for VHT at medium and high intensities. The reduction in action potential numbers for CN and CMi nociceptors was not significant. The number of action potentials (n° of AP's) are presented as mean ± SD ("two-tailed paired t-test", *p<0.05, **p<0.01, ***p<0.001, ****p<0.0001).

The number of action potentials after the blockade of TTX-S currents are presented as mean ± SD (Table 8). The results show that TTX significantly reduced the number of action potentials for LT and HT at all intensity ranges and for VHT nociceptors at 0.2-1 and 2-10mA. As expected, there is an obvious reduction in the number of action potentials by TTX for those fibres which have shown a prominent response to half-sine wave at control conditions (LT, HT and VHT at medium and high intensity ranges). The response of CN after TTX was insignificant and there was no difference in the response before and after TTX even at the highest intensity range. CMi nociceptors did not responded to half-sine wave after TTX.

Half-sine: Number of action potentials after TTX		
0.02-0.1mA	0.2-1mA	2-10mA

	0.02-0.1mA	0.2-1mA	2-10mA
LT	0.93±2.04*	2.00±3.98**	2.90±4.81****
HT	0.03±0.14**	0.89±2.10***	3.08±4.72**
VHT	0.00±0.00	0.18±0.37*	0.91±1.40**
CN	0.00±0.00	0.00±0.00	1.00±1.62
CMi	0.00±0.00	0.00±0.00	0.00±0.00

Table 8: HS- number of action potentials after TTX: Mean ± SD of number of action potentials for each fibre type tested at all intensity ranges before and after injection of TTX 1μM into the receptive field ("two-tailed paired t-test", *$p<0.05$, **$p<0.01$, ***$p<0.001$, ****$p<0.0001$).

The thresholds to induce half-sine wave action potentials differed before and after the addition of TTX delivered at a concentration of 100nM and thereafter at 1μM concentration, as demonstrated in the following example of a specimen of HT nociceptor (Fig. 35). As mentioned previously, a clear response of the unit was defined as three or more action potentials. Accordingly, the threshold of activation was considered the amount of current to generate such response.
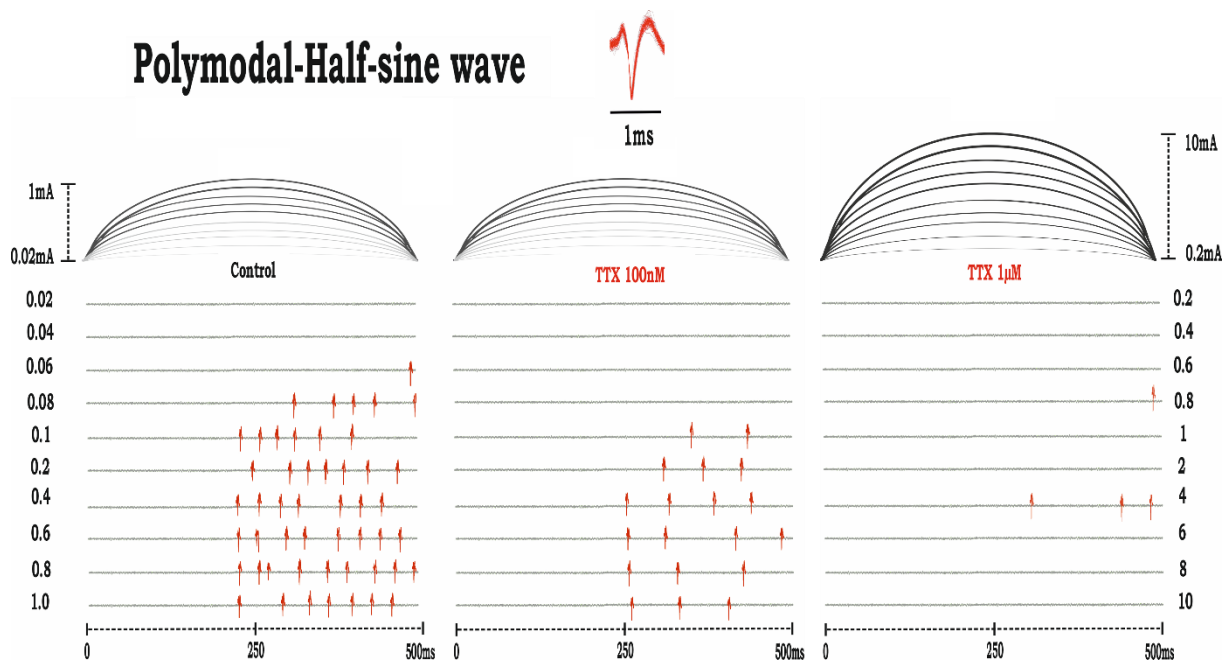
Figure 35: Specimen of HT fibre response to half-sine wave stimulus before (control) and after TTX: The thresholds for fibre activation upon half-sine wave stimulus increased tetrodotoxin dose-dependently after TTX was injected into the receptive field at concentrations of 100 nM and 1 μM.

The HT unit started responding at 0.06mA and the threshold of response was 0.08mA before TTX (control). After the injection of TTX at 100nM, the threshold increased to 0.2mA. After TTX at 1μM, only four action potentials were induced at 4mA, however, 6, 8 and 10mA stimuli were negative. Similarly, all other tested fibre types also stop responding to the initial threshold intensity of half-sine wave pulses and more current was needed to generate a similar or at last only scarce response after TTX (for detail see results below).

We first assessed the activation thresholds to rectangular stimuli. Thresholds to activate LT fibres and HT nociceptors increased significantly after TTX 1μM was

injected into the receptive field (″two-tailed paired t-test″, LT *p=0.0082 and HT (p=0.0075)*. In contrast, no difference was observed on the amount of current needed to discharge VHT, CN and CMi nociceptors before and after TTX *(p>0.05)* (Fig. 36A), but the low number of VHT, CN and CMi responding after the blockade of TTX-S currents might have influenced the statistical results obtained for those fibres. The means ± SD of stimulus current to trigger the fibres after TTX were 20.53±25.43 mA for LT, 18.67±27.26 mA for HT, 2.81±2.52 mA for VHT, 41.33±42.15 mA for CN and 13.25±11.60 mA for CMi nociceptors.
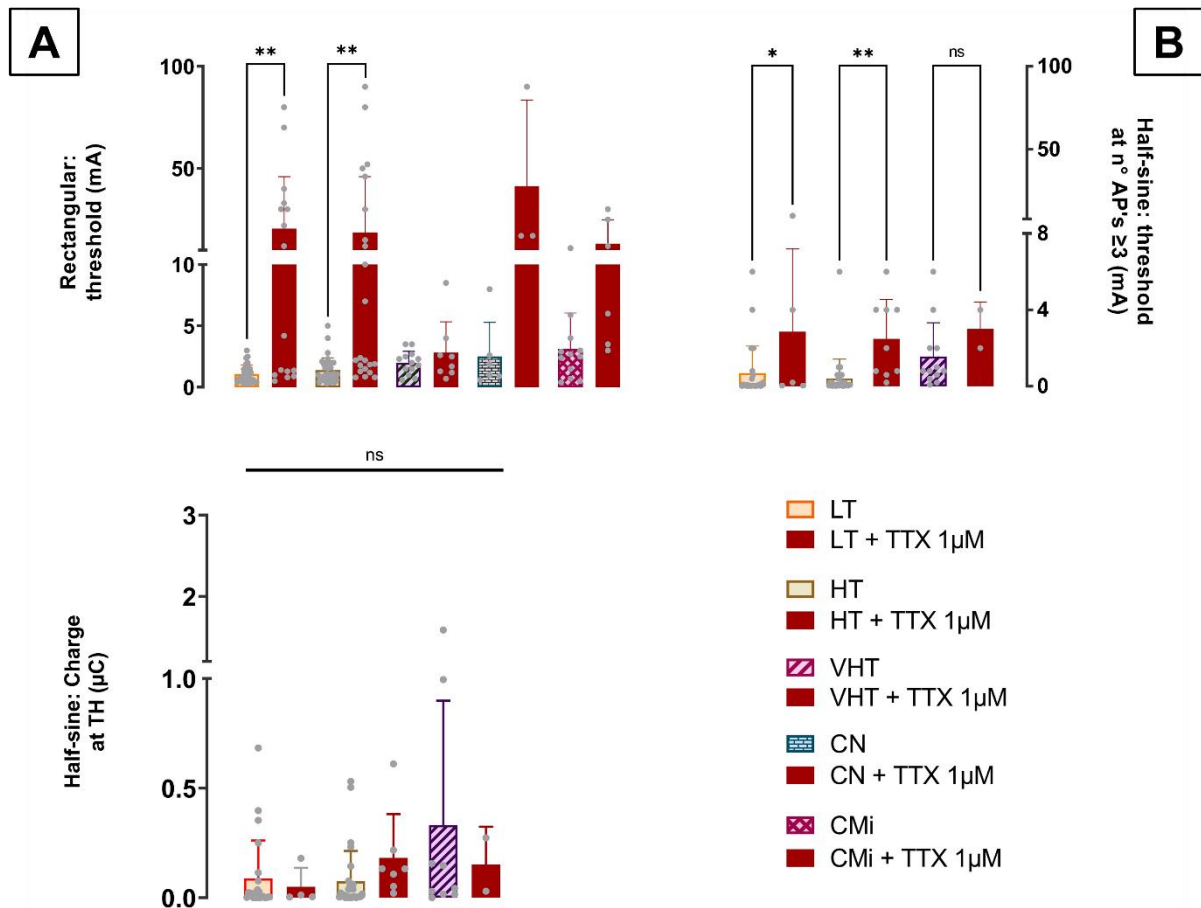
Figure 36: TTX effects on activation thresholds: There was an increase in the current thresholds for activation of LT fibres and HT (″two-tailed paired t-test″, LT *p=0.0082 and HT (p=0.0075)*, but not for VHT, CN and CMi nociceptors after TTX 1µM upon rectangular (**A**) and half-sine wave (**B**) stimuli (Repeated measures one-way ANOVA, Bonferroni post-hoc test, LT *p=0.0276* and HT *p=0.0037*). There was no difference in the amount of charge at threshold for half-sine (**C**) for LT, HT and VHT nociceptors before and after TTX. Too few CN and CMi nociceptors responded to half-sine stimulus after TTX. The values of threshold and charge are presented as mean ± SD.

Similar results were obtained for half-sine wave stimulation. The threshold to trigger a minimum of three action potentials increased for LT fibres (Repeated measures one-way ANOVA, Bonferroni post-hoc test, *p=0.0276*) and HT (*p=0.0037*) after TTX 1µM, however not for VHT nociceptors (Fig. 36B). Only 2 VHT and 1 CN were still responding to half-sine wave after TTX 1µM. No CMi responded to half-sine after the blockade of TTX-S currents. Hence, it was not possible to obtain results for CN and CMi, due to the lack of response of those nociceptors after TTX. The means ± SD of thresholds for half-sine after TTX were 2.86±4.34 for mA LT, 2.49±2.06 mA for HT, 2.81±2.52 mA for VHT, and 3.00±1.41 mA for CN.

There was no significant difference in the amount of charge at threshold for all tested nociceptors (″two-tailed paired t-test″, *p>0.05*) (Fig. 36C). It was not possible to establish a comparison of charge before and after TTX for CN and CMi, as only 1 CN and no CMi nociceptor responded to half-sine after the blockade of TTX-S currents. The means ± SD of charge after TTX 1µM were 0.05±0.09 µC for LT, 0.18±0.20 µC for HT, 0.15±0.17 µC for VHT.

The blockade of TTX-S currents significantly increased conduction delay to rectangular pulses for LT fibres (″two-tailed paired t-test″, *p=0.0055*), HT (*p<0.0001*) and VHT nociceptors (*p=0.0363*), but not for CN and CMi (Fig. 37A). The means ± SD of conduction delay after TTX 1µM were 90.32±25.6 ms for LT, 128.1±41.48 ms for HT, 136.6±34.07 ms for VHT, 111.0±41.1 ms for CN and 117.5±78.37 ms for CMi. Notably, the increase in conduction delay for CN and CMi nociceptors could be influenced by the scarce number of fibres still responding to electrical stimulation after TTX 1µM was injected.
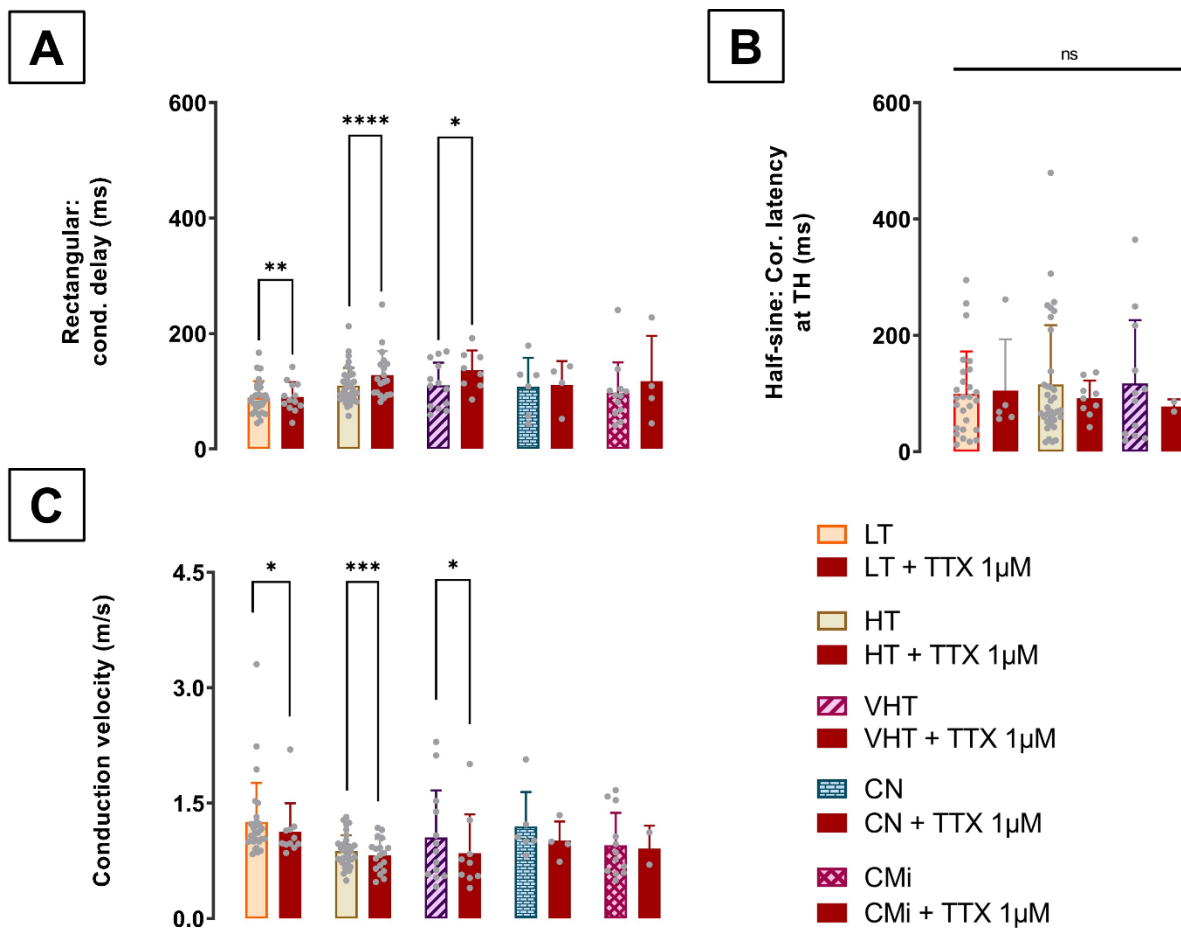
Figure 37: TTX effect on latency and conduction velocity: There was an increase in conduction delay to rectangular pulses for LT fibres (″two-tailed paired t-test″, *p=0.0055*), HT (*p<0.0001*) and VHT nociceptors (*p=0.0363*), but not for CN and CMi nociceptors after TTX 1µM was injected into the receptive field (**A**). There was no difference in half-sine wave latency at threshold after TTX for any fibre type analysed (**B**). The conduction velocity to rectangular pulses decreased after TTX for LT fibres (″two-tailed paired t-test″, *p=0.0195*), HT (*p=0.0002)* and VHT nociceptors (*p=0.0236)*, but not for CN and CMi nociceptors (**C**). The values are presented as mean ± SD.

After TTX 1µM, only 4 CN and 4 CMi nociceptors were still responding to the rectangular electrical stimulus compared to 6 CN and 12 CMi recorded at control

condition. Moreover, the number of CN and CMi fibres drop even further when analysing half-sine wave stimulus following the rectangular pulse assessments, i.e. some fibres that responded to rectangular pulses after TTX, did not respond to half-sine wave stimulation. Therefore, it was not possible to establish a comparison for latency at threshold before and after TTX for CN and CMi response to half-sine wave. LT, HT and VHT nociceptors showed no difference on latency at threshold before and after TTX ("two-tailed paired t-test", *p>0.05*) (Fig. 37B). The means ± SD of latency at threshold for half-sine wave after TTX 1µM were 105.3±87.94 ms for LT, 91.68±30.63 ms for HT and 77.70±12.16 ms for VHT.

The conduction velocity assessed upon rectangular stimulation reproduces the results obtained for conduction delay and show a decrease in conduction velocity for LT fibres ("two-tailed paired t-test", *p=0.0195*), HT (*p=0.0002)* and VHT nociceptors (*p=0.0236)* but not for CN and CMi (Fig. 37C). The means ± SD of conduction velocity after TTX 1µM were 0.85±0.96 m/s for LT, 0.82±0.2 m/s for HT, 0.85±0.50 m/s for VHT, 1.01±0.25 m/s for CN and 0.91±0.30 m/s for CMi. As mentioned before, the reduction of conduction velocity for CN and CMi nociceptors seem to be underestimated by the scarce number of fibres still responding to rectangular electrical stimulation after TTX 1µM was injected into the receptive field.

3.2.3 Summary of single nerve fibre recordings

- All fibre types respond to both sine wave and half-sine wave in an intensity-dependent manner, the higher the stimulus intensity the higher the number of action potentials. Additionally, along 60 seconds of continuous sine wave stimulation, the fibres show an accommodation of response after 10 seconds and a plateau-like response is seen in the remaining 50 seconds. After TTX was injected into the receptive field of the recorded unit, there was a clear effect in reducing the number of action potentials for LT fibres, HT and VHT nociceptors. This effect could not be seen in CN and CMi nociceptors, but the number of fibres still responding to half-sine wave were insignificant after TTX, making it impossible to establish a comparison. The reduction in the number of action potentials reflects the reduction in maximum signal amplitude obtained in CAP recordings.
- The magnitude of current to evoke a response in LT, HT and VHT is smaller compared to CMi nociceptors. LT and HT nociceptors also show an increase in the threshold for fibre activation upon both rectangular and half-sine wave stimulus after TTX. This increase was also evident in CAP recordings. An increase could not be seen for VHT, CN and CMi but this can be explained by the fact that only few fibres able to respond to a current inferior to 10mA could be analysed for the slow depolarising currents for technical reasons. The stimulator used for sine and half-sine wave stimulus could not deliver currents above 10mA, and this technical limitation may explain why responses could not be elicited after the blockade of TTX-S currents for those fibre types.
- Similar to CAP recordings, it seems that the amount of charge to generate a response is constant under sine wave stimulus. Surprisingly, there was no difference in charge of the first action potential for sine wave and charge at threshold for half-sine wave responses across all C-fibre types before and after the addition of TTX.
- In CAP recordings the blockade of TTX-S currents only increased conduction delay and reduced conduction velocity for rectangular stimulus. In single nerve fibre recordings, the blockade of TTX-S currents prolonged conduction delay for LT, HT

and VHT fibres for rectangular stimuli, but did not affect corrected latency for half-sine wave stimulation in any fibre type. Similarly, median phase upon sine wave 4Hz stimuli was only increased for LT fibres, but not for HT, VHT and CMi nociceptors. The increases in latency observed for LT, HT and VHT upon rectangular stimulus in single nerve fibre recordings is consistent with a concomitant reduction in conduction velocity. It seems reasonable, based on the latency results presented both "*in vivo*" and "*ex vivo*" for all applied stimulus profiles, to attribute any delay of C-nociceptor responses upon TTX blockade to a reduction in conduction velocity.

4 <u>DISCUSSION</u>

Data from early studies on the relationship between axonal diameter and conduction velocity have already implied the usefulness of short duration rectangular electrical stimuli in generating a synchronous compound potential. The initial aim was to cluster different types of fast myelinated fibres according to their typical conduction velocities.[93] Indeed, short depolarising rectangular pulses are most adequate to activate myelinated neurons. It was later understood that this response is due to the high expression of Nav1.6[94] in myelinated axons. Nav1.6 channels have a fast closed state inactivation, which inhibits action potential generation by slow depolarising electrical stimuli.[56] In addition, a rectangular pulse with rapid onset of activation provides a good setting for studies targeting axonal conduction. However, it fails to contribute with functional information regarding action potential initiation in sensory endings; a point of great interest when investigating the pathophysiology of nociceptors sensitization contributing to chronic pain.

First attempts to activate afferent neurons with a slow depolarising stimuli date back to 1987, when this stimulus was first proven useful in the screening of patients with painful neuropathy.[95] As previously mentioned, hyperexcitability in unmyelinated C-nociceptors is highly correlated with neuropathic pain.[19,20] Not until the last decade, this type of electrical paradigm began to be more widely used in experiments investigating small diameter unmyelinated neurons.

4.1 Why slow depolarising stimulation?

Slow depolarizing electrical stimuli have been shown more specific for the activation of unmyelinated C-nociceptors using single nerve fibre recordings in pigs, live cell imaging in mice, compound action potential recordings "*in vitro*" of human nerve fascicles, "*in vivo*" microneurography and human psychophysics in healthy volunteers as well as neuropathic pain patients.[26,96] In particular, sinusoidal stimulation of 4 Hz and single half-sine stimulation (1Hz, 500ms) were proved efficient for C-fibre activation. Both stimulation profiles mimic more physiologically relevant depolarization, however, the mechanisms behind the response to those paradigms is yet unclear.

The pathophysiology of spontaneous activity, a common symptom in neuropathic pain patients, may be better understood with a deeper knowledge of how action potentials are initiated. The generation of action potentials using mild tonic depolarization has been attributed to the capacity of sodium channels in generating ramp currents. It was described that some VGSC would act as amplifiers of weak stimuli and are fundamental to action potential initiation.[55,97] Based on the kinetics of VGSC, both Nav1.3 and Nav1.7 can generate ramp currents due to a slow transition into the inactivated state (closed state inactivation) upon slow depolarising stimuli.[55] Nav1.3 is expressed in sensory afferents only during foetal development or following nerve injury[55,56] and it is unlikely to be expressed in naive mature neurons recorded during this study. As Nav1.7 is highly expressed in peripheral C-fibres,[98] including epidermal free endings[2], this would qualify the isoform as the primary candidate to explain the responses of unmyelinated axons to slow depolarising stimuli.

4.1.1 C-fibres respond to slow depolarizing electrical stimuli (SDES)

Recordings from single unmyelinated C-fibres innervating human and pig skin demonstrated that 4Hz sinusoidal current of low intensity (<0.2mA) is able to activate

cutaneous C-fibres, whereas higher currents (>0.6mA) are required for activation of sympathetic C-fibres and A-fibres.[99,100] The C-fibre activation by cutaneous sine wave current is evidenced by the accompanying sensation of burning pain,[99] even during A-fibre compression block,[101] and an axon-reflex flare development around the site of stimulation,[102] the latter a phenomenon attributed to the activation of mechanically insensitive ("silent") C-nociceptors (CMi).[103]

The description of compound potential generation in isolated peripheral nerves by means of sine wave stimulation was originally described in human, pig and mouse nerves[26] and further explored successfully in depth in this work using nerve fascicles of pig saphenous nerve. Moreover, single units of pig saphenous nerve were recorded "*in vivo*" following the well-described technique of single nerve fibre recordings in anesthetized pigs[34,89,90] introducing the slow depolarising type of stimulus. In this study a total of 80 fibres were analysed for sine wave 4Hz stimulation (27 LT, 34 HT, 8 VHT, 3 CN and 7 CMi) and 96 fibres were recorded applying half-sine wave stimulus (29 LT, 36 HT, 13 VHT, 6 CN and 12 CMi).

Consistent with our observations based on the frequency at which LT single units were found in pig SNF recordings, LT seem to represent a large population of neurons. LT fibres are described as predominantly innervating hairy skin in rodents with endings projecting longitudinally with the hair follicles and arborising in the epidermis.[104] Another study conducting microneurography from the human peroneal nerve in the leg, found that the majority of C-fibres in distal limbs are HT or polymodal nociceptors (45%).[27] These axons were also very frequently found during single unit recordings of pig saphenous nerve. It was also described that human HT fibres receptive fields are large (106mm^2),[105] a fact that would explain the frequency with which these fibres were identified during receptive field searches in the hind limb of pigs and recorded herein, confirming the great congruency of skin structure and neuronal innervation between these species.[106]

Both LT and HT nociceptors responded vigorously to sine wave and half-sine wave stimulation at very low intensity ranges compared to VHT, CN and CMi nociceptors. The responsiveness of C-fibres to slow depolarising stimuli were quantified by the number of action potentials. The responsiveness to SDES was similarly high for LT and HT for sine wave stimuli. VHT and CMi responded with a smaller number of action potentials compared to HT nociceptors. Regarding half-sine wave slow depolarising stimulus, the number of action potentials were higher for LT fibres compared to VHT, CMi and CN nociceptors above 0.2mA. The LT fibres response to half-sine were higher than the response of HT nociceptors at stimulus intensities above 2mA, but at lower half-sine intensities (0.02-0.1mA), the number of action potentials were similar for LT and HT. In summary, both low-threshold mechano-responsive fibres and polymodal nociceptors are equally sensitive to slow depolarising stimulus. The current thresholds of activation of LT fibres and HT nociceptors are similar and significantly smaller compared to the other C-fibre types. Overall, the fibres respond to both, sine wave and half-sine wave in a current intensity-dependent manner.

4.1.2   *Different responses to sine and half-sine stimuli*

It is important to stress a crucial difference in the response pattern of C-fibres when activated by sine wave or a half-sine wave stimulus, respectively. The sensory neurons respond to half-sine wave with a burst of action potentials during and shortly after onset of the 500ms stimulus, while a single action potential is fired time locked to a certain phase in each cycle of sine wave 4Hz pulses. These synchronized responses to the 4Hz stimulation are the prerequisite for successful recordings of compound action potentials (CAP). Thus, the results obtained in the *"in vivo"* single nerve fibre recordings

are in agreement with the results obtained by *"ex vivo"* compound action potential recordings when comparing responses to electrical sine wave stimulation at 4Hz. In particular, the time required to initiate an action potential is directly comparable between corrected latency in the CAP recordings and the phase in single fibre recordings. The advantages of the "*ex vivo*" compound action potential are optimum control of stimulation site and intensity, simultaneous recording of many dozens of fibres and stable stimulation and recording conditions. The advantages of the single fibre recordings are access to the sensory endings, defined functional classes, and analysis of multi-spike responses. Both approaches provide a corresponding measure for the time to initiation of the action potential. Moreover, the amplitude on CAP recordings reflects the number of synchronously activated axons and thus would be equivalent to percentage of fibres being activated on single nerve fibre level. In contrast, analysis of non-synchronized bursts of action potentials to half-sine wave pulses requires single fibre recordings, that also allow to differentiate responses of functional C-fibre classes.

4.1.3 Differential axonal properties of C-fibre classes

The capacity to intensely respond to slow depolarising stimuli (observed for LT fibres and HT nociceptors) seems to correlate with the ability to follow a repetitive 2Hz 3-minutes stimulus, along with low or intermediate activity dependent slowing (ADS) characteristic for these C-fibre types. It was previously described that LT fibres are almost unaffected by ADS (<15%), while HT fibres have an intermediate ADS (15-23%) and CMi a high ADS (>20%) upon 2Hz stimulation.[89] VHT nociceptors resemble CMi fibres at very low stimulus frequencies (0.1 Hz), but for higher stimulation frequencies such as 5Hz behave like HT nociceptors.[107] In addition, CN nociceptors appear not much affected by ADS (<10%) in agreement to what was previously published.[89] The activity-dependent slowing phenomenon is caused by progressive slow inactivation of VGSC, intracellular accumulation of sodium ions and hyperpolarization of unmyelinated fibres upon repetitive action potential generation.[108] The authors suggest that the varying expression of sodium channels and their different slowing activation kinetics could be the cause of differences in ADS observed for C-fibres in pigs.[89] Reinforcing evidence comes from a study using $Na_V1.7$ knockout mice, which demonstrated that the absence of the isoform did not alter ADS when compared to recordings from wild-type HT fibres.[108] Accordingly, slow inactivation of $Na_V1.8$ and its high expression in CMi fibres might contribute to the high ADS observed in these nociceptors.[109,110]

In our studies, activity-dependent excitability changes were mainly investigated by accommodation of responses during the 1-minute of sine wave stimulation. Obviously, ADS will contribute to excitability changes that determine this accommodation. However, the long duration sine wave 4Hz stimulus induced an accommodating response in all fibres tested at supra-threshold current intensities, as previously demonstrated.[26] Thus, the characteristic differences in ADS between fibre classes did not translate into a corresponding accommodation pattern in the 4Hz 1-minute stimulation paradigm. However, our findings of fibre accommodation are in-line with the accommodation of pain ratings observed psychophysically and are in accordance with earlier in human microneurography studies.[91,92]

4.2 Role of TTX-s channels for C-fibre excitability

Thanks to the Nobel prized Toshio Narahashi and its 1964 publication, tetrodotoxin (TTX) became available for the study of neuronal excitability, and the research of many other drugs and toxins that modulates ion channels function were only possible following his discovery.[111] As previously stated, TTX is a sodium channel blocker that acts on the isoforms 1.1-1.4, 1.6 and 1.7. NaV1.5, 1.8 and 1.9 are known to be resistant to TTX up to a mM range.[64,99] In this study, tetrodotoxin was applied with the purpose of blocking NaV1.6 and NaV1.7 (assuming NaV1.3 is not expressed in the mature recorded units) on primary sensory afferents, based on the known expression of these VGSC in C-fibres.[112] More specifically, we investigated the role of sodium channels in the activation of C-nociceptors to slow depolarizing stimuli that occurs with intriguingly long latencies at low stimulus intensities. Recordings were performed from naive and TTX-treated single C-fibres "*in vivo*" as well as axons of pig saphenous nerve "*ex vivo*". Specific Na$_V$1.7 and Na$_V$1.6 inhibitors and/or blockers were also applied and investigated in compound potential recordings.

4.2.1 TTX impairs C-fibre firing

The TTX injection into the receptive field of single LT, HT and VHT units induced an overall reduction in the number of action potentials when applying slow depolarising stimuli. This finding was consistent with the reduction in maximum amplitude and increased half-maximum current observed in compound action potential recordings after TTX blockade.

LT fibres have a high expression of Na$_V$1.1, 1.6 and 1.7[113] and polymodal nociceptors are also known to have a big component of TTX-S VGSC based on their modest slowing-dependent activity under high frequency electrical stimulation.[112] Therefore, a reduction in the number of action potentials in LT and HT nociceptors was expected after TTX was injected into the receptive fields of these fibre classes. We further observed that the blockade of Na$_V$1.6 by µ-conotoxin was effective in abolishing A-fibre signals in compound potential recordings yet did not affect maximum amplitude in C-fibres compound potentials. These data provide evidence that Na$_V$1.6 does not play a crucial role in the response of C afferents to slow depolarising stimuli.

Comparatively, silent and CN nociceptors are assumed to have a large component of tetrodotoxin resistant (TTX-R) VGSC, and more specifically CMi nociceptors to have a pronounced slow activity-dependency.[114,112,115] Accordingly, CMi and CN might be expected to keep responding to SDES after TTX, and thus independently of the blockade of both Na$_V$1.6 and 1.7. We observed a weak response of CMi and CN nociceptors to both slow depolarising stimuli in control conditions but a more or less complete blockade of response in these fibres when TTX was injected into the receptive field. However, some of the silent fibres could still be electrically activated by intradermal rectangular pulses at higher stimulus intensities after TTX (mean ± SD: 13.25±11.6mA), whereas their responses to SDES were blocked. Unfortunately, the sine wave and half-sine wave stimuli could not be increased beyond 10mA. We therefore conclude that excitability and conduction of CMi nociceptors is facilitated by currents sensitive to TTX (TTX-S), but TTX-R currents are sufficient to ensure action potential initiation and conduction. TTX-S also contribute to CMi activation by SDES, but it is unclear whether TTX-R currents were sufficient as higher current intensities could not be tested. However, our TTX results in the CAP recordings clearly suggest that TTX-R currents are sufficient to sustain activation by SDES (see **Figure 16**) even though we cannot directly link the CAP results to CMi nociceptors. Thus, the most probable explanation for abolished SDES responses of these nociceptors after TTX is the limited stimulation intensity (maximum 10mA) in our study. This is of particular

relevance for "silent" fibres as the location and geometry of C-fibre terminals in the skin determines their response to electrical stimuli. The shorter the distance between an axon and the stimulating electrode, the lower the required stimulus amplitude to excite the nerve ending.[116] This feature also may explain low excitability of deeper located CMi nociceptors upon transcutaneous SDES.

Setting aside the reservations regarding the translational value of classifying human neurons into peptidergic and non-peptidergic,[117] a study in rodents has shown that peptidergic neurons (CGRP+, responsive to noxious heat and capsaicin) terminate in the stratum spinosum of the epidermis while non-peptidergic neurons (IB4+, responsive to mechanical pain) extend to the outermost layer of the epidermis, the stratum granulosum.[118,119] Reinforcing the abovementioned idea of a spatial differentiation of nociceptors in the skin, it was demonstrated that rat neurons with superficial receptive fields are mostly IB4 positive.[120] Even if the classification into peptidergic and non-peptidergic is not exactly applicable to human neurons, and supposedly to pigs either, the previous attempt to topographically localize these fibres among the epidermal layers indicated that a differential distribution exists. In this sense, the more superficial the fibres, the better these fibres will respond to transcutaneous electrical stimulation. It has been previously described that IB4 binding is associated with wide action potentials and large TTX-R expression of $Na_V1.8$ and $Na_V1.9$, while peptidergic neurons would have shorter duration action potentials and lower expression of $Na_V1.8$ in rat dorsal root ganglia (DRG's).[121] Following the abovementioned hypothesis, the neurons with higher expression of TTT-R NaV channels (non-peptidergic) are the ones distributed in the most superficial layers of the skin. Along this line, our experimental observations suggest VHT, CN and silent nociceptors are located deeper in the epidermis based on their low responsiveness to transcutaneous stimulation, and clear responses in few experiments when using an intracutaneous needle for applying SDES (data not shown). Nevertheless, no experiments were performed in this study to provide anatomical evidence that VHT, CN, CMi, HT and LT C-fibres have a differential distribution in the epidermal layer of pigs. The lack of anatomical data specifically differentiating unmyelinated fibres might relate to the absence of specific markers and technical limitations in terms of high-resolution approaches required for single axons with diameters less than 1µm.

CMi and cold nociceptors are thought to present a higher expression of TTX-R currents.[112] To our knowledge there is no information referring to VGSC expression in unmyelinated afferents named here very-high threshold (VHT) nociceptors.

On the other hand, our observations are in accordance with the correlation of mechanical and TTX-sensitivity, as LT fibres present the lowest mechanical threshold of activation and a high TTX-S component.[113] Based on our observations, we might speculate that the TTX-S component is progressively reduced in HT, VHT, CN and CMi nociceptors as the mechanical threshold increases.

HT nociceptors have a receptive field around 1.95cm^2 compared to 0.35cm^2 of CMi when electrically stimulated at 10mA in human skin. When the rectangular electrical stimuli are increased from 10 to 50mA, the receptive field of HT fibres was enlarged to 3.08cm^2 while the receptive field of CMi showed a 15-fold increase compared to the smaller current, suggesting much larger receptive fields of CMi compared to HT nociceptors.[122] It was also described that the thresholds of activation are very heterogeneous within the receptive field of silent fibres compared to homogenous thresholds in HT.[105,123] Considering CMi have a small receptive field for currents under 10mA and high heterogeneity in the activation thresholds,[122] we could simply infer the maximal intensity of 10mA applied for SDES in the pig skin by means of transcutaneous stimulus was not strong enough to activate them after TTX. Hence, the

apparent complete blockade to SDES could have been overcome by higher stimulus intensities, but these cannot be delivered by our constant current stimulator.

Previous work describing VHT nociceptors[107] has found similar functional results and could provide indirect evidence for the expression of TTX-S VGSC in those sensory neurons. The experimental results obtained in this study indicate that VHTs constitute a separate sub-class of C-nociceptors, rather than being silent nociceptors.[30] Here, we identified VHT fibres with markedly higher mechanical thresholds than HT nociceptors, when stimulated with Semmes-Weinstein monofilaments (VHT 39.33±21.92 g; HT 5.45±3.5 g), but with a similar electrical threshold (VHT 2±0.94 mA; HT 1.39±1 mA). The electrical threshold of CMi nociceptors (3.12±2.93 mA) differs significantly from HT but not from VHT nociceptors. Furthermore, of the 13 VHT fibres analysed in this study, 1 was not tested and 6 responded to tonic thermal stimulation (i.e. 5s, 49°C, data not shown). The response pattern of these 6 units resembled the "slow C-fibre" (SC-) response to heat[73] and it may be argued that these VHT units belong to those mechanical high threshold "SC-units". However, a more sophisticated differentiation may be achieved by modern approaches based on single cell RNA-sequencing and PCR-expression patterns, which identified more than 10 types of dorsal root ganglion (DRG)[35] and perhaps future understanding of the functional properties of new sub-classes will improve the current classification of C-fibre types.

In our study, VHT fibres, similar to CMi and CN nociceptors, were also heavily affected by TTX: 9 units responded only with 1 or no action potential to half-sine wave stimulus at higher intensity ranges and the other 4 units could not be recorded from after the blockade. As those fibres have high mechanical as well as electrical thresholds of activation, it is likely that the apparent blockade after TTX in fact increased excitation threshold beyond the maximum output of our stimulator (10mA).

4.2.2 Role of TTX-S currents on C-fibre excitability

The blockade of TTX-sensitive currents reduced conduction velocity in compound potential recordings. This was reproduced as an overall reduction in conduction velocity (CV) in LT, HT and VHT observed at the single fibre level upon rectangular stimulus, albeit in the few CMi and CN nociceptors no significant change was found. Considering LT fibres have a higher conduction velocity than the other nociceptors[34] and they are abundant in the pig saphenous nerve fascicles, they should dominate the initial rising phase of the C-compound action potential.

Our results concerning the block of $Na_V1.6$ were straight forward. μ-conotoxin PIIIa completely abolished A-fibre compound potentials, yet the C-fibre latency was not affected by the $Na_V1.6$ blockade. This result confirms the crucial role of $Na_V1.6$ for A-fibre conduction and also underpins its minor functional role in C-nociceptors.[124]

The results from CAP recordings using specific VGSC-blockers have shown no effect in reducing CV by blocking $Na_V1.6$, but the blockade of $Na_V1.7$ by both XEN907 and ProTx II caused slowing in conduction velocity for rectangular stimuli. Those results also speak in favour of an involvement of $Na_V1.7$ in facilitating C-fibre conduction. For the recordings obtained upon slow depolarization, an increase in corrected latency could not be seen; C-CAPs were still induced after blockade of TTX-S currents and had a very long latency. Based on the kinetics and distribution of $Na_V1.7$, this isoform appears the main candidate for the generation of action potentials for slow depolarization of C-nociceptors at peripheral nerve endings.[125] In view of this, it was expected that the blockade of $Na_V1.7$ would increase corrected latency for SDES. $Na_V1.8$ would still conduct the compound potential in the absence of $Na_V1.7$, but more time would be necessary to initiate the response to sine wave considering a threshold of $Na_V1.8$ activation of about 35-60mV more depolarised than $Na_V1.7$.[126] However, the

result of the generation of the first action potential by SDES at around 50ms suggests that the main determinants are biophysical membrane properties i.e. time constant and membrane resistance. In this respect, the long latencies obtained upon low-intensity sine wave stimulation were *per se* very intriguing: they suggest that the neuronal membrane can accumulate charge for dozens of milliseconds. C-fibres have a membrane time constant in the order of hundred milliseconds[127] allowing weak but tonic currents to effectively change membrane potential. Our cooling experiments convincingly show that increasing the membrane resistance increases the ability of C-nociceptors to accumulate charge and thereby the response to SDES is sensitized, even though the cooling considerably slows down $Na_V1.7$ activation. Thus, our results support a crucial role of the biophysical membrane properties of C-fibres for the initiation of the first action potential to the sine wave stimulation. The blockade of TTX-S currents in pig saphenous nerve "*ex vivo*" recordings increased the amount of current and charge independently of the stimulus paradigm applied. The blockade of $Na_V1.7$ by specific $Na_V1.7$ blockers (XEN907 and ProTx II), however was not consistent, with a XEN907 effect in increasing current and charge for both rectangular and sine wave stimulus but ProTx II $Na_V1.7$ blockade causing an increase in current and charge only for rectangular stimulation. Thus, there appears to be a redundancy among the VGSCs for the initiation of the action potential following slow depolarisation such that an isolated block of $Na_V1.7$ might be partially compensated by other low threshold and TTX sensitive sodium channels.

When looking at the "*in vivo*" single fibre recordings, the amount of charge to initiate a single action potential upon sine wave stimulation remained more or less constant as current increased from 0.05 to 1.2mA. There was no significant TTX-driven increase in the amount of charge to evoke a sine wave action potential or in the charge at threshold for half-sine wave stimulus in any fibre type tested. These results confirm our CAP recordings suggesting that biophysical characteristics of the C-fibre membrane are crucial to determine the required charge for the first action potential and that there is also some redundancy between sodium channels for its initiation. Previous data in mice already attributed these long latencies to the time needed for the neuronal membrane to accumulate charge when stimulated with weak currents.[128] Contrary to this previous result, no significant increase in C-CAP latency was caused by 1μM TTX when nerves were stimulated with sine wave 4Hz.

In an attempt to validate the function of $Na_V1.7$ as an amplifier of sine wave induced C-fibre response, the exponential curves linking stimulus intensity and corrected latency were linearized by plotting the latencies to the reciprocal stimulus intensity. There was a significant increase in the intercept after ProTx II, but this is more related to the shorter latencies caused by higher stimulus intensities (and thus rectangular-like evoked responses) rather than the long latencies we aimed to investigate by linearization.

4.2.3 Burst responses to 500ms half-sine stimulation

While the results of corrected latency in the CAP recordings were similarly found in the "phase" on single nerve fibre level, as discussed above, major differences were found for the responses to the 500ms half-sine stimulus. As mentioned previously, the fibres respond to such a stimulus with a burst of activity that can outlast the electrical stimulus ("after-stimulus discharges"). Moreover, the latency to the first action potential was much more variable and did not show the same inverse relation to intensity as observed during the 4Hz sinusoidal stimulus. This indicates that the action potential initiation by the half-sine stimulus is determined less by the transferred charge. Time-dependent secondary membrane mechanisms, such as opening of voltage-sensitive

calcium channels, may contribute considerably to this phenomenon. TTX did not significantly affect the latency at threshold of LT fibres for the half-sine stimulus and even reduced the latency for HT and VHT nociceptors. On the other hand, the threshold for action potential generation was considerably increased and number of action potentials was massively reduced. This result suggests that TTX-S currents facilitate action potential generation upon the 500ms depolarizing pulse but an increase in stimulation intensity can rescue the activation after TTX. While such increase will lead to some discharge, the full-blown tonic supra-threshold discharge pattern as observed under control conditions is not re-established. Thus, TTX-S currents apparently are crucial for sustained bursts of action potentials following half-sine stimulation.

As mentioned above, LT fibres have a high expression of Na$_v$1.1, 1.6 and 1.7[113] and polymodal nociceptors are known to have a big component of TTX-S currents based on their modest activity-dependent slowing under high frequency electrical stimulation.[112] Our TTX-results do not allow to link a certain sodium channel subtype to the sustained bursts of action potentials. In general, the repriming kinetics of sodium channels will determine the maximum discharge frequency. Na$_v$1.6 has a particularly fast repriming and its high expression in A-fibres has been linked to their high maximum discharge frequencies, whereas the slow repriming of Na$_v$1.7 can explain the lower discharge frequencies recorded in C-fibres.[129] However, the exact Na$_v$1.7 expression pattern of functional C-fibre classes is not yet known and moreover, β-subunits or other auxiliary proteins[130] can modify sodium channel kinetics – apart from the fact that major species differences additionally complicate translation of structure function relations.[131] Altogether these results confirm a major role of TTX-S currents to facilitate action potential generation in A- and C-fibres. They also facilitate the activation of C-nociceptors by slow depolarizing pulses, but increasing stimulus intensity can compensate for the lack of TTX-S currents, at least to some extent. In contrast, TTX-S currents appear to be crucial for burst-firing of C-fibres induced by 500ms half-sine depolarisations.

4.3 Clinical implications: cold allodynia

In addition to pharmacologically blocking sodium channels we also used cooling, which slows down their activation kinetics, to modify neuronal firing. In contrast to the expected inhibition of pain, cooling the skin of volunteers from a neutral temperature of 32°C to 18°C actually increased pain ratings to cutaneous 4Hz sinusoidal current stimulation. The enhanced pain ratings during cooling in humans was paralleled by a larger fraction of unmyelinated axons responding to a sinusoidal current at 20°C compared to 32°C in mice CAP "*ex vivo*" recordings.[128]

The current study using pig saphenous nerve focussed on supplementing the initial observations generated in mice CAP recordings. The results confirmed that cooling isolated pig saphenous nerve fascicles also rendered C-fibres more prone to discharge, and a larger fraction of axons was activated at lower temperatures. Not only were higher amplitudes of C-CAP signals obtained, but fibres were also activated by lower stimulus intensities at 20°C upon sine wave stimulation in contrast to activation thresholds for rectangular stimuli which were increased by cooling. Remarkably, at lower temperatures, C-fibres responded to low intensity sinusoidal current stimulation after several tens of milliseconds, as recorded herein in both mice and pig neurons. This suggests that C-fibres can accumulate charge over several tens of milliseconds under cold conditions. The average electrical charge required to evoke action

potentials in C-fibres increased in rodents with cooling,[132] yet the results obtained in pig saphenous nerve have shown no significant difference in the amount of charge required to generate action potentials in C-fibres after cooling. The increased amount of charge after cooling would speak in favour of a loss in excitability and is consistent with the anaesthetic action of cooling.

The shift of dynamic sensitivity in C-fibres to lower current intensities during cooling may contribute to the everyday experience of enhanced pain experienced on a frosty morning to mild mechanical stimuli. Evidence suggests that mild cooling can result in increased C-fibre responsiveness to slow modulations of membrane potential and thereby can contribute to enhanced sensitivity to mechanical[133] and chemical[134,135] stimuli. While activation of sodium channels is generally slowed down by cooling resulting in a reduced excitability, there are also effects that increase their excitability: cooling does not shift the activation threshold of $Na_V1.7$ but increases ramp currents and delays its deactivation.[136]

Our results suggest that the main sensitizing effect of cooling on slow depolarizing stimuli in nociceptors is based on an increased membrane resistance via closure of cold-sensitive potassium channels and thereby facilitates accumulation of charge. K^+ leak currents are essential for maintaining a negative membrane potential and decrease neuronal excitability.[137] Double-KO mice of the cold-sensitive potassium channels TREK1 and TAAK developed cold hypersensitivity at temperatures of 15°C and 20°C,[138] particularly in the nociceptor population not responsive to menthol.[139] Additionally, a reduction in leak currents at cold temperatures (14°C) has been shown in recordings of small DRG neurons compared to 30°C,[140] associated with a decrease in action potential rheobase and an increase of excitability in nociceptive-like neurons accompanied by an increase in membrane resistance.[141]

These complex changes of nociceptor excitability by cooling are already interesting under physiological conditions. However, they become much more important under pathological conditions in patients with chronic pain. In particular for neuropathic pain, in which mild cooling stimuli can provoke intense burning and stabbing pain, a symptom termed cold allodynia. This effect is not mediated by the typical cold sensitive receptors on skin afferents, such as TRPM8 and TRPA1, because activation of these receptors by topical application of their agonists (e.g. menthol, cinnamon oil) do not provoke pain in cold allodynia patients.[142,143] Accordingly, recent C-CAP responses to slow depolarization were not affected by menthol or icilin, supporting that cold-specific transduction is not involved.[128]

Rather than activation of specific nociceptive receptors, spontaneous depolarizations of nociceptors have been shown of major clinical importance in patients with painful neuropathy.[144] When sufficiently strong, such depolarizations incite action potentials and are driving spontaneous activity in nociceptors that ultimately results in ongoing pain. Importantly, the higher the axonal membrane resistance the more depolarization will be induced by a given depolarizing inward current. Thus, our experimental model of slow depolarization at varying temperatures mimics the pathophysiologic spontaneous depolarizations. If these spontaneous depolarizations are subthreshold at normal skin temperatures, mild cooling will increase the membrane resistance by closure of cold sensitive potassium channels and thereby amplify the depolarizing effect, eventually leading to suprathreshold activation. Thus, mild cooling can demask subthreshold depolarizations in nociceptors and evoke cold allodynia.

We therefore posit that cooling can enhance the sensitivity in C-nociceptors to slow changes in membrane potential either experimentally by sinusoidal stimulation or pathophysiologically by spontaneous depolarizing fluctuations. Mechanistically,

alterations in voltage-gated channels that are active around resting membrane potential are of main interest. For example, the expression of $Na_V1.7$ is increased following paclitaxel induced neuropathy[145] while following both inflammation and nerve lesion $Na_V1.9$[146,147,133] and HCN2[148] expression are both dysregulated. Under such conditions, cooling can render enhanced endogenous subthreshold currents more effective and thereby may contribute to both spontaneous pain and cold allodynia. Indirect experimental evidence for such a cooling effect is provided by phasic cooling of a histamine iontophoresis site, which transiently increased itch ratings two-fold in both healthy volunteers and chronic itch patients suffering atopic dermatitis.[134,147] Clinical evidence for a link between cold allodynia and the occurrence of paroxysmal pain has also been provided in patients with complex regional pain syndrome[149] and this is consistent with our experimental findings. Further clinical studies will be intriguing to confirm whether cold allodynia in patients could be used as diagnostic sign for superficial hyperexcitable nociceptors and that might favour therefore a topical treatment approach.

4.4   Limitations

- The higher current amplitudes obtained during the initial phase of experiments by cooling the circulating bath solution to 20°C motivated the maintenance of a temperature of 20±2°C for all following "*ex vivo*" experiments exploring neurotoxins for VGSC modulation. Nevertheless, it is not possible to exclude the influence of cooling in the kinetics of VGSC and how this might have altered the overall excitability parameters during the C-CAP recordings and consequently the interpretation of the obtained results.

- By increasing rectangular electrical current using an intracutaneous needle in single nerve fibre recordings after the injection of toxins into the receptive field of the recorded units, it is not possible to exclude that the high current needed to induce a response caused a spreading of current and thereby activating a more proximal site of the axon that potentially had not been reached by the injection. In this case, to minimise false positive responses, units with significant changes in conduction latency upon high current stimulation after administration of toxins were omitted from the analyses, which reduced the overall number of observations.

- It is not possible to exclude that the increase in threshold of activation during single nerve fibre recordings were caused by a spatial change of the nerve fibres within the cutaneous layer due to the injection bleb caused by the administration of the toxin.

- The difficulties in diluting ICA121431 and the problems with the specificity of A-803467, NaV1.3 and NaV1.8 blockers respectively, limited the experimental approach. Many of the available toxins have poor water solubility and/or specificity for the target VGSC (e.g. lack of NaV1.7 specificity of ProTx III) and this impairs the interpretation of the results obtained by sodium channel modulation.

- Occasionally, we observed a second earlier peak appearance in the in-vivo C-fibre recording signal at higher current intensities (Fig. 38, APPENDIX). The second peak could provide indirect evidence that not only the number of action potentials rise as current intensity increases, but also another branch of the unit or even different class of nociceptor with higher thresholds of activation for sine wave 4Hz were additionally recruited.

4.5   Conclusions

The activity dependent slowing (ADS) observed in C-fibres during rectangular pulse stimulation with 2Hz for 3 min (LT<HT<<CMi (VHT)) are likely to be related to a TTX-R component (i.e. most prevalent in CMi). All fibre types seem to respond to both sine wave and half-sine wave electrical stimuli in a current intensity-dependent manner, with a clear accommodation of the response after 10 seconds of an ongoing 1-minute 4Hz sine wave stimulation. However, LT fibres and HT nociceptors seem to be particularly sensitive to this type of stimulus and therefore represent ideal fibres to study action potential initiation upon slow depolarisation.

In CAP recordings, as well as SNF recordings, higher current intensity led to shorter latencies (corrected latency in CAP recordings and phase in SNF recordings). Thereby, charge required to initiate an action potential remains constant, suggesting that membranes of unmyelinated neurons can accumulate charge over tens of milliseconds in order to generate an action potential. It seems that $Na_V1.7$, based on its capacity to generate ramp currents, plays an important but not imperative role in the C-fibre responses to slow depolarising stimulus. Evidence for the effects of $Na_V1.7$ and for a redundancy between sodium channels is supported by several results in this thesis. First, the amount of current to evoke a sine wave response in LT and HT is smaller compared to VHT, CN and CMi nociceptors. Second, LT and HT have a high component of TTX-S channels whereas CMi are thought to mostly express TTX-R VGSC. Third, sine wave evoked C-CAP could still be recorded after TTX and cooling, and finally, blockade of $Na_V1.6$ did not affect C-fibre excitability parameters, but abolished A-fibre components in CAP recordings.

Notably, even if $Na_V1.3$ is unlikely to be expressed in naive peripheral sensory afferents, $Na_V1.7$ may not suffice in explaining the C-fibre response to slow depolarising stimuli. As the blockade of TTX-S currents does not affect the time to incite a response using slow depolarising stimuli, TTX-R currents and $Na_V1.8$ channels in particular could be a candidate to explain these responses.

The present experiments furthermore demonstrate that cold temperatures interfere with neuronal excitability, and less current is required to evoke a CAP by sine wave stimuli at lower temperatures. Facilitated accumulation of depolarizing charge can explain longer delays of action potential initiation at low current intensities. Apart from bio-physical properties potentially contributing to this observation, another possible explanation for this phenomenon includes the closure of K^+ channels sensitive at lower temperatures, with reduction in K^+ leak currents and an increase in membrane resistance. In context of pathologic cold hypersensitivity (cold allodynia), it will be of interest to study in patients the relevance of these channels to their symptoms and correlate the patient's sensitivity to slow depolarizing electrical stimulation with successful topical anaesthetic treatment in future.

5 <u>SUMMARY</u>

Slow depolarising stimuli represent a more suitable type of electrical stimulation to activate unmyelinated C-fibres, excluding myelinated A-fibre responses, and preferential activation of C-nociceptors provides a useful tool for clinical trials involving chronic pain patients. In this study we applied slow depolarising stimuli, as well as the traditional rectangular stimuli for comparison, to record compound action potentials and responsiveness of characterized single nerve fibres in presence of specific voltage-gated sodium channel blockers.

Our results indicate a higher sensitivity of low threshold mechanosensitive (LT) fibres and polymodal (HT) nociceptors to sine wave 4Hz and half-sine wave 500ms stimuli compared to mechano-insensitive (CMi) "*silent*" and cold sensing (CN) nociceptors. This sensitivity was attributed to the presence of tetrodotoxin-sensitive (TTX-S) Na^+ channels. The data also suggests that the presence of TTX-S, specifically $Na_V1.7$, is especially relevant in the response to high intensity and high frequency types of electrical stimulus. The TTX-induced blockade of $Na_V1.7$ and $Na_V1.6$ separately shows that $Na_V1.7$ alone determines a slowing in conduction velocity without affecting the time needed to generate a C-fibre response to slow depolarising stimulus. LT fibres and HT nociceptors still responded after TTX albeit at about ten-fold higher current intensities. Thus, either the $Na_V1.8$ component in LT and HT fibres can carry a depolarisation upon long duration depolarising stimulations or current spread to a more proximal non-blocked area of the axon initiates the action potential. Moreover, it cannot be ruled out that the contribution of other voltage gated channels, such as K^+, Ca^+ and Ca^+ dependent Cl^- channels for instance, as well as the biophysical properties of the neuronal membrane, influenced the response of C-afferents to slow depolarising electrical stimulation.

The participation of K^+ channels in the response of C-fibres to slow depolarising stimulus, rendering the nociceptors particularly sensitive to this type of stimulus at colder temperatures, provided further evidence for the relevance in studying these channels, but also shed some light on the mechanisms leading to spontaneous activity and cold hypersensitivity in neuropathic pain patients.

The development of more specific $Na_V1.8$ blockers as well as studying other neuronal membrane channels will be crucial to clarify why unmyelinated axons seem to be particularly prone to respond to slow depolarising stimulus. The knowledge about the mechanisms of peripheral activation can possibly contribute to the understanding of the pathophysiology of cold allodynia in neuropathic pain patients, providing more accurate targets for the treatment of painful neuropathy in the future.

6 <u>LITERATURE</u>

1. Dubin AE, Patapoutian A. Nociceptors: The sensors of the pain pathway. *J Clin Invest* 2010; 120: 3760–3772.
2. Bennett DL, Clark XAJ, Huang J, et al. The role of voltage-gated sodium channels in pain signaling. *Physiol Rev* 2019; 99: 1079–1151.
3. West SJ, Bannister K, Dickenson AH, et al. Circuitry and plasticity of the dorsal horn - Toward a better understanding of neuropathic pain. *Neuroscience* 2015; 300: 254–275.
4. Tracey I, Mantyh PW. The Cerebral Signature for Pain Perception and Its Modulation. *Neuron* 2007; 55: 377–391.
5. Grace PM, Hutchinson MR, Maier SF, et al. Pathological pain and the neuroimmune interface. *Nat Rev Immunol* 2014; 14: 217–231.
6. Meacham K, Shepherd A, Mohapatra DP, et al. Neuropathic Pain: Central vs. Peripheral Mechanisms. *Curr Pain Headache Rep*; 21. Epub ahead of print 2017. DOI: 10.1007/s11916-017-0629-5.
7. Bouhassira D. Neuropathic pain: Definition, assessment and epidemiology. *Rev Neurol (Paris)* 2019; 175: 16–25.
8. Posso I de P, Palmeira CC de A, Vieira ÉB de M. Epidemiology of neuropathic pain. *Rev Dor* 2016; 17: 11–14.
9. Colloca L, Ludman T, Bouhassira D, et al. Neuropathic Pain. *Nat Rev Dis Prim* 2017; 3: 1–45.
10. Hanewinckel R, Ikram MA, Van Doorn PA. *Peripheral neuropathies*. 1st ed. Elsevier B.V. Epub ahead of print 2016. DOI: 10.1016/B978-0-12-802973-2.00015-X.
11. Bouhassira D, Lantéri-Minet M, Attal N, et al. Prevalence of chronic pain with neuropathic characteristics in the general population. *Pain* 2008; 136: 380–387.
12. Maier C, Baron R, Tölle TR, et al. Quantitative sensory testing in the German Research Network on Neuropathic Pain (DFNS): Somatosensory abnormalities in 1236 patients with different neuropathic pain syndromes. *Pain* 2010; 150: 439–450.
13. Finnerup NB, Attal N, Haroutounian S, et al. Pharmacotherapy for neuropathic pain in adults: A systematic review and meta-analysis. *Lancet Neurol* 2015; 14: 162–173.
14. Jensen TS, Finnerup NB. Allodynia and hyperalgesia in neuropathic pain: Clinical manifestations and mechanisms. *Lancet Neurol* 2014; 13: 924–935.
15. Xing H, Chen M, Ling J, et al. TRPM8 mechanism of cold allodynia after chronic nerve injury. *J Neurosci* 2007; 27: 13680–13690.
16. Beise RD, Carstens E, Kohllöffel LUE. Psychophysical study of stinging pain evoked by brief freezing of superficial skin and ensuing short-lasting changes in sensations of cool and cold pain. *Pain* 1998; 74: 275–286.
17. Defrin R, Ohry A, Blumen N, et al. Sensory determinants of thermal pain. *Brain* 2002; 125: 501–510.
18. MacDonald DI, Luiz AP, Iseppon F, et al. Silent cold-sensing neurons contribute to cold allodynia in neuropathic pain. *Brain* 2021; 144: 1711–1726.
19. Serra J, Bostock H, Solà R, et al. Microneurographic identification of spontaneous activity in C-nociceptors in neuropathic pain states in humans and rats. *Pain* 2012; 153: 42–55.
20. Kleggetveit IP, Namer B, Schmidt R, et al. High spontaneous activity of C-nociceptors in painful polyneuropathy. *Pain* 2012; 153: 2040–2047.

21. Namer B, Ørstavik K, Schmidt R, et al. Specific changes in conduction velocity recovery cycles of single nociceptors in a patient with erythromelalgia with the I848T gain-of-function mutation of Na v 1.7. *Pain* 2015; 156: 1637–1646.

22. WHITWAM JG. Classification of peripheral nerve fibres: An historical perspective. *Anaesthesia* 1976; 31: 494–503.

23. Lloyd. Neuron Patterns Controlling Transmission Limb.

24. Gasser HS, Erlanger J. The Action Potential in Fibers of Slow Conduction in Spinal Roots and Somatic Nerves. *Proc Soc Exp Biol Med* 1929; 26: 647–649.

25. Manzano GM, Giuliano LMP, Nóbrega JAM. A brief historical note on the classification of nerve fibers. *Arq Neuropsiquiatr* 2008; 66: 117–119.

26. Jonas R, Namer B, Stockinger L, et al. Tuning in C-nociceptors to reveal mechanisms in chronic neuropathic pain. *Ann Neurol* 2018; 83: 945–957.

27. Schmidt R, Schmelz M, Forster C, et al. Novel classes of responsive and unresponsive C nociceptors in human skin. *J Neurosci* 1995; 15: 333–341.

28. Torebjork HE, Hallin RG. Responses in human A and C fibres to repeated electrical intradermal stimulation. *J Neurol Neurosurg Psychiatry* 1974; 37: 653–664.

29. Torebjörk HE, Hallin RG. IDENTIFICATION OF AFFERENT C UNITS IN INTACT HUMAN SKIN NERVES. *Brain Res* 1974; 67: 387–403.

30. Meyer RA, Campbell JN. A novel electrophysiological technique for locating cutaneous nociceptive and chemospecific receptors. *Brain Res* 1988; 441: 81–86.

31. Vallbo ÅB, Olausson H, Wessberg J. Unmyelinated afferents constitute a second system coding tactile stimuli of the human hairy skin. *J Neurophysiol* 1999; 81: 2753–2763.

32. Gee MD, Lynn B, Cotsell B. Activity-dependent slowing of conduction velocity provides a method for identifying different functional classes of C-fibre in the rat saphenous nerve. *Neuroscience* 1996; 73: 667–675.

33. Campero M, Serra J, Ochoa JL. C-polymodal nociceptors activated by noxious low temperature in human skin. *J Physiol* 1996; 497: 565–572.

34. Obreja O, Ringkamp M, Namer B, et al. Patterns of activity-dependent conduction velocity changes differentiate classes of unmyelinated mechano-insensitive afferents including cold nociceptors, in pig and in human. *Pain* 2010; 148: 59–69.

35. Li C, Wang S, Chen Y, et al. Somatosensory Neuron Typing with High-Coverage Single-Cell RNA Sequencing and Functional Analysis. *Neurosci Bull* 2018; 34: 200–207.

36. Usoskin D, Furlan A, Islam S, et al. Unbiased classification of sensory neuron types by large-scale single-cell RNA sequencing. *Nat Neurosci* 2015; 18: 145–153.

37. Rostock C, Schrenk-Siemens K, Pohle J, et al. Human vs. Mouse Nociceptors – Similarities and Differences. *Neuroscience* 2018; 387: 13–27.

38. Gigliuto C, De Gregori M, Malafoglia V, et al. Pain assessment in animal models: Do we need further studies? *J Pain Res* 2014; 7: 227–236.

39. Catterall WA. From ionic currents to molecular mechanisms: The structure and function of voltage-gated sodium channels. *Neuron* 2000; 26: 13–25.

40. Catterall WA, Goldin AL, Waxman SG. Nomenclature and structure-function relationships of Voltage-Gated Sodium Channels. *Pharmacol Rev* 2005; 57: 397–409.

41. Satin J, Kyle JW, Chen M, et al. A mutant of TTX-resistant cardiac sodium channels with TTX-sensitive properties. *Science (80-)* 1992; 256: 1202–1205.

42. Sivilotti L, Okuse K, Akopian AN, et al. A single serine residue confers tetrodotoxin insensitivity on the rat sensory-neuron-specific sodium channel SNS. *FEBS Lett* 1997; 409: 49–52.

43. Tzakoniati F. *A Chemical Biology Approach to Understanding the Basis of Voltage-Gated Sodium Channel Modulation*. Imperial College of London, https://spiral.imperial.ac.uk/bitstream/10044/1/65743/1/Tzakoniati-F-2018-PhD-Thesis.pdfhttps://spiral.imperial.ac.uk/bitstream/10044/1/65743/1/Tzakoniati-F-2018-PhD-Thesis.pdf (2018).

44. Black JA, Nikolajsen L, Kroner K, et al. Multiple sodium channel isoforms and mitogen-activated protein kinases are present in painful human neuromas. *Ann Neurol* 2008; 64: 644–653.

45. Fukuoka T, Kobayashi K, Yamanaka H, et al. Comparative study of the distribution of the α-subunits of voltage-gated sodium channels in normal and axotomized rat dorsal root ganglion neurons. *J Comp Neurol* 2008; 510: 188–206.

46. Renganathan M, Dib-Hajj S, Waxman SG. Nav1.5 underlies the 'third TTX-R sodium current' in rat small DRG neurons. *Mol Brain Res* 2002; 106: 70–82.

47. Felts PA, Yokoyama S, Dib-Hajj S, et al. Sodium channel α-subunit mRNAs I, II, III, NaG, Na6 and hNE (PN1): different expression patterns in developing rat nervous system. *Mol Brain Res* 1997; 45: 71–82.

48. Waxman SG, Kocsis JD, Black JA. Type III sodium channel mRNA is expressed in embryonic but not adult spinal sensory neurons, and is reexpressed following axotomy. *J Neurophysiol* 1994; 72: 466–470.

49. Ruiz M de L, Kraus RL. Voltage-Gated Sodium Channels : Structure , Function , Pharmacology and Clinical Indications. *J Med Chem* 2015; 58: 7093–7118.

50. Kaplan MR, Cho MH, Ullian EM, et al. Differential control of clustering of the sodium channels Nav1.2 and Nav1.6 at developing CNS nodes of Ranvier. *Neuron* 2001; 30: 105–119.

51. Black JA, Renganathan M, Waxman SG. Sodium channel Nav1.6 is expressed along nonmyelinated axons and it contributes to conduction. *Mol Brain Res* 2002; 105: 19–28.

52. Wood JN, Boorman JP, Okuse K, et al. Voltage-gated sodium channels and pain pathways. *J Neurobiol* 2004; 61: 55–71.

53. Richards KL, Milligan CJ, Richardson RJ, et al. Selective NaV1.1 activation rescues Dravet syndrome mice from seizures and premature death. *Proc Natl Acad Sci U S A* 2018; 115: E8077–E8085.

54. Han C, Huang J, Waxman SG. Sodium channel Na v 1.8 . *Neurology* 2016; 86: 473–483.

55. Cummins TR, Aglieco F, Renganathan M, et al. Nav1.3 sodium channels: Rapid repriming and slow closed-state inactivation display quantitative differences after expression in a mammalian cell line and in spinal sensory neurons. *J Neurosci* 2001; 21: 5952–5961.

56. Herzog RI, Cummins TR, Ghassemi F, et al. Distinct repriming and closed-state inactivation kinetics of Nav1.6 and Nav1.7 sodium channels in mouse spinal sensory neurons. *J Physiol* 2003; 551: 741–750.

57. Osteen JD, Sampson K, Iyer V, et al. Pharmacology of the Nav1.1 domain IV voltage sensor reveals coupling between inactivation gating processes. *Proc Natl Acad Sci U S A* 2017; 114: 6836–6841.

58. Männikkö R, Wong L, Tester DJ, et al. Dysfunction of NaV1.4, a skeletal muscle voltage-gated sodium channel, in sudden infant death syndrome: a case-control study. *Lancet* 2018; 391: 1483–1492.

59. Curia G, Biagini G, Perucca E, et al. Lacosamide: A new approach to target voltage-gated sodium currents in epileptic disorders. *CNS Drugs* 2009; 23: 555–568.

60. Catterall WA. Structure and function of voltage-gated sodium channels at atomic resolution. *Exp Physiol* 2014; 99: 35–51.

61. Yu FH, Catterall WA. Overview of the coltage-gated sodium channel family. *Genome Biol*; 4. Epub ahead of print 2003. DOI: 10.1186/gb-2003-4-3-20.

62. Dib-Hajj SD, Yang Y, Black JA, et al. The Na v 1.7 sodium channel: From molecule to man. *Nat Rev Neurosci* 2013; 14: 49–62.

63. Brouwer BA, Merkies ISJ, Gerrits MM, et al. Painful neuropathies: The emerging role of sodium channelopathies. *Brain* 2014; 19: 53–65.

64. Eberhardt E, Havlicek S, Schmidt D, et al. Pattern of Functional TTX-Resistant Sodium Channels Reveals a Developmental Stage of Human iPSC- and ESC-Derived Nociceptors. *Stem Cell Reports* 2015; 5: 305–313.

65. Han C, Yang Y, Te Morsche RH, et al. Familial gain-of-function Nav1.9 mutation in a painful channelopathy. *J Neurol Neurosurg Psychiatry* 2017; 88: 233–240.

66. Huang J, Han C, Estacion M, et al. Gain-of-function mutations in sodium channel NaV1.9 in painful neuropathy. *Brain* 2014; 137: 1627–1642.

67. Huang J, Yang Y, Waxman SG, et al. Depolarized inactivation overcomes impaired activation to produce DRG neuron hyperexcitability in a Nav1.7 mutation in a patient with distal limb pain. *J Neurosci* 2014; 34: 12328–12340.

68. Leipold E, Liebmann L, Korenke GC, et al. A de novo gain-of-function mutation in SCN11A causes loss of pain perception. *Nat Genet* 2013; 45: 1399–1407.

69. Li CL, Li KC, Wu D, et al. Somatosensory neuron types identified by high-coverage single-cell RNA-sequencing and functional heterogeneity. *Cell Res* 2016; 26: 83–102.

70. Ackerley R, Watkins RH. Microneurography as a tool to study the function of individual C-fiber afferents in humans: responses from nociceptors, thermoceptors and mechanoceptors. 2018; 5: 188–194.

71. Schmelz M, Schmid R, Handwerker HO, et al. Encoding of burning pain from capsaicin-treated human skin in two categories of unmyelinated nerve fibres. *Brain* 2000; 123: 560–571.

72. Serra J, Campero M, Ochoa J, et al. Activity-dependent slowing of conduction differentiates functional of C fibres innervating human skin. *J Physiol* 1999; 799–811.

73. Wooten M, Weng HJ, Hartke T V., et al. Three functionally distinct classes of C-fibre nociceptors in primates. *Nat Commun* 2014; 5: 1–12.

74. Acosta C, McMullan S, Djouhri L, et al. HCN1 and HCN2 in Rat DRG Neurons: Levels in Nociceptors and Non-Nociceptors, NT3-Dependence and Influence of CFA-Induced Skin Inflammation on HCN2 and NT3 Expression. *PLoS One*; 7. Epub ahead of print 2012. DOI: 10.1371/journal.pone.0050442.

75. Gao LL, McMullan S, Djouhri L, et al. Expression and properties of hyperpolarization-activated current in rat dorsal root ganglion neurons with known sensory function. *J Physiol* 2012; 590: 4691–4705.

76. Shon KJ, Olivera BM, Watkins M, et al. µ-Conotoxin PIIIa, a new peptide for discriminating among tetrodotoxin- sensitive Na channel subtypes. *J Neurosci* 1998; 18: 4473–4481.

77. Nielsen KJ, Watson M, Adams DJ, et al. Solution structure of µ-conotoxin PIIIA, a preferential inhibitor of persistent tetrodotoxin-sensitive sodium channels. *J Biol Chem* 2002; 277: 27247–27255.

78. Tosti E, Boni R, Gallo A. µ-Conotoxins modulating sodium currents in pain

perception and transmission: A therapeutic potential. *Mar Drugs* 2017; 15: 1–16.

79. Chowdhury S, Chafeev M, Liu S, et al. Discovery of XEN907, a spirooxindole blocker of Na V1.7 for the treatment of pain. *Bioorganic Med Chem Lett* 2011; 21: 3676–3681.

80. Chowdhury S, Liu S, Cadieux JA, et al. Tetracyclic spirooxindole blockers of hNaV1.7: Activity in vitro and in CFA-induced inflammatory pain model. *Med Chem Res* 2013; 22: 1825–1836.

81. Schmalhofer WA, Calhoun J, Burrows R, et al. ProTx-II, a selective inhibitor of NaV1.7 sodium channels, blocks action potential propagation in nociceptors. *Mol Pharmacol* 2008; 74: 1476–1484.

82. Cardoso FC, Dekan Z, Rosengren KJ, et al. Identification and characterization of ProTx-III [μ-TRTX-Tp1a], a new voltage-gated sodium channel inhibitor from venom of the tarantula Thrixopelma pruriens. *Mol Pharmacol* 2015; 88: 291–303.

83. Zilic L, Garner PE, Yu T, et al. An anatomical study of porcine peripheral nerve and its potential use in nerve tissue engineering. *J Anat* 2015; 227: 302–314.

84. Dusch M, Schley M, Obreja O, et al. Comparison of electrically induced flare response patterns in human and pig skin. *Inflamm Res* 2009; 58: 639–648.

85. Swindle MM, Smith AC. *SWINE in the LABORATORY*. 3rd ed. Charleston, USA: Taylor and Francis Group, 2016.

86. Morgaz J, Navarrete R, Granados M del M, et al. Swine model in transplant research: Review of anaesthesia and perioperative management. *World J Anesthesiol* 2015; 4: 73–82.

87. Campbell JN, Meyer RA, LaMotte RH. Sensitization of myelinated nociceptive afferents that innervate monkey hand. *J Neurophysiol* 1979; 42: 1669–1679.

88. Ringkamp M, Johanek LM, Borzan J, et al. Conduction properties distinguish unmyelinated sympathetic efferent fibers and unmyelinated primary afferent fibers in the monkey. *PLoS One*; 5. Epub ahead of print 2010. DOI: 10.1371/journal.pone.0009076.

89. Obreja O, Hirth M, Turnquist B, et al. The differential effects of two sodium channel modulators on the conductive properties of C-fibers in pig skin in vivo. *Anesth Analg* 2012; 115: 560–571.

90. Obreja O, Ringkamp M, Turnquist B, et al. Nerve growth factor selectively decreases activity-dependent conduction slowing in mechano-insensitive C-nociceptors. *Pain* 2011; 152: 2138–2146.

91. Mackel RG, Brink EE. Accommodation in single human nerve fibers in vivo. *Muscle Nerve* 1995; 18: 469–471.

92. Weidner C, Schmelz M, Schmidt R, et al. Neural signal processing: The underestimated contribution of peripheral human C-fibers. *J Neurosci* 2002; 22: 6704–6712.

93. Gasser HS, Grundfest H. Axon diameters in relation to the skpike dimensions and the conduction velocity in mammalian A fibers. *Am J Physiol Physiol* 1939; 127: 393–414.

94. Israel MR, Tanaka BS, Castro J, et al. NaV1.6 regulates excitability of mechanosensitive sensory neurons. *J Physiol* 2019; 597: 3751–3768.

95. Katims JJ, Naviasky EH, Rendell MS, Ng LK BM. Constant current sine wave transcutaneous nerve stimulation for the evaluation of peripheral neuropathy. *Arch Phys Med Rehabil* 1987; 68: 210–3.

96. Landmann G, Stockinger L, Gerber B, et al. Local hyperexcitability of C-nociceptors may predict responsiveness to topical lidocaine in neuropathic pain. *PLoS One* 2022; 17: 1–21.

97. Cummins TR, Howe JR, Waxman SG. Slow closed-state inactivation: A novel

mechanism underlying ramp currents in cells expressing the hNE/PN1 sodium channel. *J Neurosci* 1998; 18: 9607–9619.

98. Black JA, Frézel N, Dib-Hajj SD, et al. Expression of Nav1.7 in DRG neurons extends from peripheral terminals in the skin to central preterminal branches and terminals in the dorsal horn. *Mol Pain* 2012; 8: 1–11.

99. Jonas R, Klusch A, Schmelz M, et al. Assessment of TTX-s and TTX-r action potential conduction along neurites of NGF and GDNF cultured porcine DRG somata. *PLoS One* 2015; 10: 1–16.

100. Jonas R, Namer B, Schnakenberg M, et al. Sympathetic efferent neurons are less sensitive than nociceptors to 4 Hz sinusoidal stimulation. *Eur J Pain (United Kingdom)* 2020; 24: 122–133.

101. Alamri A, Bron R, Brock JA, et al. Transient receptor potential cation channel subfamily v member 1 expressing corneal sensory neurons can be subdivided into at least three subpopulations. *Front Neuroanat* 2015; 9: 1–14.

102. Stoenoiu MS, Ni J, Verkaeren C, et al. Corticosteroids induce expression of aquaporin-1 and increase transcellular water transport in rat peritoneum. *J Am Soc Nephrol* 2003; 14: 555–565.

103. Schmelz M, Michael K, Weidner C, et al. Which nerve fibers mediate the axon reflex flare in human skin? *Neuroreport* 2000; 11: 645–648.

104. Li L, Rutlin M, Abraira VE, et al. The functional organisation of cutaneous low-threshold mechanosensory neurons. *Cell* 2011; 147: 1615–1627.

105. Schmidt R, Schmelz M, Ringkamp M, et al. Innervation territories of mechanically activated C nociceptor units in human skin. *J Neurophysiol* 1997; 78: 2641–2648.

106. Lynn B, Faulstroh K, Pierau F -K. The Classification and Properties of Nociceptive Afferent Units from the Skin of the Anaesthetized Pig. *Eur J Neurosci* 1995; 7: 431–437.

107. Werland F, Hirth M, Rukwied R, et al. Maximum axonal following frequency separates classes of cutaneous unmyelinated nociceptors in the pig. *J Physiol* 2021; 599: 1595–1610.

108. Hoffmann T, Sharon O, Wittmann J, et al. *NaV1.7 and pain: Contribution of peripheral nerves*. 2018. Epub ahead of print 2018. DOI: 10.1097/j.pain.0000000000001119.

109. De Col R, Messlinger K, Carr RW. Conduction velocity is regulated by sodium channel inactivation in unmyelinated axons innervating the rat cranial meninges. *J Physiol* 2008; 586: 1089–1103.

110. Snape A, Pittaway JF, Baker MD. Excitability parameters and sensitivity to anemone toxin ATX-II in rat small diameter primary sensory neurones discriminated by Griffonia simplicifolia isolectin IB4. *J Physiol* 2010; 588: 125–137.

111. Bear MF, Connors BW, Paradiso MA. *Neuro-wissenschaften*. 3rd ed. Cambridge: Spektrum Akademisher Verlag, 2009.

112. Jonas R, Prato V, Lechner SG, et al. TTX-Resistant Sodium Channels Functionally Separate Silent From Polymodal C-nociceptors. *Front Cell Neurosci* 2020; 14: 1–13.

113. Middleton SJ, Perini I, Themistocleous AC, et al. Nav1.7 is required for normal C-low threshold mechanoreceptor function in humans and mice. *Brain*. Epub ahead of print 2021. DOI: 10.1093/brain/awab482.

114. Zimmermann K, Leffler A, Babes A, et al. Sensory neuron sodium channel Nav1.8 is essential for pain at low temperatures. *Nature* 2007; 447: 855–858.

115. Luiz AP, MacDonald DI, Santana-Varela S, et al. Cold sensing by Na V 1.8-

positive and Na V 1.8-negative sensory neurons. *Proc Natl Acad Sci U S A* 2019; 116: 3811–3816.

116. Grill WM, Mortimer JT. Stimulus Waveforms for Selective Neural Stimulation. *IEEE Eng Med Biol Mag* 1995; 14: 375–385.

117. Tavares-Ferreira D, Shiers S, Ray PR, et al. Spatial transcriptomics of dorsal root ganglia identifies molecular signatures of human nociceptors. *Sci Transl Med* 2022; 14: 1–36.

118. Crawford LTK, Caterina MJ. Functional Anatomy of the Sensory Nervous System: Updates From the Neuroscience Bench. *Toxicol Pathol* 2020; 48: 174–189.

119. Zylka MJ, Rice FL, Anderson DJ. Topographically distinct epidermal nociceptive circuits revealed by axonal tracers targeted to Mrgprd. *Neuron* 2005; 45: 17–25.

120. Fang X, Djouhri L, McMullan S, et al. Intense isolectin-B4 binding in rat dorsal root ganglion neurons distinguishes C-fiber nociceptors with broad action potentials and high Nav1.9 expression. *J Neurosci* 2006; 26: 7281–7292.

121. Wu ZZ, Pan HL. Tetrodotoxin-sensitive and -resistant Na + channel currents in subsets of small sensory neurons of rats. *Brain Res* 2004; 1029: 251–258.

122. Schmidt R, Schmelz M, Weidner C, et al. Innervation territories of mechano-insensitive C nociceptors in human skin. *J Neurophysiol* 2002; 88: 1859–1866.

123. Schmelz M, Schmidt R, Ringkamp M, et al. Sensitization of insensitive branches of C nociceptors in human skin. *J Physiol* 1994; 480: 389–394.

124. Chen L, Huang J, Zhao P, et al. Conditional knockout of Na V 1 . 6 in adult mice ameliorates neuropathic pain. *Sci Rep* 2018; 8: 1–17.

125. Bennett DL, Clark XAJ, Huang J, et al. The role of voltage-gated sodium channels in pain signaling. *Physiol Rev* 2019; 99: 1079–1151.

126. Vijayaragavan K, O'Leary ME, Chahine M. Gating properties of Nav1.7 and Nav1.8 peripheral nerve sodium channels. *J Neurosci* 2001; 21: 7909–7918.

127. Bostock H, Campero M, Serra J, et al. Velocity recovery cycles of C fibres innervating human skin. *J Physiol* 2003; 553: 649–663.

128. Pakalniskis J. *Modulation of neuronal excitability in ex-vivo and in-vitro systems*. University of Heidelberg, https://archiv.ub.uni-heidelberg.de/volltextserver/28255/1/diss20_e021.pdf (2019).

129. Mcdermott LA, Weir GA, Themistocleous AC, et al. Defining the Functional Role of Na V 1 . 7 in Human Article Defining the Functional Role of Na V 1 . 7 in Human Nociception. *Neuron* 2019; 101: 905-919.e8.

130. Effraim PR, Estacion M, Zhao P, et al. Fibroblast growth factor homologous factor 2 attenuates excitability of DRG neurons. *J Neurophysiol* 2022; 128: 1258–1266.

131. Zhang X, Priest BT, Belfer I, et al. Voltage-gated Na + currents in human dorsal root ganglion neurons. *Elife* 2017; 6: 1–23.

132. Pakalniskis J, Soares S, Rajan S, et al. Human pain ratings to electrical sinusoids increase with cooling through a cold-induced increase in C-fibre excitability. *Pain* 2023; 00: 1–13.

133. Boada MD, Eisenach JC, Ririe DG. Mechanical sensibility of nociceptive and non-nociceptive fast-conducting afferents is modulated by skin temperature. *J Neurophysiol* 2016; 115: 546–553.

134. Pfab F, Valet M, Sprenger T, et al. Temperature modulated histamine-itch in lesional and nonlesional skin in atopic eczema - A combined psychophysical and neuroimaging study. *Allergy Eur J Allergy Clin Immunol* 2010; 65: 84–94.

135. Pfab F, Valet M, Sprenger T, et al. Short-term alternating temperature enhances histamine-induced itch: A biphasic stimulus model. *J Invest Dermatol* 2006; 126:

2673–2678.

136. Han C, Lampert A, Rush AM, et al. Temperature dependence of erythromelalgia mutation L858F in sodium channel Nav1.7. *Mol Pain* 2007; 3: 1–10.

137. Goldstein SAN, Bockenhauer D, Kelly IO, et al. POTASSIUM LEAK CHANNELS AND THE KCNK FAMILY OF TWO-P-DOMAIN SUBUNITS. *Nat Rev Neurosci* 2001; 2: 175–184.

138. Noe J, Zimmermann K, Deval E, et al. The mechano-activated K channels TRAAK and TREK-1 control both warm and cold perception. 2009; 28: 1308–1318.

139. Li X, Toyoda H. Role of leak potassium channels in pain signaling. *Brain Res Bull*. Epub ahead of print 2015. DOI: 10.1016/j.brainresbull.2015.08.007.

140. Viatchenko-karpinski V, Ling J, Gu JG. Characterization of temperature-sensitive leak K + currents and expression of TRAAK , TREK-1 , and TREK2 channels in dorsal root ganglion neurons of rats. *Mol Brain Res* 2018; 1–9.

141. Kanda H, Gu JG. Effects of cold temperatures on the excitability of rat trigeminal ganglion neurons that are not for cold-sensing. *J Neurochem* 2017; 141: 532–543.

142. Namer B, Kleggetveit IP, Handwerker H, et al. Role of TRPM8 and TRPA1 for cold allodynia in patients with cold injury. *Pain* 2008; 139: 63–72.

143. Wasner G, Naleschinski D, Binder A, et al. The effect of menthol on cold allodynia in patients with neuropathic pain. *Pain Med* 2008; 9: 354–358.

144. North RY, Odem MA, Li Y, et al. Electrophysiological Alterations Driving Pain-Associated Spontaneous Activity in Human Sensory Neuron Somata Parallel Alterations Described in Spontaneously Active Rodent Nociceptors. *J Pain* 2022; 23: 1343–1357.

145. Li Y, North RY, Rhines LD, et al. Drg voltage-gated sodium channel 1.7 is upregulated in paclitaxel-induced neuropathy in rats and in humans with neuropathic pain. *J Neurosci* 2018; 38: 1124–1136.

146. Amaya F, Wang H, Costigan M, et al. The voltage-gated sodium channel Nav1.9 is an effector of peripheral inflammatory pain hypersensitivity. *J Neurosci* 2006; 26: 12852–12860.

147. Lolignier S, Bonnet C, Gaudioso C, et al. The Nav1.9 Channel Is a Key Determinant of Cold Pain Sensation and Cold Allodynia. *Cell Rep* 2015; 11: 1067–1078.

148. Emery EC, Young GT, Berrocoso EM, et al. HCN2 ion channels play a central role in inflammatory and neuropathic pain. *Science (80-)* 2011; 333: 1462–1466.

149. Lunden LK, Kleggetveit IP, Schmelz M, et al. Cold allodynia is correlated to paroxysmal and evoked mechanical pain in complex regional pain syndrome (CRPS). *Scand J Pain* 2022; 22: 533–542.

7 <u>APPENDIX</u>
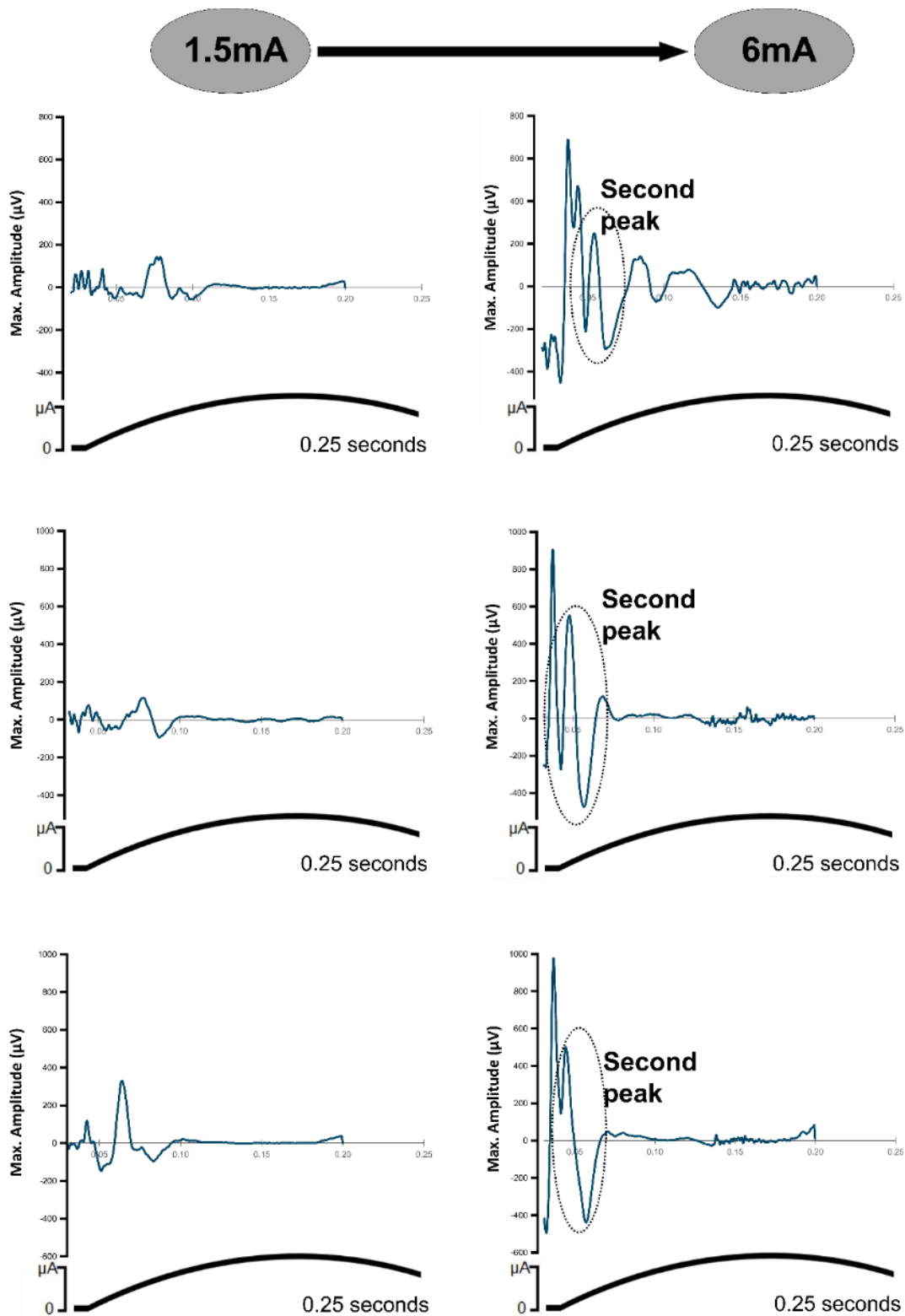
Figure 38: High stimulus intensity induced 2nd C-CAP Peak: Three specimens of C-CAP signal B90905B (**top panel**), C00604A (**middle**) and C00618A (**bottom panel**) recorded from saphenous nerve fascicles upon sine wave stimulus. The appearance of a 2nd peak become evident as stimulus intensity increased from 1.5 to 6µA during the stimulus-response curves generation. The second peak might be indirect evidence for the recruitment of C-fibres with higher thresholds of activation and slower conduction velocities. The specimens were recorded in different days and from different pigs.

8   <u>CURRICULUM</u>

PERSONALIEN

Name und Vorname: Sabrina da Silva Soares

Geburtsdatum: 14/10/1984

Geburtsort: Brasilien

SCHULISCHER WERDEGANG

1991-2001   Primar und Sekundarschule

UNIVERSITÄRER WERDEGANG

01 2019 - jetzt   Promotion zum Dr. sc. hum.

Universität Medizin Mannheim- Heidelberg Universität

Soares, S., Wühl, E., Schlund, A., Schneider, T., Sohns, K., Rukwied, R., Schmelz, M., Kränzlin, B. Acepromazine and Medetomidine Influence on a Diabetes Related Study in Aachen Minipigs. Laboratory Animals (*submitted manuscript*)

Pakalniskis J*, Soares S*, Rajan S, et al. Human pain ratings to electrical sinusoids increase with cooling through a cold-induced increase in C-fibre excitability. Pain 2023; 00: 1–13.

Schneider T, Filip J, Soares S, et al. Optimized Electrical Stimulation of C-Nociceptors in Humans Based on the Chronaxie of Porcine C-Fibres. J Pain. Epub ahead of print 2023. DOI: 10.1016/j.jpain.2023.01.009.

Jonas R, Namer B, Schnakenberg M, Soares S, Pakalniskis J, Carr R, Schmelz M, Rukwied R: Sympathetic efferent neurons are less sensitive than nociceptors to 4 Hz sinusoidal stimulation. *Eur. J. Pain (United Kingdom)* 24: 122–133, 2020

10 2016 – 2018   Master-Abschluss in Angewandter Pharmakologie

Coimbra Universität

Sabrina S. Soares*, Elmira Bekbolatova*, Maria Dulce Cotrim, Zuriyadda Sakipova, Liliya Ibragimova, Wirginia Kukula-Koch, Thais B. Sardella Giorno, Patrícia D. Fernandes, Diogo André Fonseca and Fabio Boylan. and Pharmacology of the Kazakh Crataegus Almaatensis Pojark: An Asian Herbal Medicine. Antioxidants 2019, 8, 300; doi:10.3390/antiox8080300

Hugo F, Fernandes A, Soares S, et al. Pharmacological, toxicological and phytochemical analysis of Spondias dulcis parkinson. Nat Prod Res 2023; 0: 1–5.

02 2012-2014   Residenzprogramm in Anästhesiologie

UFRGS Universität

07 2006- 2011   Studiums in Tiermedizin

UFRGS Universität

9 <u>ACKNOWLEDGEMENTS</u>